On the Mechanisms of Cardiomyopathy in a Human Induced Pluripotent Stem Cell-derived Cardiomyocyte Model of Infantile-Onset Pompe Disease

By

Kunil Kaushik Raval

A dissertation submitted in partial fulfillment of
the requirements for the degree of

Doctor of Philosophy
(Cell and Molecular Biology)

at the

UNIVERSITY OF WISCONSIN-MADISON

2014

Date of final oral examination: 6/25/2014

The dissertation is approved by the following members of the Final Oral Committee:

Timothy J. Kamp, Professor of Medicine
Deane F. Mosher, Professor of Medicine
Aseem Z. Ansari, Professor of Biochemistry
Gary E. Lyons, Professor of Cell and Regenerative Biology
John C. Ralphe, Associate Professor of Pediatrics

TABLE OF CONTENTS

ACKNOWLEDGEMENTS

I first thank my Mom and Dad, Tiba and Kaushik Raval. From a very young age, perhaps even birth or before, they instilled in me a hunger for knowledge, and not just the academic or scientific type. I would often be asked, "What did you learn today, Kunil?" even during the summer months when there was no school. If, when, I have children, they will also be raised to always be curious and never be satisfied for too long. Looking back to those early days I see that becoming a philosopher, one who loves knowledge, was pure destiny.

I remember in science class being in awe that I could calculate the circumference of the earth with a piece of string and a protractor. I was haunted by the inescapable process of entropy and humbled when I finally grasped evolution and what it implied about my relation to the entire living world. For these great insights I have to thank Mr. Barker and Mr. Sealey, my science teachers, who to this day I have not met anyone more inspiring. They were the ones who made me realize through years of science fair projects that I had the capacity, as we all do but most never find out, to create knowledge and not just study it.

Closer to the present I must thank my mentor, Dr. Kamp. Dr. Kamp gave me an unusual amount of freedom in the lab for reasons I cannot explain. He never stopped me from doing an experiment or pressured me to pursue one hypothesis over the other. He did not have the answers to my research troubles, of which there were many. When failure was commonplace, he was calm. During those brief moments of excitement in the lab, he remained calm. I learned from him that no one has the answers I seek. If I want to know something, I had to conduct an experiment (I had to ask nature). If I conducted a clear, carefully crafted experiment, I would receive a clear and carefully crafted answer. If I asked too many questions at once, or a series of open-ended questions, then the response was likewise and I did not learn anything. I realized

this truth during my 5 years of wandering in the unknown. Dr. Kamp allowed me to wander, and for that I am grateful.

To the fellow graduate student in Dr. Kamp's lab, Pratik Lalit, with whom I shared many late nights culturing cells and writing grants, and who perhaps at this moment is still doing experiments somewhere, I must also thank. We struggled through countless ambiguous experiments, forced ourselves to stay awake during unusually long lab meetings and seminars, and laughed at the peculiarities of other professors and post-docs. I hope our paths cross again.

I am a lucky man to have met my companion and partner, Aurelia Faure, in Dr. Kamp's lab, in the basement of the Medical Sciences Center. She was a visiting student from France in 2011, we became close, and decided upon her return to France that she should apply to graduate school to be in Madison. With more luck she was accepted for the coming year, and I made trips to France until then. There is much to be thankful for, thanks that will take a lifetime to express.

Finally, I have to thank you, the reader. The circumstance of arriving at this thesis I am not privileged to, but just know you are now part of an exclusive club. I am well aware that most of the text and figures beyond this acknowledgements section will go unread, or at the most flipped through for color images. Here's the gist to save you the time. There is a deficit of golgi-based protein glycosylation in human cardiomyocytes that lack lysosomal resident acid α-glucosidase enzymatic activity (manifests infantile-onset Pompe disease). It has taken me 5 years to write that one statement, but that statement is truth. That is, until someone provides evidence to the contrary, but until that time comes that statement stands as my one contribution to humanity's never ending quest for the truth. Veritas. May there be many more truths to be had, both in the lab and in life. Thank you.

Kunil Raval

On the Mechanisms of Cardiomyopathy in a Human Induced Pluripotent Stem Cell-derived cardiomyocyte model of Infantile-Onset Pompe Disease

Kunil K. Raval

Under the supervision of Timothy J. Kamp, Professor of Medicine

At the University of Wisconsin-Madison

ABSTRACT

Infantile onset Pompe disease, caused by the loss of lysosomal glycogen hydrolyzing enzyme acid α-glucosidase (GAA) activity, presents with a hypertrophic cardiomyopathy at birth. Without enzyme replacement, death occurs within 1 year of life. We have evaluated the leading hypotheses of contractile insufficiency and autophagic dysfunction as mechanisms of Pompe cardiomyopathy in a human induced pluripotent stem (iPS) cell derived cardiomyocyte (iPSC-CM) model. Pompe patient skin fibroblasts were reprogrammed into iPS cells and differentiated into cardiomyocytes that have undetectable GAA activity and pathognomonic glycogen-filled lysosomes. The iPSC-CMs were combined with a fibrin scaffold to make strips of engineered cardiac tissue (ECT). Pompe and Control ECTs had no consistent differences in contractile force or kinetics. Autophagic function was measured through inhibition and then re-establishment of lysosomal activity. Control and Pompe iPSC-CMs demonstrated no remarkable differences in autophagosomal clearance. Higher electrophoretic mobilities of protein-sodium dodecyl sulfate complexes and more basic isoelectric points were noticed in the lysosomal associated membrane proteins (LAMPs) from Pompe compared to control iPSC-CMs. We determined that these lighter and more basic LAMPs lacked golgi modification, which typically include poly-N-acetyllactosamine and sialic acids, that could be partially reproduced in Control iPSC-CMs through destruction of the golgi apparatus. No abnormalities in golgi structure were observed in Pompe iPSC-CMs. Therefore, we have identified an unknown deficit in golgi-based glycosylation that may contribute to Pompe cardiomyopathy through mechanisms shared by the congenital disorders of glycosylation or LAMP2 deficiency (Danon Disease), both of which have cardiac phenotypes similar to Pompe disease.

CHAPTER 1: An Introduction to Pompe Disease

Portrait of Dr. Pompe by Christa Loonen (1)

Johnanne Cassianus Pompe was a Dutch physician born in 1901 and lived during the most unfortunate time in Europe. In competition with the Germans, he and the medical staff in Holland were in a race to publish on a novel class of diseases called the glycogen storage disorders (GSD) so that a Dutch name would be represented amongst the German ones, such as Von Gierke's disease (GSD Type I). An opportunity arrived in 1930, when Dr. Pompe was responsible for the post-morten analysis of an infant girl with the disease that would soon bear his name. His paper (2) in 1932, titled "Over idiopathische hypertrophie van het hart" (about the idiopathic hypertrophy of the heart), described a vacuolar myopathy with glycogen accumulation from histologic sections of the patient's myocardium. The disease was a new one, and rightfully named Pompe disease, or GSD Type II.

Events turned for the worst in his native Holland during Nazi occupation. Dr. Pompe enlisted in the army as a physician and after defeat joined the Dutch resistance. He made use of his underground laboratory, unknown to the occupiers, to shelter Jewish peoples and transmit short wave radio signals meant for the UK on intelligence gathered in the streets. During the last days of the war the Nazi's found his laboratory, he was judged guilty of espionage, and was executed by firing squad on April 14, 1945 (1).

I. GENETIC AND BIOCHEMICAL ETIOLOGY OF POMPE DISEASE

Infantile-onset Pompe disease is a lysosomal and glycogen storage disorder caused by the loss of acid α-glucosidase (GAA) enzymatic activity. This enzyme is responsible for the hydrolysis of glycogen into free glucose within the acidic environment of the lysosome (3). The catalytic process is depicted in the reaction below.

$$\text{Glycogen (glucose)}_n \xrightarrow[\text{GAA}]{\text{Lysosome, pH 4}} \text{n(glucose)}$$

Without the ability to digest glycogen into glucose, the lysosomes gradually accumulate glycogen, become enlarged beyond a normal diameter, and occupy the cytoplasm of all cell types as a glycogen-filled lysosome. Image 1 below depicts an electron micrograph of diseased lysosomes residing in skeletal myocytes from the soleus muscle of an infantile-onset Pompe patient (4).

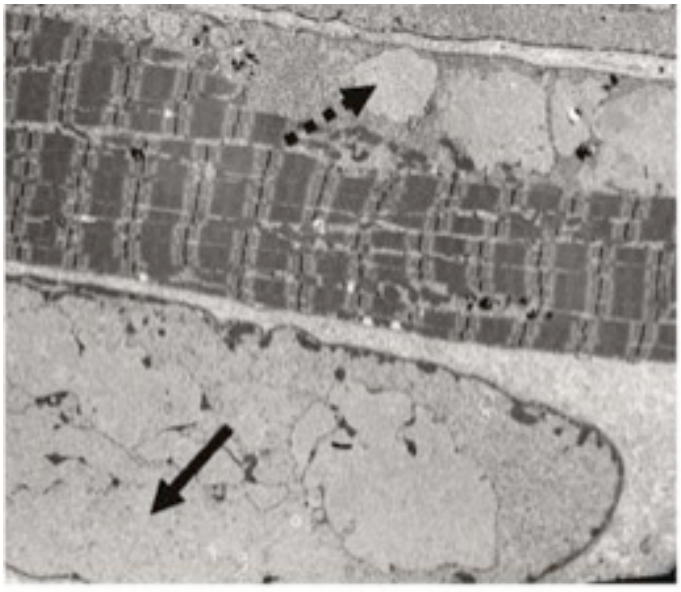

Image 1 Glycogen-filled lysosomes within skeletal myocytes biopsied from a patient with infantile-onset Pompe disease. The arrows point to glycogen engorged lysosomes. The top myocyte demonstrates the progressive replacement of contractile elements (repetitive structures

of the sarcomere) with enlarged lysosomes. The bottom myocytes reveals complete absence of contractile protein and in its place glycogen filled lysosomes and free cytoplasmic glycogen.

Glycogen accumulates in all lysosomes of all cell types, however, the striated muscles of the skeletal and cardiac type are most affected both in structure and function (5). A clear explanation for why the skeletal and cardiac muscle are primary targets of pathology is to be desired, but the thought is these cell types are the most reliant on their intracellular organization for function that is easily disrupted by the existence of large, randomly placed, abnormal structures. Other cell types that are crudely described as "bags of organelles and proteins" are not as sensitive to the disorganization of cellular structures (6). For example, the distances and orientation between the sarcoplasmic reticulum (SR) responsible for calcium cycling, the sarcomere that relies on calcium cycling for signals to contract and relax, and the mitochondria that provides energy to both the sarcomere and the SR is tightly controlled. Placement of glycogen-filled lysosomes anywhere would slow the diffusion of Ca^{2+}, ATP, or O_2 (7), compromising contractile function (8,9). Other cell types, such as a hepatocyte, also have a busy cytoplasm, but the precise relative location of organelles and protein complexes is not as essential for its catalytic and synthesis responsibilities.

The physical presence of the lysosome does interfere with contractile function by mis-aligning the direction of the sarcomeric arrays (10). Therefore, if we represent one sarcomere as a vector, the maximum amount of force produced would occur if all vectors were pointing in the same direction. With non-contractile elements (glycogen-filled lysosomes) sandwiched between sarcomeric arrays, each vector will now have a component in other dimensions, thereby reducing the magnitude in any single dimension. Moreover, an enlarged lysosome pushing against an adjacent sarcomere will lengthen the distance between 2 Z-lines. In response, a sarcomere

further away will shorten (distance between 2 Z-lines will decrease) to accommodate the lengthening of the other, since total length of all sarcomeres is constant. The force produced by a single sarcomere is partly dependent on the overlap of actin-myosin filaments in the resting state. Therefore, upon contraction in muscle with non-contractile inclusions, each sarcomere will produce a different amount of force depending on its relation to the glycogen-filled lysosome. This will not only reduce the total force production, but it will introduce internal stresses that will tear the muscle apart – a sarcomere that is contracting with more force than it's neighbor will pull its neighbor away from its usual location (there will be a non-equilibrium).

The non-contractile inclusion model predicted a 6% loss of force as a result of disturbed sarcomeric arrangement and lengths, closely matching the force loss in the early stages of Pompe disease of 7% compared to healthy muscle. Therefore, during the early stages of disease, the buildup of glycogen-filled lysosomes accounts for skeletal muscle force loss per unit muscle mass. However, Pompe muscle also experiences wasting – a loss of total muscle mass – and as the disease progresses the amount of force loss per unit muscle mass drops to 50% that of normal muscle (11). Thus, other pathologic factors are accountable.

To address the inconsistencies of the model above in explaining the additional loss of muscle force during later stages of Pompe disease, the authors of (12) measured force from skinned fibers from the Pompe mouse model. By skinning the fibers, they were examining only the actin-myosin interaction, independent of the cell's calcium cycling machinery or energy status. The force of Pompe skinned fibers was approximately 50% that of healthy fibers, indicating that there was a disruption of sarcomeric arrangement. X-ray diffraction of myofilaments revealed a loss of the normal hexagonal organization of 6 actin filaments surrounding a central myosin filament. More specifically, the fraction of myosin filaments

within binding range of actin in the relaxed state was reduced by ≈ 50%, implying that during contraction, 50% of the myosin heads would not form cross-bridges with actin even though the myosin ATPase was actively cycling ATP.

To summarize so far, during the initial stages of Pompe myopathy non-contractile inclusions occupy regions between sarcomeres, disrupting their organization and lengths resulting in a 5-7% loss of force per unit muscle mass. Over time, the total muscle mass in Pompe disease decreases and the existing muscle produces 50% less force normalized to muscle content compared to healthy control myofibers. Two questions exist: 1) what is causing the loss of muscle mass and 2) what is the cause of disturbed actin-myosin arrangement? Earlier in the introduction, I mentioned the contractile proteins were being "replaced" by glycogen-filled lysosomes (13) as was evident in the electron micrograph of image 1. What is causing the "replacement" that defines atrophy? For answers we must first have a background on autophagy.

Autophagy, or "self-eating" from the Greek, is the process whereby intracellular constituents such as organelles and proteins are recycled into their monomeric components (14). For example, a mitochondria that has passed its prime (>2 weeks old) will be degraded into its lipid, amino acid, and carbohydrate components by the hydrolytic enzymes contained in the acidic lumen of the lysosomes (15). How the mitochondria (and other entities destined for lysosomal degradation) enter the lysosome is the key to understanding how and why glycogen ends up in the lysosome. The mitochondria being targeted for degradation is enclosed by a membrane called the autophagosome. The autophagosome can be considered the "trash-bag" in the autophagic process (16). The autophagosome then fuses with the lysosome, releasing all the materials enveloped to the action of the lysosomal hydrolases. Once digested, the monomers are released back into the cytoplasm for use as building blocks or as energy substrates.

Autophagy is the process by which glycogen enters the lysosome. Glycogen is a ubiquitous, ancient polymer that evolved to fulfill the role for glucose storage exclusively in eukaryotes. To store glucose in it's monomeric form would burden the cell with an osmolarity incompatible with life. However, with glycogen, approximately 30,000 glucose molecules can be stored at 1 molecule of glycogen; the osmolarity of glycogen is 1/30000 that of an equivalent amount of glucose. Therefore, glycogen is present in the cytoplasm of all eukaryotic cells (17).

Since glycogen is ubiquitous in the cytoplasm, the process of surrounding the mitochondria also includes nearby glycogen particles that are enclosed non-specifically. These glycogen particles then find themselves in the lysosome, with the only escape being through hydrolysis back to glucose and exit via glucose transporters. Since GAA is the sole enzyme responsible for degrading glycogen in the lysosome, the absence of this enzyme will result in stagnant glycogen particles in the lysosome (18).

Fusion of autophagosomes with the lysosome is not the only process by which glycogen entry is facilitiated (19,20). Dr. Raben and collegues have shown that when the autophagosome-lysosome fusion process is inhibited – the fusion being referred to as macro-autophagy – glycogen still enters and remains in the lysosome of cultured myotubes derived from Pompe mouse muscle. Therefore, glycogen is thought to also enter the lysosome via the process of micro-autophagy, or the endocytosis of glycogen directly by the lysosome.

Why the lysosome would endocytose glycogen is under debate, however, two hypotheses are being considered. One is based on the non-specific engulfment of glycogen concomitant with the specific endocytosis of proteins marked for degradation (via ubiquitin, for example). The other postulates a role of the lysosome in glycogen metabolism. That is, the lysosome specifically takes in glycogen for degradation into glucose and release back into the cytoplasm.

Some have calculated that approximately 10% of all glycogen is degraded by the lysosome, with the other 90% being digested by phosphorylase in the cytoplasm (21). However, I think the second hypothesis represents an inefficient process. If the cell requires glucose for fuel (glycolysis) or for the pentose phosphate pathway, it first has to be phosphorylated. The enzyme phosphorylase degrades glycogen to glucose-1-phosphate with no ATP necessary. When the lysosome degrades glycogen it releases free glucose, which requires phosphorylation via hexokinase with consumption of ATP. Therefore, it seems unlikely that the lysosome would be responsible for supplying glucose for energy or as a substrate on purpose (an evolved function), since there is a far more energetically efficient manner to do so. Fortunately, to understand Pompe disease we only need to know that glycogen does enter the lysosome and needs to escape by being converted back into glucose monomers.

The mechanistic link between lysosomal glycogen accumulation and Pompe pathology is in the extensive literature on autophagic dysfunction in Pompe disease published primarily by Dr. Nina Raben at the NIH with her mouse model and access to patient muscle biopsies. We had described previously the process of autophagy as a mechanism by which glycogen enters the lysosome. From histologic analysis of Pompe muscle tissue, large regions of cellular debris, autophagosomes, and lysosomes with partially digested materials exist within the core of type II (glycolytic fibers) (19). Immunoblots from type II Pompe fibers also reveals enormous ubiquitinated protein accumulation. Surprisingly, such autophagic build-up is absent from oxidative type I fibers and in the heart where lysosomal glycogen accumulation predominates (22-24). It should be mentioned that the skinned myofiber studies above were performed on psoas muscle, which in the mouse is >90% glycolytic type II.

Glycogen-filled lysosomes have been shown to have a neutralized lumen at pH 7, meaning that all the hydrolases are non-functional (25). Therefore, the hypothesis was forwarded that as glycogen accumulates, lysosomal function is compromised, resulting in autophagic buildup that includes toxic protein aggregates, ubiquitinated proteins, old mitochondria that spew oxidative radicals, and overall cellular malaise (26). The reason for specificity to the type II fibers in the mouse was accounted for by the overall higher amount of cytoplasmic glycogen in these tissues, due to their reliance of glycolysis for fuel. Type I fibers, having limited glycogen stores would perhaps take longer for lysosomes to concentrate glycogen and therefore manifest pathology. In human muscle samples, the autophagic debris is not limited to type II fibers; autophagosomal buildup does not discriminate between fiber types, suggesting that differences in pathologic mechanisms exist between mouse and human Pompe disease (27,28).

The presence of overwhelming toxic material and mitochondria on the verge of collapse is thought to result in myofiber atrophy through necrotic/apoptotic pathways. It was further hypothesized that the non-specific association of misfolded proteins or their degradation products with actin and myosin could be the mechanism for the loss of hexagonal architecture required for force production in the full capacity (12). If the hypothesis is that the diseased lysosomes with glycogen are non-functional and therefore cannot facilitate autophagy, then one should be able to measure the rate of autophagosomal consumption by the lysosomal system in skeletal myocytes and show that the rate is lower in the Pompe group.

To study autophagic flux, researchers rely on the reporter protein microtubule-associated light chain 3 (LC3). LC3 is synthesized in a soluble cytoplasmic form called LC3I by the ribosome. Upon autophagosomal membrane formation, LC3I is lipidated with

phosphatidylethanolamine and anchors itself in the autophagosome (AP) membrane. The amount of LC3II protein, which can be quantified via immunoblot because of its higher electrophoretic mobility over LC3I, is representative of the AP content of a cell population (29).

Indeed, LC3II levels are dramatically higher in skeletal muscle biopsies from Pompe patients, indicating that either the rate of AP formation is elevated or the rate of consumption is hindered. However, when myoblasts were isolated from the same muscle that exhibited higher LC3II levels, myotubes differentiated from those myoblasts in culture had LC3II levels equivalent to controls (28). Another reference (25) also indicated that Pompe myotubes from the mouse model, although exhibiting glycogen-filled lysosomes, do not present with autophagic accumulations as is observed in vivo. Measurements of flux in the isolated in vitro Pompe lysosomal system were not attempted.

The fact that the autophagic buildup vanishes in vitro is of value. As mentioned above, the higher LC3II levels could be due either a higher level of AP formation or slower AP consumption (or both). By showing that LC3II levels are normal in vitro implies that the lysosomal system in Pompe myotubes is adequate to handle the APs being formed in the culture dish. One can easily induce temporary AP buildup in healthy cells via nutrient starvation, either by removing glucose from the media or by starving animals (30,31). One of the primary functions of autophagy is to provide fuel to maintain homeostasis in times of famine – the fuel is provided by degradation of non-vital proteins and lipid membranes into fatty acids for the TCA cycle and amino acids for gluconeogenesis. Perhaps the rate of AP production is increased in Pompe myocytes in vivo due to a yet unknown stressor that is not being reproduced in culture. Although some lysosomes are neutralized, there may be a sufficient population of functional

lysosomes to maintain AP degradation at a normal rate. That rate, however, may not be adequate in the environment of AP production that exists in vivo.

If autophagic dysfunction were the source of Pompe skeletal muscle pathology, then slowing autophagy down or inhibiting it all together should restore force production. Such an experiment has been conducted by preventing AP formation all together (19), however, the muscle of both Pompe and healthy mice undergoes atrophy and destruction at a faster rate than what is seen in autophagy-intact Pompe mice. By suppressing glycogen synthesis activity via knockout of glycogen synthase protein (32), Pompe mice that survived gestation and birth manifested no classic Pompe pathology. Therefore, beyond the loss of GAA resulting in glycogen-filled lysosomes, further downstream pathology remains ill-defined with autophagy being a suspect. The fact that the myocardium in the Pompe mouse lacks any evidence of AP accumulation in the environment of enormous amounts of lysosomal glycogen accumulation further diminishes our confidence that the lysosomal system is malfunctioning because of the incompetence of glycogen-filled lysosomes.

Let us assume then that the autophagic accumulation observed in skeletal muscle of mouse and humans with Pompe disease is a reactive mechanism to the true pathology, not the provoking pathology itself. Research from the Genzyme corporation, the manufacturers of recombinant GAA used in the treatment of Pompe disease (to be discussed later), shows that the rate of glycogen synthesis in a variety of tissues from the Pompe mouse model are dramatically higher while the rates of glycogen breakdown via glycogen phosphorylase activity are reduced (33). For example, the in vitro activity of glycogen synthase from the Pompe heart was approximately 10-fold higher per milligram total protein. In skeletal muscle there was a 2-4 fold reduction in AMP dependent phosphorylase activity. In heart, skeletal muscle, and liver, the

amount of glycogen synthase protein was significantly elevated. All together, the Pompe mouse seems to be in an anabolic state, with free glucose preferentially being stored as glycogen rather than being used as fuel or as a synthetic substrate (for nucleotide sugars used for post-translational glycosylation, or shuttled to the pentose-phosphate pathway). Levels of the glucose transporter GLUT4, glycogen 6-phospate (G6P), and hexokinase activity were also elevated in the cardiac and skeletal muscle of Pompe mice, further promoting the imbalance between glycogen synthesis and breakdown. The fold changes this paper reports – such as the 20-fold increase in G6P in Pompe skeletal muscle – may indicate that the amount of glycogen in the lysosome has a signaling function and/or lysosomal glycogen degradation is important in overall glycogen metabolism. Why sensing an overload of glycogen in the lysosome would promote even more glycogen synthesis seems counterintuitive. How elevated glycogen synthesis leads to autophagic accumulation may occur via independent sensing of low ATP/ADP ratios, due to the lack of glycogen breakdown into glucose. If the cell is sensing a low energy state it may be triggering the starvation response and upregulating autophagy. However, glycogen synthesis/breakdown and ATP/ADP ratios are linked via the AMP sensor AMP kinase. Usually in situations of low ATP, AMP kinase will stimulate the entry of glucose into the cell and inhibit anabolic processes such as glycogen synthesis (34). However, if ATP levels are normal and glucose is still being imported due to constitutively activating mutation in AMP kinase, then glycogen synthesis occurs, probably due to excessive glucose without a need for ATP (35). It seems like two opposing processes are occurring in the Pompe myocytes. The higher influx of glucose into the cell indicates the cell is in need of energy substrate – the internal supply of glucose is not sufficient. However, the imported glucose is not being used for fue because energy status is fine – instead, it is being marked for glycogen synthesis, similar to AMP kinase

mutations causing glycogen storage disease mimicking hypertrophic cardiomyopathy. The cell, therefore, is in a perpetual state of unnecessary glucose import and therefore stores all that glucose as glycogen. Unfortunately, that paper (33) did not measure AMP kinase activation, calculate the ATP/ADP/AMP status, or look at insulin levels that could also be forcing glucose entry and glycogen synthesis.

To summarize our mechanistic understanding, infantile-onset Pompe disease begins with mutations in the GAA allele that result in zero enzymatic activity. The loss of the enzyme's function results in the inability of lysosomes to hydrolyze glycogen into glucose. Lysosomes increase in size as they fill with undigested glycogen. In consequence these diseased lysosomes disrupt sarcomeric structure by physically pushing on the myofilaments as non-contractile inclusions. Another consequence glycogen accumulation in the lysosome is the loss of acidity, rendering the resident acid hydrolases inactive. Wether or not the incompetence of the glycogen-filled lysosomes results in global autophagic dysfunction is still under debate, however, we do know that autophagosomal buildup does occur in Pompe skeletal muscle. In addition, we observe skeletal myofiber atrophy (loss of contractile proteins) and a disorganization of the actin-myosin hexagonal arrangement. Glycogen metabolism is also abnormal with an enormous increase in glycogen synthesis, glucose uptake, and diminished glycogen breakdown. How the malfunctioning glycogen metabolism relates, if at all, to autophagic accumulation requires further investigation.

One will notice from searches in the literature that the majority of mechanistic work has been discovered in Pompe skeletal muscle rather than in the heart. The reasons are 2-fold. The first requires an overview of the current treatment method for infantile Pompe patients. Based on the etiology being the loss of GAA activity, the logical therapeutic would be the intravenous

administration of recombinant human GAA (rhGAA) that has the correct targeting motifs (glycosylations, signaling peptides) to enter first the cell and then the lysosome (36).

The rhGAA produced by the Genzyme corporation, now a subsidiary of Sanofi, is very effective at reversing the glycogen accumulation and hypertrophic cardiomyopathy of the Pompe heart if treatment begins before 5 months of age (37). Continuous treatment suppresses all cardiac pathology indefinitely with the first patients ever administered now in their late teenage years without heart complication. Beyond 5-months of age systolic function declines into congestive heart failure where secondary pathology (edema, valve/outflow track malfunction, localized ischemia, inflammatory response) becomes irreversible. In addition, if treatment begins too late as the immune system becomes more competent, antibodies will be created towards the rhGAA and huge amounts of the drug will be needed to over-ride antibody inactivation.

The skeletal muscle, on the other hand, responds poorly to rhGAA treatment over time. Patients will experience an initial resolution of musculoskeletal symptoms, however muscle contractile function will then decline and exist in a perpetual state incompatible with an independent lifestyle (feeding, moving, breathing without assistance). Researchers find that the rhGAA does enter muscle cells, but is eventually trapped in an endocytic vesicle waiting to reach the lysosome. The endocytic (materials gathered from outside the cell) and autophagic (materials gathered from inside the cell) systems converge on the lysosome for recycling. Therefore, the thought is autophagic backup creates a sort of “traffic jam” where materials destined for the lysosome, such as rhGAA that has been endocytosed, never make it there or are slow to reach the destination. Fortunately, there are methods being commercialized for humans to target rHGAA for direct uptake by the lysosome, thereby bypassing the endocytic system.

Thus, patients have much more to benefit from a greater understanding of autophagic dysfunction in skeletal muscle than investigations of the heart, which responds perfectly to rhGAA.

The second reason for greater interest in Pompe skeletal muscle pathology follows from the disease's natural history, alluded to above. There is actually a spectrum of Pompe disease, categorized based on the age of onset. The form focused on in this thesis is the infantile-onset form, caused by a *complete* loss of GAA activity. If GAA activity is present below the threshold for normal biology to proceed but above 0, then patients will present later in life with age of onset directly correlated with level of residual activity (the higher the activity, the later the age of initial presentation). These late-onset cases always manifest with skeletal muscle weakness, as this is the reason patients seek out a doctor. The cardiac phenotype ubiquitous in the infantile form is very rare in late onset form (38).

In infantile-onset Pompe disease, patients are born with a hypertrophic cardiomyopathy but this diagnosis is not immediately recorded as the patient appears healthy at birth without need of a chest x-ray. However, during the first month of life the caretaker (usually the mother) will notice that the infant does not feed well and is unable to move arms or legs against any force. When held in the supine position, the limbs will dangle with no ability to raise them – this observation is known as "floppy baby syndrome". Soon after and the immediate reason for a revisit to the hospital is the onset of respiratory distress. The baby will breathe as if short-of-breath and struggle with inhaling such that the accessory muscle of respiration in the neck will become prominent with every cycle. If left untreated the infant will die within a month due to the inability to breathe or eat and if given respiratory support and nutrition, death will occur within 1-year due to congestive heart failure (CHF)(39). Therefore, the skeletal muscle

pathology is the more pressing issue when confronted with the infantile-form as it will lead to death earlier than the cardiac dysfunction, which takes time to manifest. There are exceptions, however. Early outflow tract obstruction, which occurs where the hypertrophic heart physically blocks the exit of blood into the aorta upon systole, can lead to early death due to the rapid onset of CHF(40).

Mechanistic knowledge of Pompe skeletal muscle pathology has brought renewed interest in explaining Pompe cardiomyopathy because of their differences. Whereas weakness and autophagic accumulation are hallmarks of the skeletal muscle, no reports of contractile insufficiency or accumulations of APs have been reported in the heart (24). True, the heart does go into failure late in the natural history, but there is extensive remodeling to a dilated state by this time, blurring the distinction between myofiber and structural (shape of the heart) deficits. There is a distinction between the skeletal and cardiac muscle reaction to the absence of GAA activity; the origin of that dichotomy is worthy of inquiry.

Although both human and mouse Pompe muscle display the similar pathologies of weakness and autophagic accumulation, there are as mentioned above key differences that allude to divergent mechanisms based on the species under study. While AP and ubiquitinated protein accumulation is seen exclusively in the fast twitch glycolytic type II muscle, both the slow type I and fast-twitch type II muscles in humans are equally affect by autophagic dysfunction. Therefore, for the sake of understanding the Pompe cardiomyopathy in humans, we decided to use human cardiomyocytes afflicted by Pompe disease to avoid confounding differences in mouse and human pathology.

Disease Modeling with Induced Pluripotent Stem Cell-Derived Cardiomyocytes

Immediately following the publication that human fibroblasts could be reprogrammed into induced pluripotent stem (iPS) cells via expression of 4 transcription factors (41,42) that control gene expression in the pluripotent state, many scientists predicted the immediate value of such cells would first be realized in the ability to model patient-specific diseases in difficult to obtain tissues (brain, heart) well before their clinical use as sources of regenerative tissue (43).

The first iPS cell derived cardiomyocyte model (iPSC-CM) was of LEOPARD syndrome (44), a rare, autosomal dominant multisystem disease caused by mutations in the PTPN11 gene that codes for SHP2 phosphatase. This enzyme is part of the RAS-mitogen-activated protein kinase signaling pathway that when inactive results in the constellation of syndromes that make up its acronym (lentigines, electrocardiographic abnormalities, ocular hypertelorism, pulmonary valve stenosis, abnormal genitalia, retardation of grown, and deafness). Although not included in the acronym, hypertrophic cardiomyopathy is a hallmark of the disease and, if death does occur the cardiomyopathy is usually to blame. As the first of its kind model, the paper focuses on characterizing the iPS cells by doing DNA fingerprinting, looking at the endogenous expression of reprogramming factors, methylation patterns at those reprogramming factor promoters, and genome wide changes in expression levels between the fibroblast and iPS cell state. Such extensive genetic characterization of the iPS cells is no longer standard protocol for iPSC-CM disease models. Instead, proof that the iPS cells are pluripotent and have a normal karyotype suffices. Pluripotency is assessed via formation of teratomas, a mass of tissue formed from cells that are allowed to differentiation without direction (45). The iPS cells are injected into the sub-dermal layer of immune-compromised mice and allowed to multiply and differentiate at random (most likely directed by local signaling). If, in the teratoma,

representative tissue of all 3 embryonic germ layers (endoderm, mesoderm, ectoderm) are found, then the iPS cell is deemed to have the capacity to differentiate into any somatic cell if given the correct signaling cues, earning the cell line in question the title of being true pluripotent stem cells. Giemsa (G)-band karyotyping, with Giemsa staining AT rich regions of the chromosome to create a light-dark banding pattern on condensed chromosomes, is able to reveal large translocations, duplications, or deletions that could arise during the reprogramming process, since such chromosomal abnormalities may provide selective growth advantages.

In the LEOPARD syndrome paper, cardiomyocyte differentiation was facilitated with embryoid body (EB) formation – or large spherical clusters of suspended cells – that once plated in culture dishes would form spontaneously contracting areas, a characteristic unique only to cardiomyocytes. The EB differentiation method is one borrowed from mouse ES cell literature, but when applied to human iPS cells gives low yields. At best, 1-2% of EBs from iPS cells contains contracting areas with the process first having to be optimized through testing the differentiation protocol with different lots of fetal bovine serum (FBS). The whole process is very undefined, but at the time that method was sufficient. Isolated contracting areas were plated as single cells for study with the author reporting that LEOPARD iPSC-CMs had on average a larger surface area and a higher percentage of cells with Nuclear factor of activated T-cells (NFAT) translocated into the nucleus. The NFAT transcription factor is known to turn on genes associated with hypertrophic remodeling, thus, the authors conclude that the model is capable of recapitulating at least some aspects of the cardiomyopathy observed in patients (46).

Dilated cardiomyopathy caused by mis-sense mutations in troponin T, a structural protein in the troponin complex that regulates calcium signaling for the actin-myosin interaction, is an example of the next phase in iPSC-CM disease modeling (47). In this model the authors

demonstrate that iPSC-CMs originating from DCM patient fibroblasts have disorganized myofilaments and lower amplitudes of calcium cycling that culminates in reduced force generation measured with atomic force microscopy. The phenotype is exacerbated when exposed to a long-term β adrenergic stimulus. Due to the need for greater quantities of iPSC-CMs, the authors use the EB method of differentiation and then sort cells based on the surface expression of cardiomyocyte progenitor markers. Culture of the progenitors gives higher yields and purities of CMs once differentiation is complete. As predicted, the paper does not spend enormous resources characterizing the iPS cells; a teratoma assay and G-band karyograms are presented instead. In comparison with the LEOPARD model, the DCM model advances the field by showing that contractile dysfunction, both in calcium handling and force production, can be modeled with iPSC-CMs. The authors also corrected the phenotype by applying a known treatment being developed in the mouse model of the same DCM. By overexpressing the sarcoplasmic reticulum calcium reuptake protein SERCA2, the DCM iPSC-CMs had a correction of phenotype with calcium transients, sarcomere organization, and absolute force resembling that of the healthy controls. Although the relationship between cTnT mutation and weak contractility was not studied beyond the insight into reduced calcium transient amplitude, the entire process linking the genotype-to-phenotype is being recapitulated. It will be interesting to see if these authors or someone else in the field takes this model one step further by discovering something new about the disease, or if publishing the initial model was an end in itself. Likewise for the LEOPARD syndrome model.

The most recent evolution of iPSC-CM disease modeling I had the opportunity to write a review for publication in Nature Medicine (48,49). Barth syndrome is a rare X-linked genetic disorder caused by mutations in the tafazzin (*TAZ*) gene that results in dilated cardiomyopathy,

skeletal myopathy, and neutropenia. Tafazzin has a mitochondrial function, and this study using human Barth syndrome iPSC-derived cardiomyocytes identifies increased mitochondrial reactive oxygen species (ROS) as a key intermediate causing cardiac contractile dysfunction.

In the early 1980s, Dutch physician Peter Barth reported a family with an extensive history of male infants presenting with dilated cardiomyopathy, neutropenia, and skeletal myopathy (50), the majority of which succumbed to combined infection and heart failure within a year after birth. Subsequent studies have demonstrated that Barth syndrome is an X-linked monogenic disease caused by mutations in tafazzin (*TAZ*) (51), an acyltransferase essential in the modification of cardiolipin (CL), a key phospholipid enriched in mitochondrial inner membranes. Thus, mutations in *TAZ* provide an obvious link to mitochondrial abnormalities, but the precise mechanisms leading to pathology such as cardiomyopathy are not well understood. Therefore, iPSCs were generated from two Barth syndrome patients harboring distinct mutations in *TAZ* to identify ROS production as an intermediate in the pathophysiology of Barth syndrome.

Wang *et al* first differentiated iPSCs derived from the two Barth syndrome patients into cardiomyocytes (termed iPSC-CMs) and demonstrated that they exhibited the impaired cardiolipin acylation diagnostic of Barth syndrome. Mature cardiolipin is known to have a role in the functioning of oxidative phosphorylation by stabilizing the electron transport chain (ETC) super complex and also in trapping protons on either side of the mitochondrial membrane. Compared to controls, Barth syndrome iPSC-CMs had a proton leak across the inner membrane and a reduced efficiency of the F_1F_0 ATP synthase resulting in an increased basal O_2 consumption, and ultimately a depleted ATP pool.

A feature identified in pathological samples from Barth syndrome cardiac tissue is myofilament disarray. To be able to directly compare the effects of *TAZ* mutations on sarcomeric

structure in the iPSC-CMs, the paper shows quantification of sarcomeric organization in single cells seeded on micropatterned fibronectin rectangles that mimic the structure and dimensions of adult heart cardiomyocytes. Intriguingly, they observed a significant decrease in organization in the sarcomeres in the disease line with a *TAZ* frame-shift mutation, but the sarcomeres had normal structure in the disease line with a missense mutation. Therefore, this disease model is the first to acknowledge a patient-specific difference in phenotype due to a monogenic disorder.

To test for contractile deficits known to be part of the pathophysiology of Barth's syndrome, the authors used their previously published heart-on-chip technology (52). Both Barth syndrome iPSC-CM contractions were weaker than wild type cell lines, although there were differences in the characteristics of contractile dysfunction. Culture in glucose (all previous experiments were done in galactose containing media to promote oxidative phosphorylation) of the iPSC-CMs results in increased ATP levels by promotion of glycolysis; however, this did not improve force production in disease constructs, indicating that deficient mitochondrial ATP synthesis is not directly responsible for cardiac contractile deficits.

In perhaps the most important part of their study, the researchers used the iPSC-CM platform to test small molecule therapeutic interventions. Of the three interventions tested, linoleic acid, an essential unsaturated fatty acid precursor of mature CL, was most promising as it largely corrected the mitochondrial metabolic abnormalities and alleviated contractile dysfunction. They hypothesized that this might be because it encouraged an alternative cardiolipin synthesis pathway. However, they also thought that it might be able to scavenge mitochondrial reactive oxygen species; they were in fact able show that it curtailed mitochondrial ROS production which was found to be elevated in Barth Syndrome iPSC-CMs. In addition, the mitochondrial targeted antioxidant, mitoTEMPO, dramatically reversed the

observed contractile defects. Thus, this study clearly implicates mitochondrial derived ROS as a key intermediate linking the genetic defect to contractile dysfunction. However, translating this finding to patients may not be as straightforward as this application in tissue culture, but it is an important landmark in the search for better treatments.

Based on the data given in the study here, one obvious question for future study is the correlation of genotype with phenotype as potentially important differences were observed in the two different patient mutations studied, such as the different pattern of contractile dysfunction observed with the heart-on-chip assay. It would be interesting to know further clinical information regarding disease features in the patients sampled – it was noted that they were adult males, which suggests a milder phenotype. Perhaps the greatest impact of this work and model will be on advancing our understanding of mitochondrial and cardiolipin biology that is central to cardiac dysfunction seen in ischemic heart disease and aging mediated by ROS.

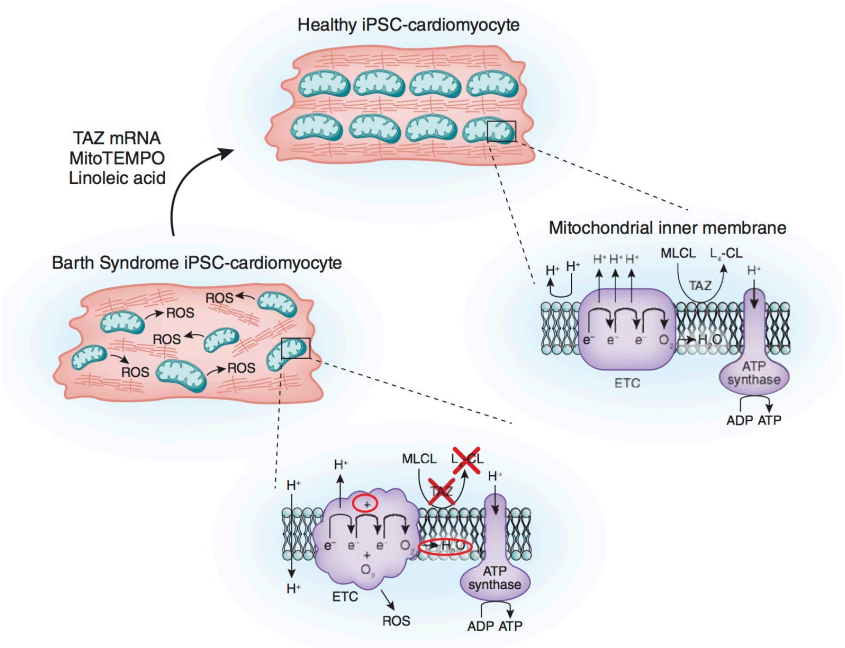

Image 2. Proposed pathophysiology of Barth syndrome cardiomyopathy revelaed by iPSC model. Healthy iPSC-CM have organized myofilaments and mitochondria with active transacylase tafazzin (TAZ) producing L_4-CL (mature cardiolipin) rich inner mitochondrial membrane with normal electron transport complex (ETC) and ATP synthase function. In contrast, a Barth syndrome iPSC-CM with mutant TAZ lack of L_4-CL leading to mitochondrial abnormalities with ETC complex malfunction and increased reactive oxygen species (ROS) production that contributes to myofilament disarray and contractile dysfunction. Modified mRNA (mod-RNA) encoding TAZ can rescue the disease phenotype as can buffering mitochondrial ROS with mitoTEMPO or providing a precursor for L_4-CL, linoleic acid.

In between the 3 iPSC-CM models above others were published and were of equivalent or lesser impact. One such model was of infantile-onset Pompe disease (53). The authors attempted standard reprogramming with Pompe patient skin fibroblasts but were not able to sub-culture any iPS colonies because cell death predominated. The only way they were able to make Pompe iPS cells was through the temporary expression of GAA during the reprogramming process and they equated the need for GAA to part of the diseases phenotype. Moreover, once reprogrammed, they noted that the Pompe iPS cells grew at a much slower rate and that when differentiated by using the EB method, the Pompe cardiomyocytes were only viable for 1 month. These findings may be artifacts of cell culture because they do not model the reality of the disease where normal development occurs in the expected time frame of gestation and following birth have functioning hearts until the end-stages of the disease.

The authors also investigated autophagy with qualitative immunostaining comparisons with LC3 and LAMP1 between healthy and Pompe iPSC-CMs. They presented one image where LC3 looked abundant in the Pompe iPSC-CM cytoplasm relative to a healthy cytoplasm

that had reduced fluorescence intensity. From the images the authors conclude that they have evidence of autophagic dysfunction, thereby confirming what has been noted in skeletal muscle from the mouse model and patients. The statements regarding autophagy are less than convincing. One can find images that suit opposing hypotheses and so rigorous quantification of multiple images or other semi-quantitative methods, such as western blots densitometry of LC3II – is necessary. In this research we address the issue of autophagy and provide evidence stronger than single images that autophagic dysfunction is not observed in the Pompe iPSC-CMs.

The authors then investigated differences in energy utilization based on the finding that mitochondria with abnormal appearance have been reported in patient muscle biopsies (54). Mitochondria from Pompe iPSC-CMs had a reduced basal oxygen consumption compared to control, however, treatment with rhGAA had no effect in correcting the deficit. Instead, treatment with L-carnitine had a subtle but statistically significant increase in oxygen consumption with the proposed mechanism that L-carnitine improves that transport of fatty acid substrates into the mitochondria for oxidation. Inhibiting the formation of autophagosomes also produced no effect on oxygen uptake, suggesting that the immediate deficit in Pompe disease may be related to glycogen metabolism and not to the presence of glycogen-filled lysosomes. Perhaps rhGAA was not administered for long enough (they treated for 21 days), or the set point of substrate utilization – glucose to fatty acid ratios – was permanently established during differentiation in the environment of glycogen accumulation. The authors should have treated with rhGAA during differentiation to see if the time of treatment would modulate oxygen handling.

Engineered Cardiac Tissue Models of Cardiomyopathy

Like the Barth syndrome iPSC-CM models, we are interested in using our Pompe iPSC-CMs to manufacture artificial tissue constructs with which to study contractile function. The Pompe heart maintains systolic function during the early stages of disease. The clinical description of Pompe cardiomyopathy is of LV wall and septum thickness at first presentation. Occasionally, hypertrophy is diagnosed in utero. Systolic function in a study of 40 patients was 100% preserved (LVEF > 40%) from 0-5 months of age but then declined as the natural history progressed. Another study also reported mostly normal ejection fractions and fractional shortenings of the LV in Pompe patients from 0-6 months of observation (37,39,55). Therefore, the functional decline of the Pompe heart occurs during the adverse remodeling phase towards the end, when the left ventricle dilates and because of its shape becomes inefficient at moving blood. Whether or not there is an intrinsic contractile deficit that ultimately leads to failure is unknown. One could hypothesize that the individual Pompe cardiomyocyte is fine, and that low blood O_2 levels as a result of weak respiratory muscles forces the heart to contract with more force to move the same amount of O_2 as fully oxygenated blood. The heart then hypertrophies in response to the increased work load and this is what we are observing and perhaps, wrongly attributing to glycogen accumulation.

If the hypertrophy is not a response to environmental stress, then there must be an intrinsic problem with the cardiac muscle that is causing it to increase in size. We look to the congenital hypertrophic cardiomyopathies (HCMs) for insight. These HCMs are caused by mutations of sarcomeric proteins that affect the ability of cardiomyocytes to contract (56,57). Then, in response to the abnormal contraction, the heart responds through hypertrophy as a compensatory mechanism for the deficits resulting from the malfunctioning sarcomeric protein.

For example, mutations in myosin binding protein C (MyBPC) is known to cause HCM, however, until recently the mechanism remained unknown because the mouse model hearts were studied after hypertrophy had all ready occurred within 10 days of birth. People knew that at birth the heart was of a normal size, but then rapidly remodeled to its pathologic form. The majority of studies focused on either the function of MyBPC in the sarcomere or a description of the changes in left ventricular structure and function during remodeling. How the underlying disruption of MyBPC translates to hypertrophy was not addressed.

The concept of a pre-hypertrophic model of MyBPC HCM is now helping to resolve the critical connection. In reference (58), neonatal cardiomyocytes isolated from newborn mice that produced no MyBPC protein were used to create engineered cardiac tissue (ECT) with which contractile force and kinetics of force generation and relaxation can be measured without hypertrophic signaling that would be present if the cells were allowed to continue developing in vivo. One can think of the cardiomyocytes in the ECT as existing in a developmentally suspended state. The main conclusion is that without MyBPC, contractile kinetic rates increase, meaning the rates of force generation and relaxation at any given contraction frequency are faster. However, the faster kinetics are not a direct result of faster calcium cycling kinetics, but rather from an increase in the probability that myosin-actin cross bridges will form once the troponin complex allows such an association to occur. The probability of their detachment also increases when the troponin complex shields actin from interacting with myosin. Although we now know the exact contractile pathology, how faster cross-bridge cycling kinetics can trigger hypertrophic remodeling remains unknown. Perhaps the faster cycling is being perceived by the heart as being in a state of increased demand, as is the case in hypertrophy due to hypertension or aortic valve stenosis.

IV. Conclusions

Sufficient background has been given to understand the early data presented in this thesis on the generation of iPS cells, characterization of the Pompe biochemical phenotype, differentiation into cardiomyocytes and the presence of glycogen filled lysosomes, the Pompe ECT model, and autophagy studies. However, other studies presented in this thesis dealing with post-translational glycosylation require a more specialized background and will be given in those chapters.

CHAPTER 2: Generation of the induced pluripotent stem cell derived cardiomyocyte model of infantile-onset Pompe disease

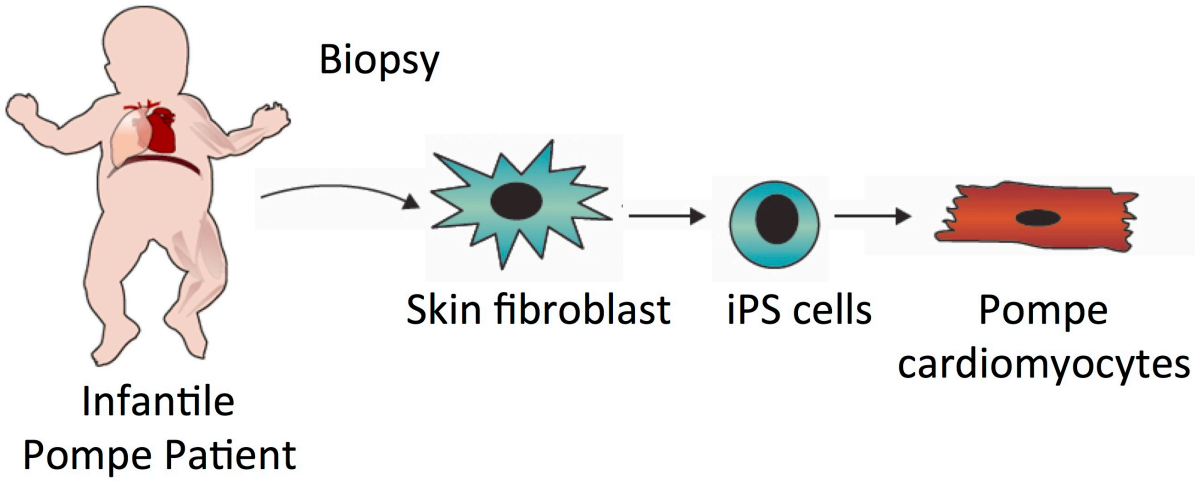

In this chapter we detail the events by which skin fibroblasts from patients with infantile-onset Pompe disease are reprogrammed into induced pluripotent stem cells and then differentiated into cardiomyocytes. Although the process and results are described in a scholarly, objective writing style, we ask that you step back from the text as a modern scientist and think about the awe someone from the past (pre-2006) would think about the first sentence. We are taking someone's skin cells and turning them into heart cells. Just as the nuclear physicists showed that transmutating the elements was possible (and not the realm of magicians), we biologists are also realizing that each cell, like each element, is the sum of its parts and those parts can be added and subtracted to convert one into the other.

Experimental Procedures

Generation of iPS cells from skin fibroblasts Pompe patient fibroblasts were obtained from the Coriell Institute for Medical Research. Information from each of the lines is presented in appendix IA, copied directly from the Coriell website. Details of the reprogramming methodology are given in reference (59). We worked with with Dr. Junying Yu and Dr. James Thomson, the first and senior author, respectively, on the initial human skin fibroblast-to-iPS cell reprogramming paper (41). We used the 6-factor protocol in reference (58) that adds KLF4 and cMYC to the original 4 factors (OCT4, NANOG, SOX2, LIN28) with traditional lentiviral integrating vectors to improve reprogramming efficiency above that of the original 4-factor protocol. Each iPS cell line is clonal – derived from a single cell.

Karyotyping of new iPS cell lines We used the Wisconsin Stem Cell institute (WiCell) fee-for-service cytogenetics facility for G-band karyotyping 4 passages following establishment of clonal iPS cell lines. We refer you to their facility for the details of the protocol. Each line was certified as karyotypically normal by a certified cytopathologist.

Teratoma assays with new iPS cell lines To form teratomas, 6-10 million iPS cells are injected subcutaneously between the shoulders on the back of female SCID-Beige mice. The mice are completely immune-incompetent. Following 6-8 weeks of growth the mice are sacrificed and the teratoma (lump of tissue) is excised, fixed with PFA, embedded in paraffin, sectioned at 8 microns, hydrated, and stained with haematoxylin and eosin. A certified pathologist assesses the tissue to identify representatives of the 3-embryonic germ layers. Again, we used the WiCell teratoma service for all steps in the protocol.

Standard iPS cell culture protocol Immediately after reprogramming and clonal cell line establishment, iPS cell were co-cultured with irradiated mouse embryonic fibroblasts (MEFs) fed

with DMEM/F12 + Serum Knockout Replacer with 100 ng/mL basic fibroblast growth factor (bFGF) to maintain the pluripotent state. After a few passages, cells were transferred to the MEF-free matrigel/TeSR culture system (60) and were maintained with this system indefinitely throughout all of the thesis work. Splitting was performed as single cells with 1 mM EDTA (Versene from Gibco) and 5 μM rho-associated kinase (ROCK) inhibitor (Y-27632) on the first day of re-platting. ROCK inhibitor aids in the survivial of single iPS cells.

Pluripotency Marker Immunostaining IPS cell cultures were grown to 60% confluence on glass coverslips, fixed with 10% Neutral Buffered Formalin (NBF), permeabilized with 1% triton X-100, blocked with 5% goat serum, incubated with anti-OCT4 and anti-SSEA4 at 4^{o}C overnight, incubated with an alexafluor conjugated secondary antibody, counter stained with DAPI, mounted on a glass slide with anti-fade, and visualized on an epifluorescence microscope.

Cardiomyocyte differentiation protocol Cardiomyocytes were differentiated from iPS cells by using a protocol developed on the UW Campus by Dr. Xiaojun Lian (61). The iPS cells were seeded at 0.5 million cells per well of a 12-well dish and allowed to grow for 4 days. On the 4th day the glycogen synthase kinase 3 inhibitor CHIR99021 (LC Laboratories) was added at 15 μM in RPMI/B27 without insulin and added at 1 mL/well. CHIR99021 was prepared in DMSO at a concentration of 75 mM so that 2 μL in 12 mL of media would produce a 12 μM solution. Using B27 without insulin is essential. The following day (exactly 24 hours later), the media was exchanged with fresh RPMI/B27 without insulin at 2 mL/well. Two days later (exactly 48 hours after media change, 3 days after the addition of CHIR99021), 1 mL/well in each well was extracted and mixed with an equal amount of fresh RPMI/B27 without insulin. 5 μM of the Wnt pathway inhibitor, IWP4 (Stemgent) was added from a stock of 5 mM in DMSO to the mixture of old and new media and added at 2 mL per well. 2 days later (5 days after initiation of

differentiation), the media was exchanged with fresh RPMI/B27 without insulin. 2 more days later (7 days after day 0 of differentiation), the media was exchanged with RPMI/B27 with insulin. Media was exchanged every 2 days with RPMI/B27 containing insulin until cells were ready for experimentation. Contracting cells were noticed anywhere from day 7 to day 15 (7 to 15 days after day 0 of the protocol, when CHIR99021 was added). Each cell line has to be optimized for differentiation with appropriate guidelines for optimization given in (62). Specific conditions were necessary for each of the lines of this thesis. For GM20089, cells had to be seeded at 2 million cells/well of a 12 well plate. For GM04912 and IMR90c4, 1 ug/mL of insulin was needed on day 0 to maintain cell survival.

Preparation of iPSC-CMs for downstream experimentation At 30 days following initiation of differentiation, cells were dissociated with 10x TryPLE (Gibco) as clumps and re-plated onto gelatin coated T75 flasks in DMEM/20% FBS for two days and then maintained for another 8 days in RPMI/B27. Cells were then dissociated as single cells with 10x TryPLE and either 1) used for engineered cardiac tissue (ECT) formation, 2) replated onto gelatin coated 12 well plates (first 2 days in DMEM/20% FBS followed by RPMI/B27) at 1 million cells/well for protein studies or 3) plated at a variety of densities on glass coverslips for immunocytochemistry. For electron microscopy, contracting regions were microdissected from original differentiation plates and re-plated on glass coverslips as 3D clusters. Following 10 days of culture, cardiomyocytes were ready for downstream experimentation.

IPSC-CM myofilament immunostaining IPSC-CMs on coverslips were fixed in 10% NBF, permeabilized in 1% triton x-100, blocked with 5% goat serum, and immunostained with anti-sarcomeric α-actinin (Sigma) overnight at 4^{o}C, incubated with an alexafluor conjugated

secondary antibody, stained with DAPI, preserved on a coverslip with antifade, and visualized with an epifluorescence scope.

Acid α-glucosidase mutational analysis Pompe line GM04912 (Pompe 2) gDNA, purified from iPS cells with DNeasy kit (Qiagen) was PCR amplified with primers in table 1 and Sanger sequenced. The exon 18 deletion of Pompe line GM20089 (Pompe 1) was amplified with primers in table 1 and the products were visualized on agarose gel. GoTaq green (Promega) was used for all reactions. Sanger sequencing involved cutting out the PCR products of interest from an agarose gel, purifying the DNA with a Qiaquick gel extraction kit (qiagen), running a Big Dye cycle sequencing reaction (applied biosystems) with purified template DNA and fluorescent NTPs, cleaning the reaction of all free fluorescent NTPs with a magnetic bead based protocol, and submiting purified DNA oligomers to the sequencing facility at the biotechnology center at UW-Madison.

Acid α-glucosidase enzymatic activity We measured GAA activity in iPS cells by incubating total cell protein lysates with a fluorophore conjugated glucose substrate that mimics the α1,4 glucose-glucose bond of glycogen that GAA has evolved to hydrolyze. The substrate is called 4-methylumbelliferyl-α-D-glucoside (4-MUG) and is hydrolyzed to release glucose and the fluorophore 4-methylumbelliferone (4-MU). When assayed at a pH of 4, the reaction is specific to GAA (only the lysosomal enzymes operate that this pH, and of those enzymes only GAA can cleave the glucose-glucose bonds of glycogen). When assayed at a pH of 7, the reaction still proceeds, but is catalyzed by the cytoplasmic form of GAA called neutral α-glucosidase (NGA). The reaction is performed in a 96-well all black plate and fluorescence is measured with the TECAN fluorescence plate reader. Details of the protocol are given in appendix I in a standard

operating protocol obtained from the Duke glycogen storage disease laboratories. The protocol is routinely used for clinical diagnosis of Pompe disease from patient skin fibroblast samples.

Acid α-glucosidase western blotting IPS cells were harvested by directly adding RIPA buffer to each well after being washed once with PBS (no Ca^{2+} or Mg^{2+}). Cells were transferred to a microfuge tube, sonicated, and then subjected to a methanol:chloroform:water biphasic extraction according to reference (63). Briefly, to 100 μL of protein lysates, 400 μL of MeOH, 200 μL of chloroform, and 300 μL of water were added and vortexed to create an emulsion. The sample was centrifuged at 9000 g for 3 minutes and the upper layer was removed with a pipette, leaving the protein disc in the middle and the chloroform layer below. 500 μL of MeOH was then added, the tube vortexed, and centrifuged at 9000 g for another 3 minutes. The supernatant was decanted and the protein pellet was allowed to dry for 5 minutes. Protein pellets were re-dissolved in 5% SDS solution and stored at -80^{o}C until analysis. Samples were boiled in 5% β-ME before electrophoresis. SDS-PAGE was performed with Bio-Rad 4-15% criterion precast gel for 42 minutes at 201 V and proteins were transferred in a Criterion Blotter with Plate Electrodes to Immobilion-FL PVDF membranes (Millipore) for 18 hours 11 minutes at 11V in Towbin's buffer. An anti-GAA antibody was obtained as a gift from the Duke glycogen storage disease laboratories.

Electron Microscopy Cardiomyocyte clusters were fixed in 2.5% paraformaldehyde/3% gluteraldehyde in 0.1M cacodylate buffer overnight at 4°C, post-fixed in 1% osmium tetroxide, dehydrated in ethanol gradient and embedded in Durcapan (Fluka), sectioned at 60 nm and stained with Lead Citrate and Uranium Acetate. All images were taken on a Phillips CM120 TEM. For the low glucose culture, iPSC-CM clusters were fed with no glucose DMEM with 1% FBS for 18 hours before fixation.

Cell Size Assay The iPSC-CMs were plated on coverslips at a low density such that cells do not come in contact with each other. After 10 days of culture (2 days in DMEM/F12 with 20% FBS followed by culture in RPMI/B27 with insulin), cells were fixed for myofilament immunostaining with cardiac troponin T (isoform Ab-1, Thermo). Fields of cells (20x objective) were photographed with an epifluorescence scope and cell size was quantified by outlining the troponin T positive circumferences in Image J (NIH), which converted pixel number into square centimeters when given the image magnification.

RESULTS

Reprogramming of Pompe disease fibroblasts into induced pluripotent stem cells – Skin fibroblasts from 2 unrelated infantile-onset Pompe patients, designated Pompe 1 and Pompe 2, were reprogrammed into iPS cells using overexpression of a set of transcription factors as previously described (59). In addition, skin fibroblasts from the healthy mother of the Pompe 1 line, referred to as Control 1, were also reprogrammed. Consistent with the cells being reprogrammed to a pluripotent state, nuclear immunolabeling for the pluripotency-related transcription factor OCT4 was present as was cell surface immunolabeling for stage-specific embryonic antigen 4 (SSEA4) (Fig. 1A). The cell line karyotypes were confirmed as normal 46XX in Pompe 1 and Control 1 and 46XY in Pompe 2 (Fig. 1B). The new cell lines were tested for pluripotency using a teratoma assay in immunocompromised mice. As shown in Fig. 1C, formation of all three embryonic germ-layers occurred for each of the new iPS cell lines. The other human iPS cell line studied in this work, called Control 2, was previously reprogrammed from lung fibroblasts and characterized (41). Table 2 summarizes the source and properties of the cell lines used in this study.

Pompe iPS-cells have disease-causing acid α-glucosidase mutations resulting in undetectable mature protein and enzymatic activity – The mutations in *GAA* in the original Pompe fibroblasts were evaluated in the corresponding iPS cell lines. The Pompe 1 cell line has a homozygous exon 18 deletion of approximately 550 bp in *GAA* as demonstrated by the PCR product in Fig. 2A of the genomic DNA region surrounding exon 18. The Control 1 iPS cell line, originating from skin fibroblasts of the mother of Pompe 1, is heterozygous for the exon 18 deletion in the *GAA* gene. In comparison, the Control 2 iPS cell line is homozygous wild-type for exon 18 of *GAA*.

The Pompe 2 line is a null compound heterozygote at the *GAA* locus with one allele containing a deletion of a T nucleotide at cDNA position 1441 (Fig. 2B), resulting in a frameshift and pre-mature stop codon 39 amino acids downstream. The other allele has a G to A transition at position 2237 (Fig. 2B), producing a UAG stop codon at that location. For comparison are the wild-type sequences from Control 2's genomic DNA.

To test the impact of the Pompe mutations on the expression of GAA protein, western blotting of iPS cell protein lysates with an anti-GAA antibody revealed the active lysosomal 70 and 76 kDa forms of GAA in control but not Pompe lines (Fig. 3A). No significant immunoreactivity for GAA was found from the Pompe 2 sample, but the Pompe 1 sample demonstrated the GAA precursor at a molecular weight of 110 kDa (64). This is consistent with a previous report that the deletion of exon 18 allows for a precursor peptide to be translated, but not processed into an active form (65).

To ascertain whether the mutations in the Pompe cell lines affects GAA function, protein lysates from iPS cells were assayed for GAA activity via incubation with the substrate 4-methylumbelliferyl-α-D-glucoside (4-MUG) at a pH of 4. Hydrolysis of this substrate releases

the fluorophore 4-methylumbelliferone (4-MU) and free glucose. Both Pompe lines had no detectable GAA activity compared to the control lines that demonstrated activity in the expected range (Fig. 3B). The GAA activity of Control 1 was approximately ½ that of Control 2, suggestive of a gene dosage effect since Control 1 has one functional *GAA* allele while Control 2 has both copies active. As an assay control, 4-MUG was incubated at pH 7 to measure neutral-α-glucosidase (NGA) activity. Equivalent NGA activity was measured in all lines, confirming the catalytic deficit in Pompe disease is due to the hydrolysis of the α1-4 glucosidic bond at the typical acidic pH of the lysosome.

Pompe iPS-cells can differentiate into cardiomyocytes The small molecule differentiation protocol produced spontaneously contracting cardiomyocytes from Control and Pompe iPS cells. Both Pompe and Control iPSC-CMs demonstrated pan-cytoplasmic α-actinin staining (Fig. 4A) that revealed highly organized and parallel Z-line architecture (Fig. 4B).

Pompe iPS-derived cardiomyocytes have pathognomonic glycogen-filled lysosomes— A feature found in striated muscle from patients with Pompe disease is lysosomal glycogen accumulation (13). We examined the ultrastructure of Control and Pompe iPSC-CMs under standard culture conditions by using electron microscopy. The cytoplasm of both Pompe and Control iPSC-CMs revealed abundant glycogen β-particles in Fig. 5A, a feature found in embryonic cardiomyocytes (66). In order to resolve lysosomal from cytoplasmic glycogen, the iPSC-CMs were cultured in media without glucose overnight. Ultrastructure of Control iPSC-CMs deprived of glucose (Fig. 3B) shows a disappearance of glycogen β-particles. The Pompe iPSC-CMs also have a depleted cytoplasmic glycogen pool, however, glycogen β-particles remain in membrane-isolated lumens (Fig. 5B and 5C). In contrast, lysosomes from Control 1 iPSC-CMs are identified with electron dense material without evident glycogen. Likewise, the Control 2 and Pompe 2 iPSC-CMs show

an equivalent distinction in lysosomal structure (data not shown).

Cell surface area comparisons between Pompe and Control iPSC-CMs To test the hypothesis that the HCM is due to an increase in cardiomyocyte size, we measured the surface area of single cell plated iPSC-CMs from Control and Pompe groups. Table 3 has calculated average surface areas that reveal a trend towards smaller cell sizes in the Pompe lines, however, no statistically significant differences in cell size were observed.

DISCUSSION

The purpose of this research was to develop a human iPSC-CM model of Pompe cardiomyopathy. Reprogramming of Pompe patient fibroblasts to iPS cells was possible with a 6-factor cocktail and did not require the temporary expression of GAA during the reprogramming process as was previously necessary in an existing iPSC-CM model of Pompe disease (53). Furthermore, the Pompe 1 and Pompe 2 iPS cell lines did not have dramatically slower doubling times than the control iPS cell lines and cardiomyocytes differentiated from the Pompe iPS cells demonstrated no observable differences in culture viability as was reported in. These discordant observations in Pompe iPS cell and iPSC-CM growth and survival characteristics in our study compared to the study in may be due to the differences in factors used for reprogramming and the method of cardiomyocyte differentiation. Another paper demonstrated the successful reprogramming of both infantile and Pompe fibroblasts into iPS cells without the use of transient GAA expression (67).

Our phenotypic characterization of Pompe iPS cells is in agreement with the known cause of infantile onset Pompe disease, namely undetectable levels of GAA activity due to mutations in the GAA allele that results in the lack of enzymatically active protein. Once differentiated into cardiomyocytes, we were able to identify the pathognomonic glycogen-filled

lysosomes exclusively in the Pompe iPSC-CMs. Surprisingly, both Control and Pompe iPSC-CMs displayed enormous amounts of cytoplasmic glycogen that was at first difficult to distinguish from lysosomally trapped glycogen. However, following glucose removal from the media the presence of glycogen filled lysosomes became definitive through what we hypothesize was consumption of all cytoplasmic glycogen made necessary by the absence of glucose substrate. The preponderance of cytoplasmic glycogen in iPSC-CMs may be representative of their early developmental state; studies of rat cardiomyocyte maturation shows an embryonic cytoplasm full of glycogen that is thought to act as both an energy substrate and a place-holder for myofilament assembly (66).

The cell surface area assay did not reveal an enlargement of Pompe iPSC-CMs compared to controls, which would be a strong indicator of hypertrophy. We are unsure if the equivalent or slightly smaller size of the Pompe cells would argue against individual myocyte hypertrophy, since the cells may beexisting in a pre-hypertrophic state supported by their immature morphology. Perhaps the Pompe cells are unable to grow to a larger size due to lysosomal dysfunction or disruption of glycogen metabolism or the differentiation protocol may favor atrial or nodal myocyte formation from the Pompe lines and the larger ventricular types from the control lines. Cell surface area is not the ideal measure of hypertrophy, since Pompe pathology may be affecting the ability for iPSC-CMs to adhere and spread on the plastic substrate. Volumetric measurements, perhaps with z-stacks with a confocal microscope, may be more relevant.

In conclusion, we were able to take skin fibroblasts from a patient with infantile onset Pompe disease, reprogram them into iPS cells, and differentiate those iPS cells into cardiomyocytes. The iPS cell lines were karyotypically normal, expressed pluripotency markers,

and were able to differentiate into the 3 embryonic germ layers. The Pompe disease causing mutations in the fibroblast lines were maintained in the iPS state along with the downstream consequences of a loss of GAA protein and enzymatic activity. The Control and Pompe iPSC-CMs had normal sarcomeric structure and organization, however, only the Pompe iPSC-CMs revealed glycogen filled lysosomes. The Pompe iPSC-CMs did not present with larger cell surfaces that would indicate a hypertrophic process Therefore, the iPSC-CM model of infantile-onset Pompe disease has been established. The remaining chapters will investigate potential pathologic mechanisms of the new Pompe cardiomyocytes.

TABLE LEGENDS

Table 1 Primers for GAA genotyping Genomic DNA from iPS cells were amplified with the tabulated primer pairs and the GoTaq Green (Promega) polymerase mix. The DNA products were analyzed as described in the methods.

Table 2 IPS-cell line nomenclature, GAA genotype, and phenotype del ex18: deletion of exon 18; WT: wild-type; 1441delT: deletion of a T nucleotide at GAA cDNA position 1441; 2237G>A: G to A transition at GAA cDNA position 2237.

Table 3 Quantification of iPSC-CM surface areas The mean surface area, the standard deviation, and number of cells counted are presented.

Figure Legends

Fig. 1. Characterization of iPS cells reprogrammed from patient dermal fibroblasts A. Immunofluorescence of iPS cell cultures probed with anti-OCT4 (nuclear) and anti-SSEA4 (plasma membrane), markers of pluripotency. Scale bar = 100 μm for panels and 10 μm for insets. **B.** Giemsa-band Karyograms from each line. Control 1: 46XX; Pompe 1: 46XX; Pompe 2: 46XY. **C.** H&E stained sections of iPS cell teratomas. Examples of endoderm, mesoderm, and

ectoderm are represented from each reprogrammed line. Endoderm – Control 1: Hepatoid cells; Pompe 1: Primitive gut epithelium; Pompe 2: Respiratory epithelium. Mesoderm – Control 1: Cartilage; Pompe 1: Smooth muscle; Pompe 2: Cartilage. Ectoderm – Control 1, Pompe 1 & Pompe 2: Retinal Pigmented Epithelium. Scale bar = 50 μm.

Fig. 2. The acid α-glucosidase genotype in Pompe and Control iPS cell lines. A. PCR products of the genomic DNA region that includes GAA exon 18 from Pompe 1, Control 1, and Control 2 iPS cell lines separated on a 0.8% agarose gel. ex18: exon 18. Del ex18: deletion of exon 18. **B.** Sequencing chromatograms of PCR products from Pompe 2 iPS cell genomic DNA at locations of the 2 point mutations. Aligned wild-type sequences underneath are from Control 2 iPS cells. Arrows point to the deletion of a T nucleotide in one allele and the G>A transition in the other copy. Regions of interest were PCR amplified and directly sequenced. Nucleotide position numbers refer to the GAA cDNA sequence.

Fig. 3. The acid α-glucosidase biochemical phenotype in Pompe and Control iPS cell lines. A. An immunoblot of iPS cell total protein lysates probed with anti-GAA. The precursor form is approximately 110 kDa and enzymatically active forms are represented by a dark band above and a light band below the 75 kDa marker. Anti-GAPDH was used as a loading control. **B.** Enzymatic activity assay of total protein lysates from the 4 iPS cell lines for the ability to hydrolyze 4-methylumbelliferyl-α-D-glucoside (4-MUG) into glucose and the fluorophore 4-methylumbelliferone (4-MU) at pH = 4 for lysosomal GAA and at pH = 7 for cytoplasmic neutral α-glucosidase**.** Activity is measured as nmol of 4-MU released per mg of protein per hour. N = 4 biological replicates (cells taken from different passages) for each line.

Fig. 4 Sarcomeric structure and organization in Control and Pompe iPSC-CMs A. The epifluorescence images are of the Z-line protein sarcomeric α-actinin immunostaining in Control

1 and Pompe 1 iPSC-CMs. **B.** Regions of the images in A are increased in magnification. For all images Scale bar = 10 μm and DAPI stains the nuclei blue.

Fig. 5. Ultrastructure of Pompe and Control iPSC-CMs A. Electron micrographs of Control 1 and Pompe 1 iPSC-CMs cultured in media containing 4.5 g/L glucose. Scale bar = 5μm **B**. Electron micrographs of Control 1 and Pompe 1 iPSC-CMs cultured in zero g/L glucose for 24 hours before imaging. Scale bar = 5 μm **C**. Expanded regions from panel B. scale bar = 0.5 μm. Legend: N = Nuclei; CG = cytoplasmic glycogen; M = mitochondria; HL = healthy lysosome; LG = lysosomal glycogen; MF: myofilaments; MF_x : Myofilaments in cross-section.

Table 1

Mutation	Direction	Primer Sequence (5'-3')
del ex18	Forward	CTCCTCACACCATCCCCATT
del ex18	Reverse	CACGTACCAGCTCATTCACG
G>A	Forward	CATACGTTCCTCTTTCCGCC
G>A	Reverse	AATTCAGCCTCTTCCTGTGC
delT	Forward	CAATCCACATGCCGTCGAAG
delT	Reverse	AGCTGCTCATTGACCTCCAG

Table 2

Official Name	Common Name	GAA genotype	Pompe Phenotype
GM20123	Control 1	WT/del ex18	Healthy
IMR90c4	Control 2	WT/WT	Healthy
GM20089	Pompe 1	del ex18/del ex18	Infantile Pompe disease
GM04912	Pompe 2	1441delT/2237G>A	Infantile Pompe disease

Table 3

Cell Line	*Mean Surface Area μm^2	SD μm^2	# of cells
Control 1	3369	2445	312
Control 2	4696	2488	118
Pompe 1	1833	1506	214
Pompe 2	2189	1600	152

* ANOVA analysis with Bonferroni post-hoc correction revealed no significant differences in cell size between the cell lines.

Figure 1

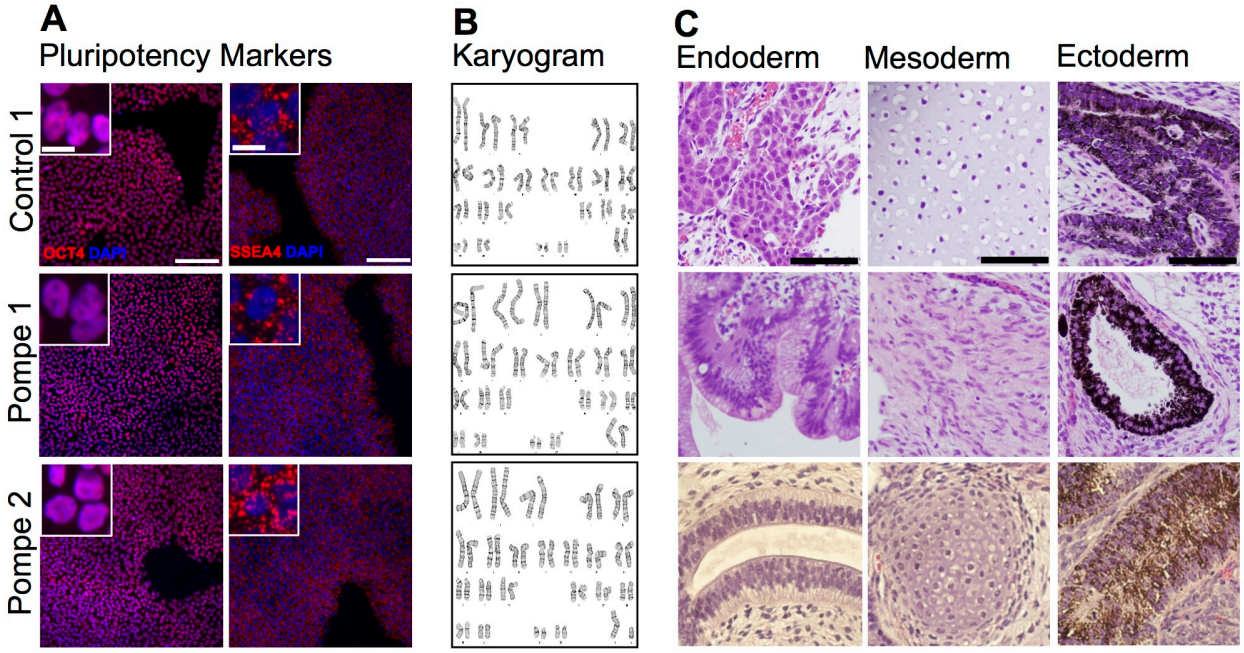

Figure 2

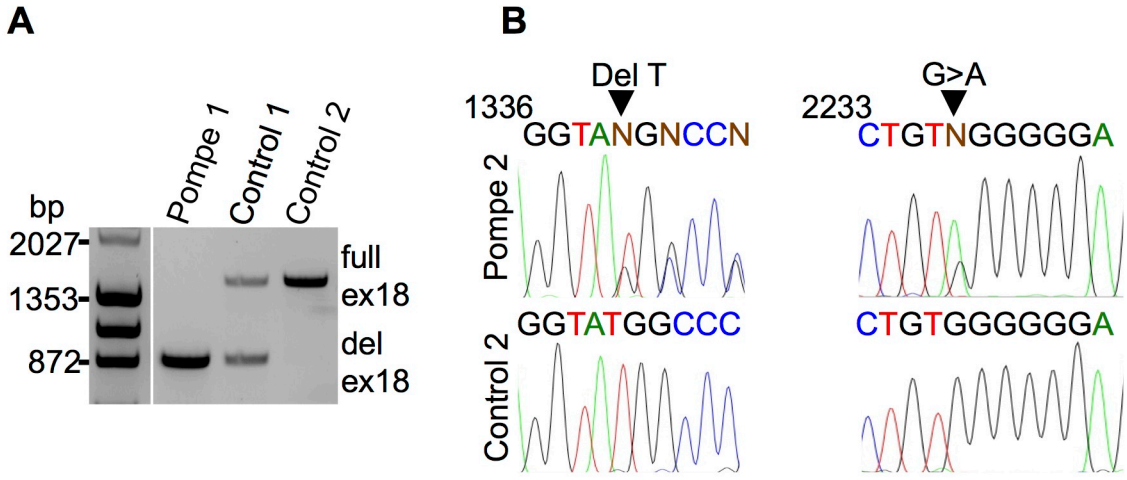

Figure 3

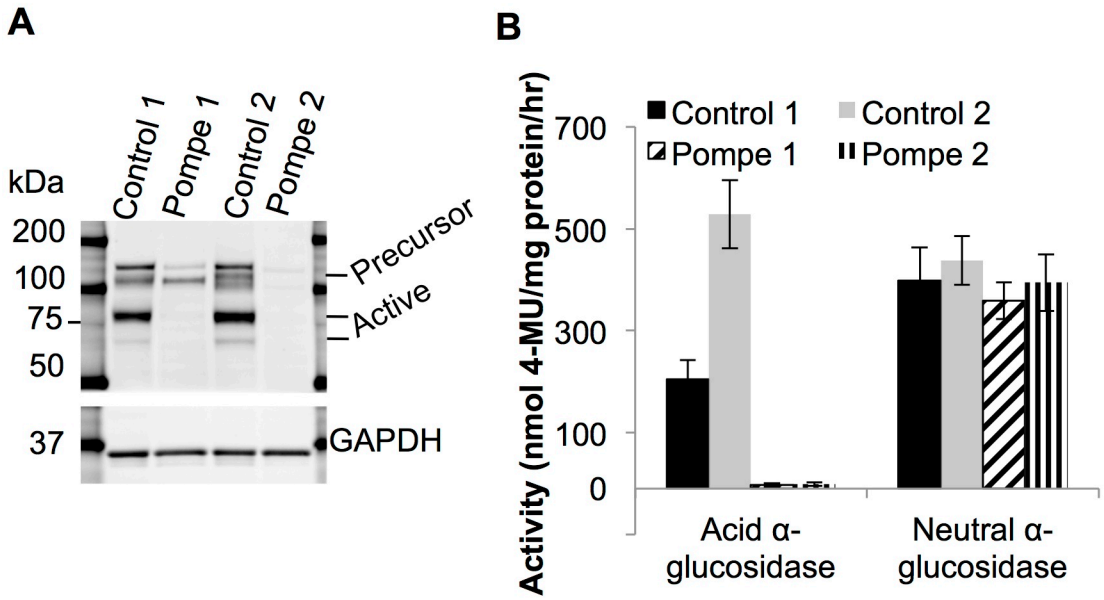

Figure 4

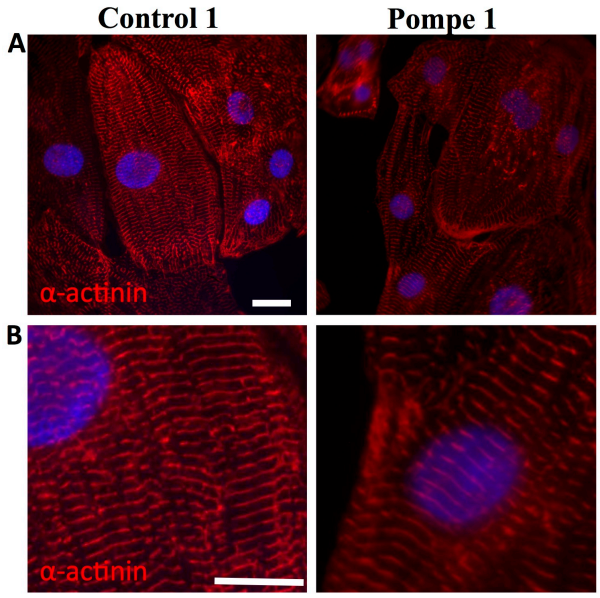

Figure 5

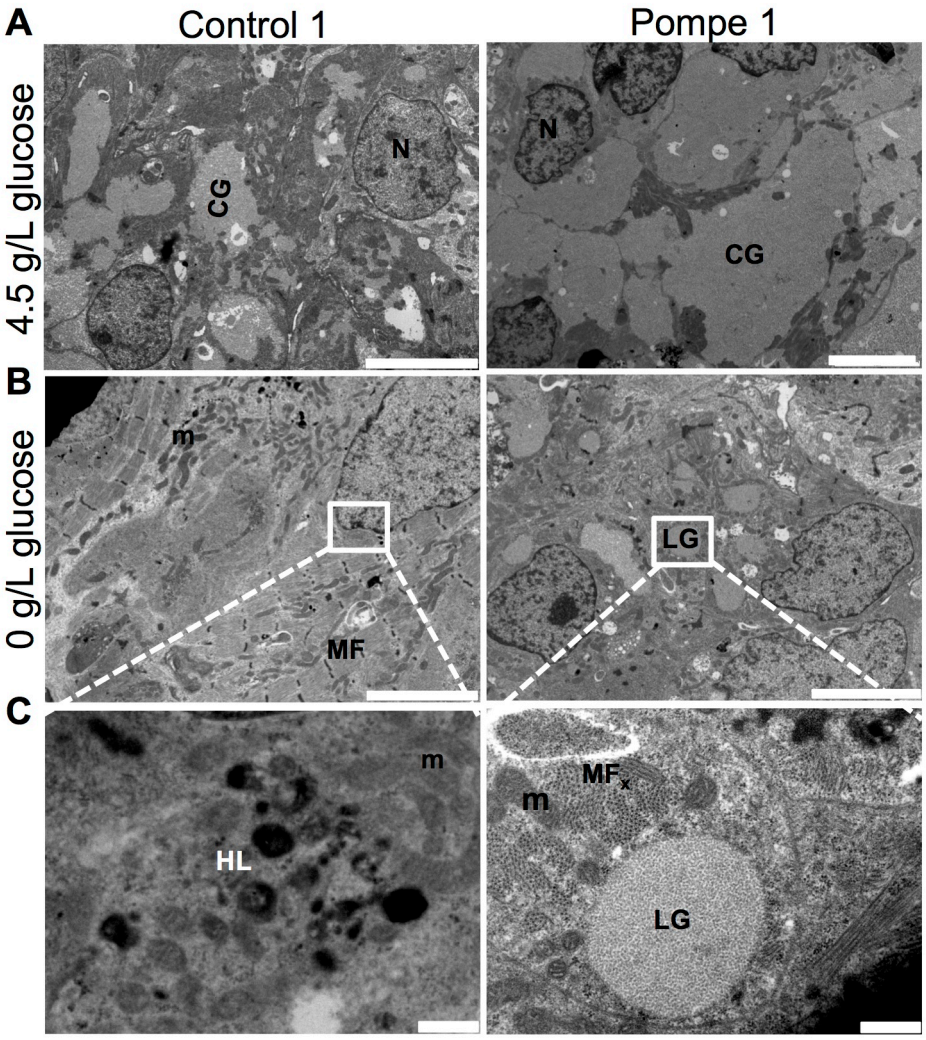
A
Control 1
Pompe 1
4.5 g/L glucose
N
CG
N
CG
B
0 g/L glucose
m
MF
LG
C
m
HL
MFx
m
LG

CHAPTER 3: The Engineered Cardiac Tissue Model of Infantile Onset Pompe Disease

In this chapter we explore the potential of using iPSC-CMs to create 3-dimensional contractile tissue that resembles myocardium. We show that not only is production of engineered cardiac tissue (ECT) with human iPSC-CMs reproducible, but that we can measure contractile kinetics (force vs. time) to 3 significant figures. The etiology of familial forms of hypertrophic cardiomyopathy can be traced to changes in the force generation and kinetics of a contraction cycle, so we used our system to determine if cardiac tissue produced with Pompe iPSC-CMs had differences in the magnitude of force production and contractile kinetics compared to controls.

Methods

Cardiac Troponin T Flow Cytometry Differentiated cardiomyocytes were dissociated from T75 flasks and used to prepare fibrin-based ECTs with a protocol adapted from (68). One million cardiomyocytes from the single cell suspension were fixed in 2% PFA and processed for cTnT (Cardiac Isoform Ab-1, Thermo) flow cytometry to determine CM purity. Flow cytometry was performed with the FACScalibur and analyzed with FloJo software.

Engineered Cardiac Tissue Preparation and Functional Testing Differentiated cardiomyocytes were dissociated from T75 flasks and used to prepare fibrin-based ECTs with a protocol adapted from (68,69). Only ECT data from CM preparations that were >80% $cTnT^{+}$ were included in contractile analysis. The remaining CM suspension was cultured for 3 hours on a rotating platform at 45 RPM in a 10 cm petri dish in ECT media. The composition of ECT media is described in (58) as "mouse media". Cell clumps from rotational culture were then mixed with scaffold reagents in the following ratios: 1.2 million cells: 5 mg fibrinogen: 0.5 units of thrombin in 200 μL total volume of ECT media. Each ECT is then prepared from 200 μL of the mixture pipetted into 20 mm x 3 mm cylindrical molds of the Flexcell Tissue Train silicone membrane culture plate (Flexcell International) according to methods detailed in (58). Solidified ECTs were then maintained for 2 weeks in ECT medium containing tranexamic acid (Sigma) at 400 μM and aprotinin (Sigma) at 33 μg/mL. A subset of ECTs were externally paced with the C-pace apparatus (IonOptics) for 1 week at 2.5 Hz after an initial 1 week of culture before being harvested for functional studies. Force measurements were made in a model 801B small intact fiber test apparatus (Aurora Scientific) as previously decribed (58) while being perfused with Krebs-Henseleit buffer and externally paced. A stationary arm and force transducer (model 403A, Aurora Scientific), to which the ECT is attached at both ends with sutures, were controlled

by a micrometer for stretch length measurements. Twitch recordings from which contractile kinetics were measured were obtained at the length of maximum isometric force.

ECT Histology and Immunofluorescence For ECT histology, the tissues were immersed in Dent's fixative overnight at 4°C, embedded in paraffin and sectioned at 8 μM thickness. Once on glass slides and rehydrated with an ethanol gradient, the sections were stained with H&E or cTnT. All nuclei were detected with DAPI.

Results

Contractile function of engineered cardiac tissue produced with Control and Pompe iPSC-CMs—Given the limited understanding of cardiac contractile function in Pompe disease in the setting of profound cardiac hypertrophy, we produced engineered cardiac tissue (ECT) with iPSC-CMs to assess contractile performance. Following 2 weeks of culture, the ECTs remodeled into linear strips of spontaneously contracting tissue (Fig. 6A) that were cellularized (Fig. 6B) with cardiomyocytes located circumferentially as visualized with cTnT immunofluorescence (Fig. 6C). Electron micrographs of Control and Pompe ECTs, respectively, displayed elongated nuclei and longitudinally oriented myofilaments (Fig. 6D and 6E). Only in the Pompe ECT, however, were glycogen filled lysosomes evident.

Contractile performance of the ECTs was evaluated by characterizing isometric force (F) production in response to a step-wise increases in length (L). As shown in Fig. 7, the Control 1 and 2 ECTs have matching F-L curves. Pompe 2 ECTs had a higher contractility while Pompe 1 ECTs had a lower contractility than both Control ECTs, calculated as $\Delta F/\Delta L$ in table 4. In summary, the Pompe 1 and 2 F-L curves diverge from each other and are distinct from the control group. Therefore, we are unable to distinguish whether the unique characteristics of the

Pompe 1 and 2 ECT F-L relationship are due to cell-line-to-cell-line variation or Pompe pathology manifesting in a patient-specific manner.

ECTs were stimulated at 2.5 Hz and isometric force generation was measured. Pompe 1 ECTs demonstrated significantly accelerated kinetics of contraction compared to the other lines tested (Fig. 8A, Table 5). However, we noted differences in the intrinsic rates at which the ECTs contracted during the 2 weeks of culture during ECT maturation. Pompe 1 ECTs had an intrinsic rate (2.2 Hz) that was at least double the intrinsic rate of the other lines studied (Table 5). Therefore, we conducted another series of experiments in which all ECTs were conditioned by pacing at 2.5 Hz for one week in culture prior to force measurements to provide a uniform rate of contraction. Pacing for one week accelerated the contraction kinetics for the three lines that had slower intrinsic rates to a greater extent than for Pompe 1 ECTs that had a fast intrinsic rate (Fig. 8B). For the conditioned ECTs, the normalized force (F/F_{max}) and the first derivative ($dF/dt/F_{max}$) vs. time (Fig. 8C and 8D) relationships along with ANOVA comparisons of kinetic parameters (Table 5) showed no clear differences between ECTs prepared from the 2 Control and 2 Pompe cell line.

To quantify total kinetic variability, the sum of the differences in normalized force (F/F_{max}) between each combination of the 4 lines (6 pairs total) were plotted on the y-axis at each time point collected when paced at 2.5 Hz every 0.001 s. As shown in Fig. 9, ECTs from the 4 lines that were paced had reduced kinetic variability in comparison to ECTs tested following culture at their intrinsic rate. Maximum variability occurred towards the middle of force decay at slightly less than 0.3s with another region of high variability noted during force generation around 0.1s. Minimum variation was noticed at time of peak force.

Discussion

The clinical description of Pompe cardiomyopathy is of LV wall and septum thickness at first presentation. Occasionally, hypertrophy is diagnosed in utero. Systolic function in a study of 40 patients was 100% preserved (LVEF > 40%) (37) from 0-5 months of age but then declined as the natural history progressed. Another study (39) also reported mostly normal ejection fractions and fractional shortenings of the LV in Pompe patients from 0-6 months of observation. With further time in the absence of treatment, the hypertrophic cardiomyopathy progresses to a dilated phenotype with systolic dysfunction. No clear differences in contractile performance between the two control lines and two Pompe lines were observed. The fact that we did not find delayed relaxation in the Pompe ECTs as seen clinically may indicate that changes in observed relaxation are secondary to macroscopic remodeling of the heart rather than being intrinsic to the cardiomyocytes or alternatively, this could be secondary to limitations in the model. Additionally, the lack of significant contractile abnormalities suggests that contractile dysfunction is unlikely to be the primary stimulus of the hypertrophic phenotype in Pompe cardiomyopathy.

Since the iPSC-CMs bear ultrastructural resemblance to neonatal cardiomyocyte morphology, ECTs made with immature CMs may be confirming the lack of functional deficits during the earliest stages of Pompe disease. We were interested in comparing contractile kinetics between 4 iPS cell lines that demonstrated variability in intrinsic rates. For the slower cell lines with average intrinsic rates <1.5 Hz (Pompe 2, Control 1 and Control 2), weeklong pacing at 2.5 Hz increased force relaxation kinetics, producing a leftward shift in the F/F_{max} vs. time curves. Previous tissue constructs made with iPSC-CMs (70) report faster calcium reuptake kinetics – the upstream mechanism controlling force relaxation – in response to chronic pacing at 6 Hz

along with evidence of a more developed sarcoplasmic reticulum calcium handling system. Our results share more similarities with exercise induced enhancements in calcium re-uptake rates (71) rather than the slowing of calcium cycling seen in tachycardia-induced cardiomyopathy (72). Changes in ECT kinetics due to pacing in culture, therefore, is supportive of physiologic adaptation rather than a pathologic process. ECTs kinetics from Pompe 1 with an intrinsic rate of 2.1 Hz were unaffected by pacing at 2.5 Hz and had the fastest kinetics of all the 4 cell lines. Thus, the effect of long-term contraction rate on kinetics is independent of the method of pacing, whether it is internally or externally driven.

Table Legends

Table 4 Contractility of Pompe and Control ECTs. ΔF/ΔL was calculated with measurements in the linear rise phase of the F-L curves in Fig. 5A. Data is presented as slopes averaged from individual ECTs ± S.E.

Table 5 Comparison of kinetic parameters and maximum force measured at a pacing frequency of 2.5 Hz between ECTs contracting at their unpaced rate or paced at 2.5 Hz for 1 week prior to testing. Time to peak: time from external pacing voltage initiating the contraction to peak force generation. Time to 50% force relaxation: Time from maximum force to 50% maximum force during relaxation. The Ns for each group refer to the number of ECTs tested.

Figure Legends

Fig. 6. Structural characterization of ECTs produced with Control and Pompe iPSC-CMs **A.** Photograph of an ECT in perfusion chamber before testing. The left end is tied to a stationary arm and the right end will soon be attached to the force transducer. Scale bar = 1 mm **B.** Photomicrograph of an H&E stained longitudinal ECT section post-testing. Scale bar = 50 μm **C.** Immunofluorescence image of a sectioned ECT immunolabeled with anti-cTnT to identify cardiomyocyte location. Scale bar = 50 μm. DAPI stains the nuclei blue. **D.** Representative electron micrographs of a Control ECT. Scale bar = 5 μm **E**. An electron micrographs of a Pompe ECT. N = Nuclei; MF = myofilaments; LG = lysosomal glycogen. Scale bar = 5 μm

Fig. 7 Contractile Force as a Function of ECT Length Plots of isometric force (F) vs. Δ length (L). Length was measured as the distance between the 2 sutures securing the ECT ends. ΔL=0 was defined as the maximum length that produced no force. Error bars are ± S.E.

Fig. 8. Contractile kinetic studies of ECTs produced with Control and Pompe iPSC-CMs. A. Force normalized to maximum force (F/F_{max}) vs. time curves for a single contraction at 2.5 Hz from ECTs contracting at their intrinsic rate (unpaced) while in culture for 2 weeks prior to testing. On average 30 contractions are averaged for each ECT **B.** The F/F_{max} vs. time curves measured at 2.5 Hz for both Control and Pompe ECTs either allowed to contract at their intrinsic rate for 2 weeks in culture, or paced at 2.5 Hz for 1 week before measurement. The Ns for each cell line in both paced and intrinsic rate groups are given in table 3. **C.** F/F_{max} vs. time curves for a single contraction at 2.5 Hz from ECTs that were paced in culture for 1-week at 2.5hz.. **D.** First derivative (dF/dt) of the F/Fmax vs. time curves in C. dt = 0.001 sec. All error bars are ± S.E.

Fig. 9 Variability in contractile kinetics between ECTs Variability in kinetics between the 4 cell lines tested from a single contraction at 2.5 Hz. During every 0.001s interval the sum of the differences between normalized force of each pair of cell lines was plotted on the y-axis. The ECTs used in the calculation were either allowed to contract at their intrinsic rate during ECT formation (intrinsic rate group) or were paced at 2.5 Hz for 1-week in culture (paced group) prior to testing. Error bars in black represent propagated errors calculated with standard errors of normalized force at each time point.

Table 4

ECT I.D.	*ΔF/ΔL (mN/mm)
Control 1	0.38 ± 0.02
Control 2	0.37 ± 0.04
Pompe 1	0.25 ± 0.02
Pompe 2	0.55 ± 0.03

***** All pairs of ANOVA comparisons with Bonferroni corrections have significant differences except for {C1,C2}.

Table 5

ECT ID	Unpaced rate in Hz (Ns)	Paced rate in Hz (Ns)	[2]Unpaced Time to Peak (ms)	[3]Paced Time to Peak (ms)	[4]Unpaced time to 50% relaxation (ms)	[5]Paced time to 50% relaxation (ms)	[6]Unpaced peak force (mN)	[7]Paced peak force (mN)
C1	1.1±0.2 (34)	2.5 (24)	185±4	[1]175±4	107±2	[1]99±2	1.2±0.1	1.1±0.1
C2	0.8±0.2 (14)	2.5 (9)	187±5	[1]166±3	121±3	[1]98±2	0.9±0.2	0.9±0.1
P1	2.2±0.3 (26)	2.5 (14)	164±4	157±3	95±2	90±2	0.9±0.1	[1]0.4±0.1
P2	0.6±0.2 (24)	2.5 (11)	195±5	[1]173±8	111±2	106±3	1.5±0.2	1.0±0.3

[1]Paced value is significantly different from unpaced value ($p < 0.05$, unpaired t-test with unequal variance)
[2]P1 is significantly different from all other values ($p<0.05$, ANOVA*)
[3]No significant differences were noticed between all comparisons (ANOVA)
[4]Significant differences were found in all comparisons except between the C1,P2 pairing ($p<0.05$, ANOVA)
[5]Significant differences were only found between the P1,P2 and P1,C1 pairings ($p<0.05$, ANOVA)
[6]P1 is significantly different from P2 ($p<0.05$, ANOVA)
[7]P1 is significantly different from C1 ($p<0.05$, ANOVA)
*The Bonferroni correction method was used with all ANOVA calculations

Figure 6

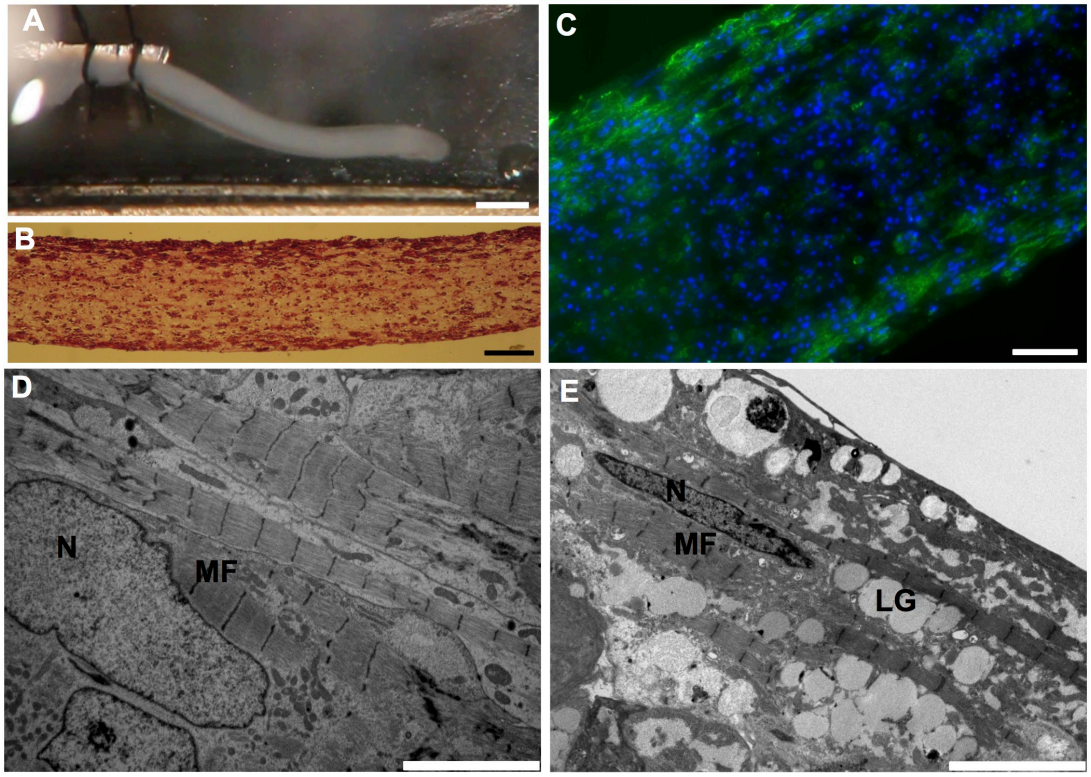

Figure 7

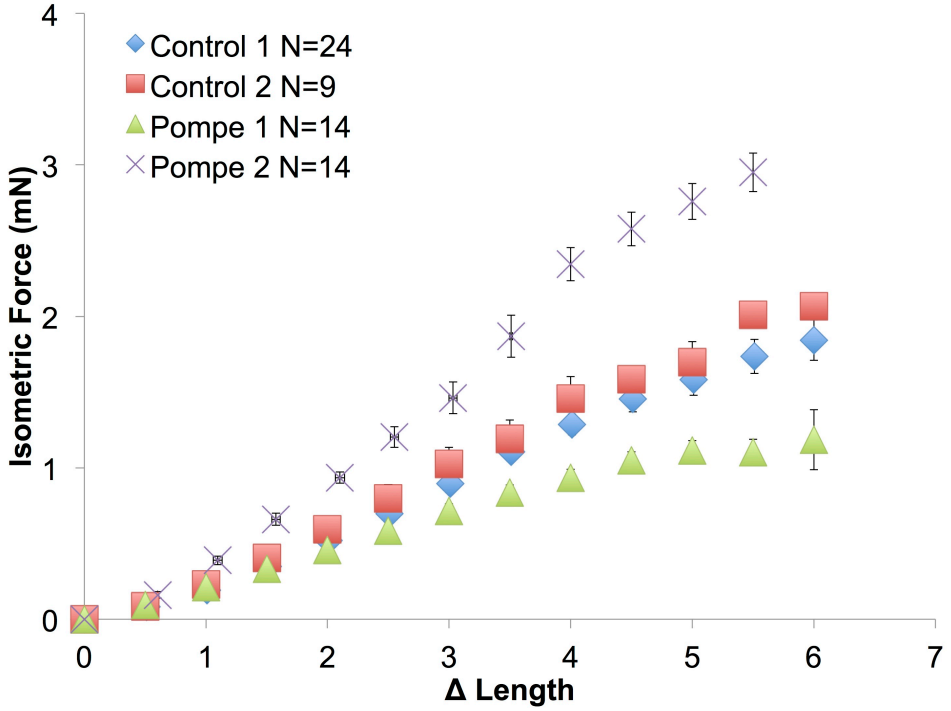

Figure 8

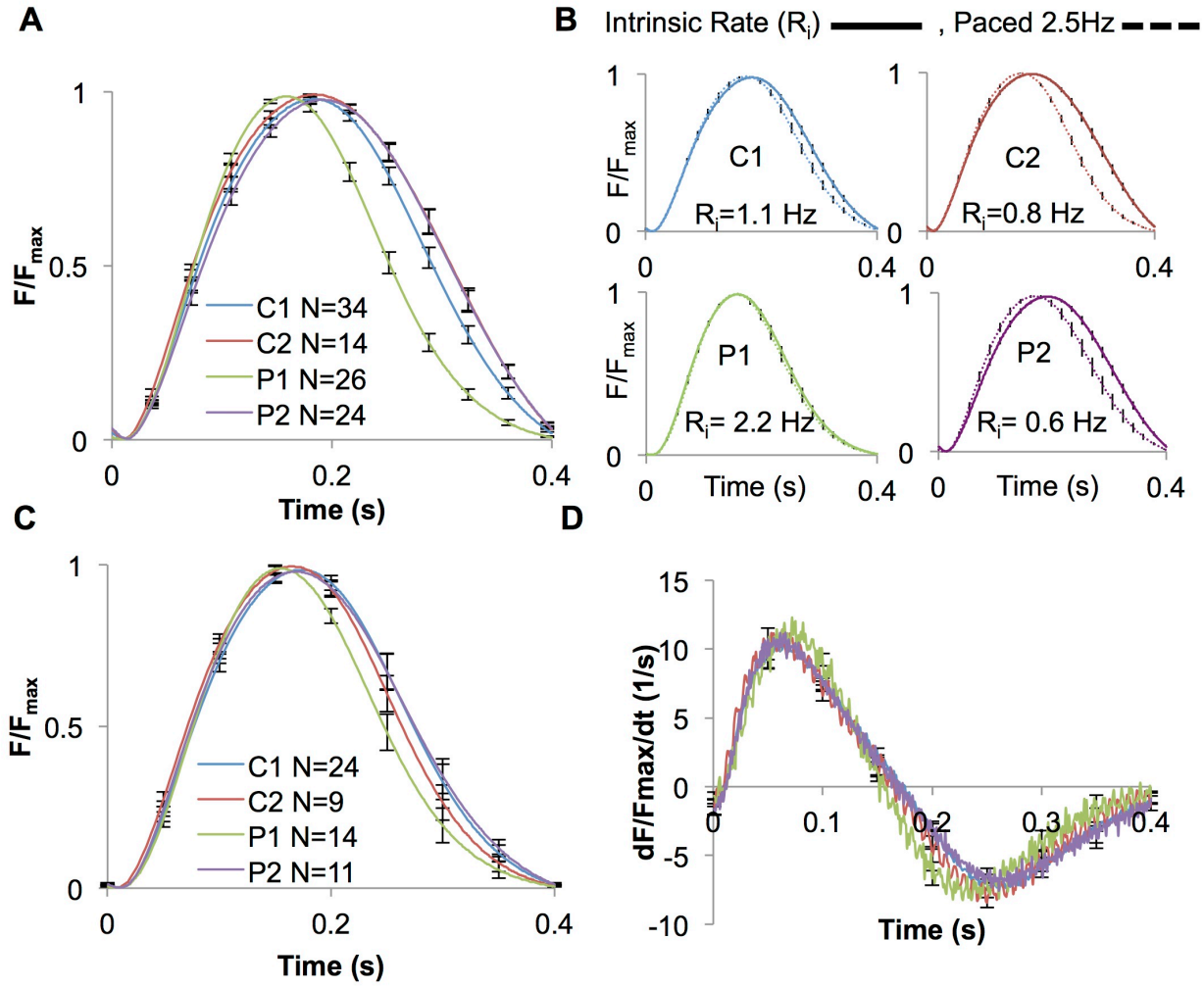

Figure 9

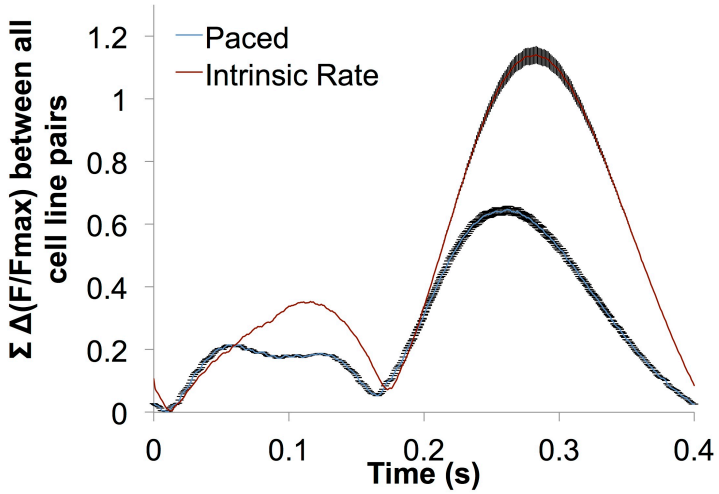

CHAPTER 4:

Autophagic Function in Pompe and Control iPSC-CMs

April 14, 2013. Tuscany, Italy. Gordon Conference on Autophagy and Lysosomal Biology. Today I had the opportunity to meet Dr. Nina Raben, the scientist whose work I am building upon with the autophagy studies in iPSC-CMs. Unfortunately, she was not very excited to meet me once she realized that my data indicated a lack of autophagic dysfunction in the Pompe cardiomyocytes (her work at the NIH has been to prove that the etiology of Pompe myopathy is autophagic dysfunction). She said I was wasting my time studying Pompe disease in the heart, since the available treatment is able to completely cure the cardiomyopathy. There are more patient applications, she argued, in studying the skeletal muscle of Pompe patients since this is where autophagic dysfunction thought to cause the gradual loss of effectiveness of enzyme replacement therapy (with recombinant acid α-glucosidase) is occurring. "There is nothing new to learn about the Pompe heart," and "You will not graduate any time soon if you study the heart with iPSC-CMs," are quotes from her. Everyone in the history of science who has every said something along those lines, that what has been discovered is everything there is to discovery, has time and time again been wrong. I cannot garuntee that I will find anything new in my studies of Pompe iPSC-CMs, but history is on my side.

--- Kunil Raval

Additional Background

All of the autophagy studies are based on the principle of temporary inactivation of lysosomal enzymes followed by reactivation. When lysosomes are inactive, autophagosomes accumulate since they are always being produced and consumed in dynamic equilibrium. In the normal state, the steady state level of autophagosomes is kept to a minimum and is constant. Upon "lysosomal arrest", the autophagosomal population is no longer in equilibrium and they begin to accumulate. Upon lysosomal reactivation, the accumulated autophagosomes are consumed back to equilibrium levels. The rate at which the autophagosomes are consumed is indicative of the lysosomal system's capacity to turnover the autophagosomes. The experimental design is summarized in the cartoon below (73).

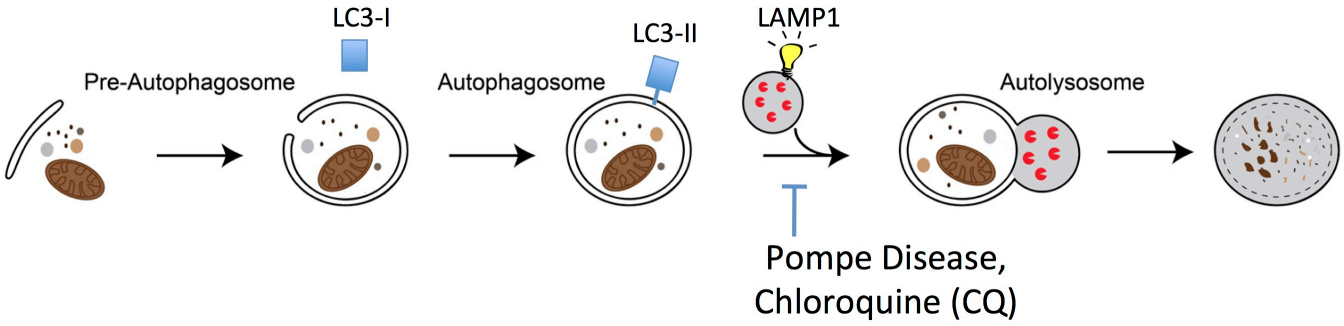

Image 3 The Macro-autophagic process An independent membrane surrounds materials to be degraded, such as old mitochondria and un-needed protein complexes. The enclosed membrane is called an autophagosome and has a specific membrane surface marker called LC3II, that is formed via lipidation of soluble LC3-I. The lysosome, with its own surface marker lysosomal associated membrane protein 1 (LAMP1), fuses with the autophagosome to allow the acid hydrolyases to degrade the intracellular materials into monomers. Current hypotheses propose that Pompe disease is associated with lysosomes that do not digest autophagosomal materials effectively. Pharmacological lysosomal inhibition is possible with the drug chloroquine.

Lysosomal inactivation is mediated by the drug chloroquine (CQ). CQ is a tertiary amine compound (image 4) that has been used for malaria prophylaxis. The drug's mechanism of action is to pass through cell membranes due to its hydrophobicity. Within an acidic compartments such as the lysosome or an equivalent acidic structure in *Plasmodium falciparum* (malaria) that functions as the digestive system, the tertiary amine is protonated to become charged. The positive charge makes CQ impermeable to hydrophobic membranes, trapping the molecule in the acidic compartment. However, because CQ becomes charged by acting as a base (classic Bronsted acid-base reaction), the acidic compartment becomes neutralized as more CQ molecules accumulate. In a neutral environment, the lysosomal enzymes (or enzymes in the acidic compartment of malaria) are inactivated and no longer can hydrolyzed materials that are being delivered (74). As such, the continually produced autophagosomes accumulate while they wait to fuse with and be digested by lysosomes that no longer function.

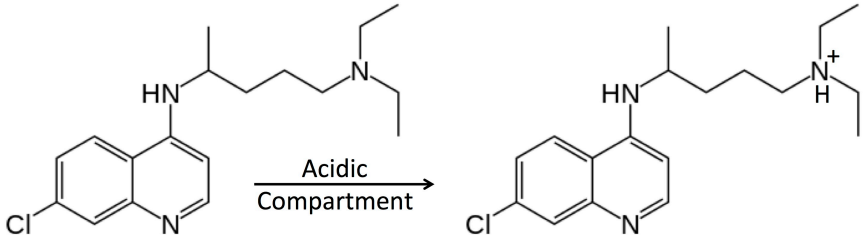

Image 4 Acid-Base Properties of Chloroquine. The Chloroquine molecule can be protonated at the tertiary amine to become charged and more hydrophilic.

Methods

Protein Isolation and 1-D Western Blotting – Protein from cardiomyocyte cultures was harvested by directly adding RIPA buffer to each well after being washed once with PBS (no Ca^{2+} or Mg^{2+}). Cells were transferred to a microfuge tube, sonicated, and then subjected to a methanol:chloroform:water biphasic extraction according to reference (63). For ECTs, RIPA buffer was added to an ECT, after functional testing, in a 1.5 mL microfuge tube and mechanically dissociated with a plastic mortar that fits a 1.5 mL tube and then sonicated. Protein pellets were re-dissolved in 5% SDS solution and stored at -80C until analysis. Samples were boiled in 5% β-ME before electrophoresis. SDS-PAGE was performed with Bio-Rad 4-15% criterion precast gel for 42 minutes at 201 V and proteins were transferred in a Criterion Blotter with Plate Electrodes to Immobilion-FL PVDF membranes (Millipore) for 18 hours 11 minutes at 11V in Towbin's buffer. Blotting was performed with the following primary antibodies: anti-LC3 (Cat. No. NB100-2220. Novus Biologicals), LAMP1 (clone H4A3, DSHB), LAMP2 (clone H4B4, DSHB), and GAPDH (Cat. No. G9545, Sigma). Washes were performed in TBS with 0.05% Tween-20 (TBST) and blocking with 5% goat serum.

Chloroquine Treatments – The autophagy studies were facilitated via chloroquine (CQ) treatment of cell culture and ECTs. Chloroquine was purchased from Sigma and dissolved in PBS at 20 mM so that a 1:1000 fold dilution in media would make a 20 μM solution for treatment. The CQ treatment lasted 2 days with no media exchanges. Beyond 2 days of CQ treatment the cells exhibit signs of necrotic death. The recovery period occurred after exchange with CQ-free media.

Results

Macro-autophagic function is preserved in Pompe iPSC-CMs– Recent studies in Pompe skeletal muscle have implicated an inability of the lysosomal system to maintain normal levels of autophagic flux as a major contributor to the pathogenesis of myofiber destruction (12). However, the role of autophagic dysfunction in the myocardium of infantile-onset Pompe patients is unknown (75). To examine autophagosomal turnover in the Pompe iPSC-CM model, we forced autophagosome accumulation by blocking lysosomal acidification with chloroquine (CQ). Removal of CQ from the media re-establishes lysosomal function and autophagosomal clearance (73). To detect the autophagosomal system, we examined the microtubule-associated protein light chain 3 (LC3) which is synthesized in a soluble cytoplasmic form (LC3-I) and upon induction of autophagy, becomes lipidated and anchors in the autophagosome membrane as LC3-II. Immunofluorescence studies demonstrate LC3 fluorescence on D0 is diffuse through the cytoplasm, highlighting the LC3I form; however, following CQ exposure the fluorescence becomes more intense and punctate, representing conversion to the membrane localized LC3II form (Fig. 10A). These results demonstrate that the treatment with CQ cause autophagosomal accumulation in the iPSC-CMs.

Western blots with anti-LC3 were evaluated for iPSC-CMs during CQ treatment and recovery along with anti-GAPDH loading controls (Fig. 10B). Densitometric ratios of LC3II/GAPDH show that all lines experienced a rise in LC3II following 48 hours of 20 μM CQ treatment (Fig 10C); the rise was between 15-20 fold above baseline ratios. At day 1 of recovery (R1), all lines presented with an LC3II decline, except for Pompe 2 iPSC-CMs, which consistently reported a rise in LC3II at R1. By 8 days of recovery (R8), all Control and Pompe iPSC-CMs were able to reduce their LC3II burden towards baseline (D0) levels. Therefore, a

CQ-based autophagic challenge did not reveal persistent autophagosomal (LC3II) accumulation or a slower autophagic flux in Pompe iPSC-CMs compared to the Control iPSC-CMs.

The lysosomal system also changes dramatically when exposed to CQ, visualized in Fig. 11A with anti-lysosomal associated membrane protein 1 (LAMP1) marking the lysosomes (76). Before CQ treatment, LAMP1 labeling is punctate in Control iPSC-CMs, but outlines larger lysosomal structures in Pompe cells. In response to CQ, both Pompe and Control cells experience an expansion of the lysosomal population, both in quantity and/or size.

The LAMP1 immunoblots in Fig. 11B show an increase in intensity following CQ treatment for the Control iPSC-CMs, but in the Pompe iPSC-CMs an unexpected change in electrophoretic mobility of LAMP1 was observed. LAMP1-SDS complexes from control cells have an apparent molecular weight of 100 kDa, while LAMP1 in the Pompe lines present as a smear with a prominent band below 100 kDa. Following CQ treatment, the intensity of the lower mobility LAMP1 band in the Pompe lines increases concomitant with diminishing amounts of the higher mobility forms. The mobility of LAMP1 in the Control lines remains the same upon CQ exposure. We also investigated the immunoblotting patterns of LAMP2 (Fig. 11C), which co-exists with LAMP1 as a glycoprotein on the lysosomal membrane. Like LAMP1, LAMP2 presents as a single band in the Control lines, but as multiple bands of higher mobility in the Pompe lines. Also like LAMP1, Control lines experience an increase in LAMP2 intensity with no change in mobility as a result of CQ exposure while Pompe cells demonstrate a reduction in LAMP2 SDS-complex mobility in response to CQ.

Discussion

Since autophagic dysfunction has been recognized as an important feature of the Pompe skeletal myopathy (77), we examined for autophagic incompetence in the iPSC-CM model. Elevations of the autophagosmal marker LC3II in Pompe iPSC-CMs were not observed under standard culture conditions in contrast to LC3 immunoblots of Pompe skeletal muscle (28). The lack of basal LC3II accumulation agrees with the Pompe cultured mouse myotube model where the obvious LC3II elevation in vivo is absent in vitro (78). Since in vitro conditions may not be as demanding on the autophagic system as is experienced in vivo, we stimulated autophagosomal accumulation via CQ treatment. There was no significant difference in the rate at which the lysosomal system consumed accumulated autophagosomes even though a population of those lysosomes in the Pompe iPSC-CMs at baseline were enlarged and glycogen-filled. Thus, results from this model system argue that autophagic dysfunction is not central to the early Pompe cardiomyopathy.

Higher mobility LAMP1 and LAMP2 species in Pompe iPSC-CMs compared to controls were first noticed while quantifying changes in lysosomal mass via immunoblot densitometry during CQ treatment and recovery. The apparent molecular weight difference in the LAMPs had been observed before between Pompe and control heart and skeletal muscle, but was either attributed to natural variation in glycosylation (79) or an explanation was not pursued (77).

Figure Legend

Fig. 10. Autophagosomal flux in Control and Pompe iPSC-CMs during recovery from CQ mediated lysosomal arrest A. Immunofluorescence image of LC3 in Control and Pompe iPSC-CMs before and after 2 days of CQ treatment. DAPI stains the nuclei blue. Scale bar = 10 μm. **B.** LC3 immunoblots of total protein lysates during CQ treatment and recovery with GAPDH controls. LC3I is converted into LC3II upon autophagosomal formation. 3 replicate experiments (CMs differentiated from different iPS cell passages) are shown for each line with one lane representing cells from 1 culture well. D0: Day 0. Cells were harvested immediately before CQ treatment; CQ: Cells exposed to CQ for 2 days before protein collection. R1,R4,R8: Recovery from CQ treatment. CQ was removed from the media and cells were cultured for 1, 4, and 8 days in normal media before harvest. **C.** Quantification of LC3II/GADPH ratios relative to the maximum ratio set to 1. The x-axis is labeled to correspond with immunoblot time points. Each x-axis mark represents 1 day with the black bar indicating CQ exposure. Error bars are ± S.E.

Fig. 11. Analysis of LAMPs from Control and Pompe iPSC-CMs before and after CQ treatment A. LAMP1 immunofluorescence in Control and Pompe iPSC-CMs before (D0) and after 2 days of CQ treatment. DAPI stains the nuclei in blue. Scale bar = 10 μm. **B.** LAMP1 immunoblots from Pompe and Control iPSC-CMs before and after CQ treatment. Data is presented in duplicates. **C.** LAMP2 immunoblots from Pompe and Control iPSC-CMs before and after CQ exposure.

Figure 10

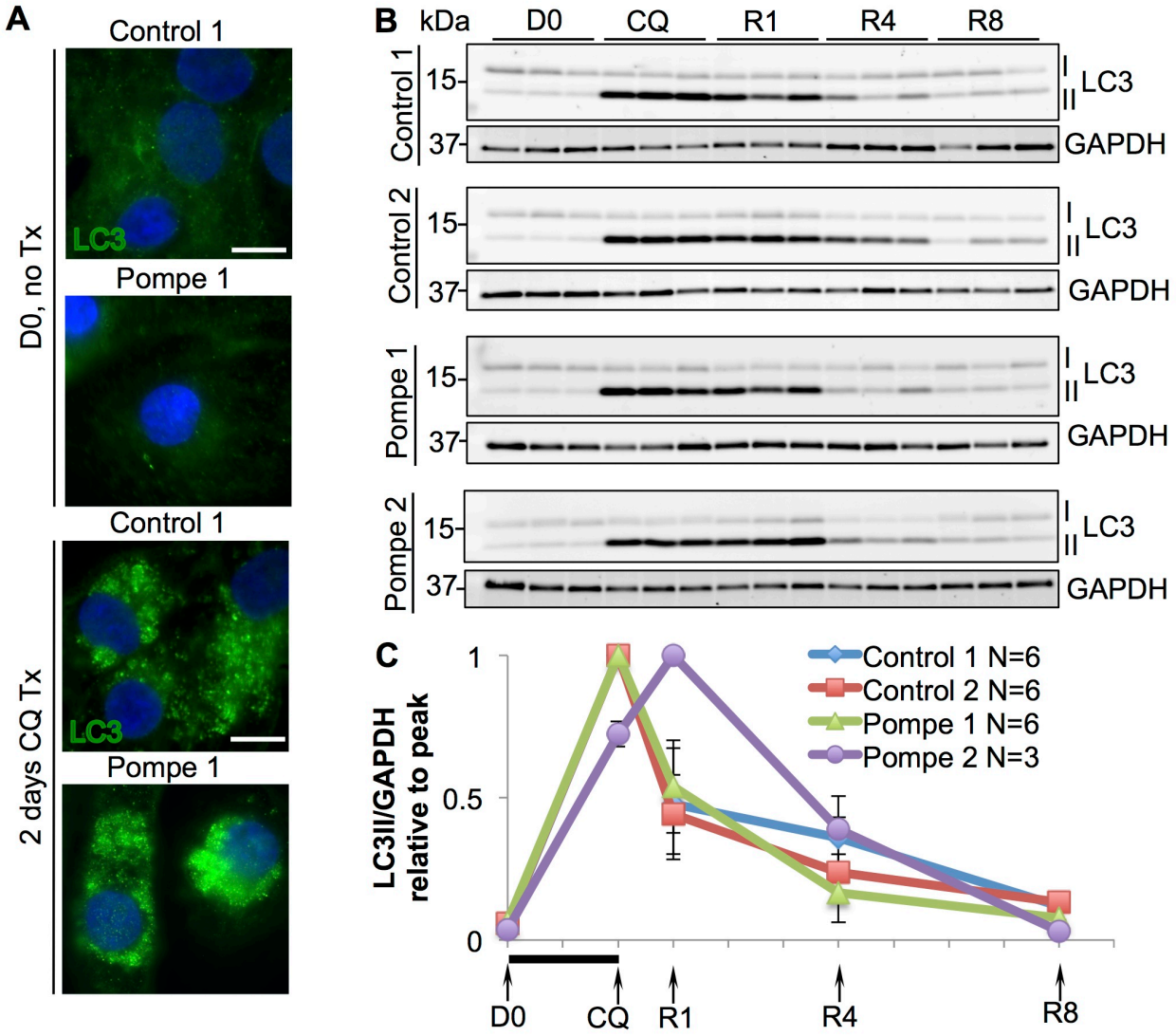
A
Control 1
LC3
Pompe 1
D0, no Tx
Control 1
LC3
Pompe 1
2 days CQ Tx
B
kDa
D0
CQ
R1
R4
R8
Control 1
Control 2
Pompe 1
Pompe 2
15
37
I
II
LC3
GAPDH
C
LC3II/GAPDH relative to peak
1
0.5
0
Control 1 N=6
Control 2 N=6
Pompe 1 N=6
Pompe 2 N=3
D0
CQ
R1
R4
R8

Figure 11

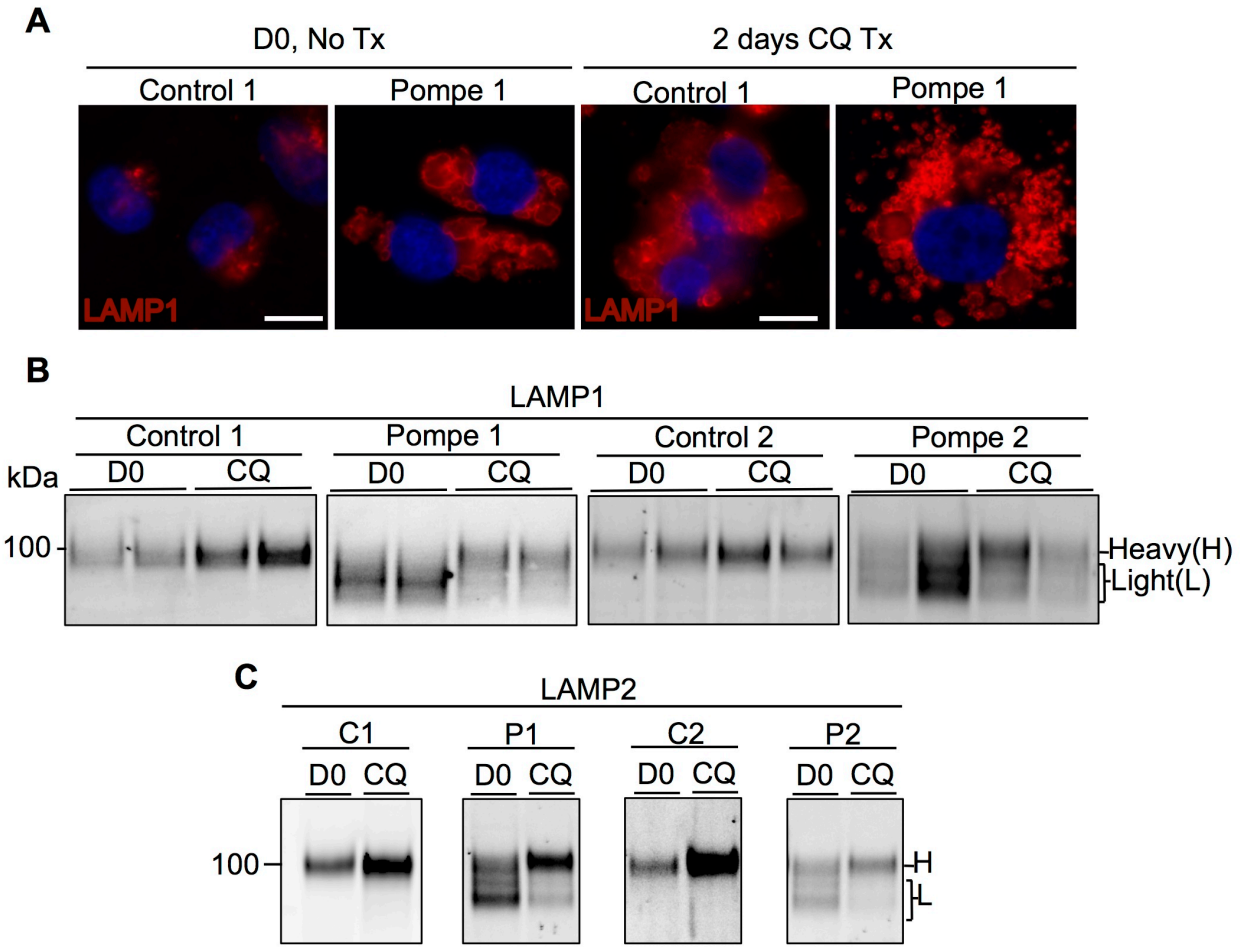
A
D0, No Tx
2 days CQ Tx
Control 1
Pompe 1
Control 1
Pompe 1
LAMP1
LAMP1
B
LAMP1
Control 1
Pompe 1
Control 2
Pompe 2
kDa
D0
CQ
D0
CQ
D0
CQ
D0
CQ
100
Heavy(H)
Light(L)
C
LAMP2
C1
P1
C2
P2
D0 CQ
D0 CQ
D0 CQ
D0 CQ
100
H
L

Chapter 5:

Glycosylation study of the lysosomal associated membrane proteins (LAMPs) in Control and Pompe iPSC-CMs

In the previous 2 chapters, I tested existing hypotheses on the mechanisms of Pompe cardiomyopathy, namely contractile and autophagic dysfunction. I could find neither in our iPSC-CM model. With time running out for my PhD studies, I decided to follow up on a peculiar finding made in the last chapter, one that had actually been observed during the ECT studies, but was disregarded as trivial. The key observation was of LAMP1 (and LAMP2) from Pompe iPSC-CMs having a lower apparent molecular weight (higher mobility) after separation by SDS-PAGE and immunodectection than LAMPs from Control iPSC-CMs. My decision to pursue the cause of higher mobility LAMPs in Pompe cardiomyocytes proved to be the most productive aspect of my thesis, and is my truly novel contribution to our understanding of Pompe disease.

"In the fields of observation, chance favors only the prepared mind" – Louis Pasteur, December 7, 1854. Lille, France.

Additional Background

The lysosomal associated membrane proteins (LAMPs) are heavily glycosylated by N- and O-linked ER-to-golgi glycosylation. The peptide maps of both LAMP1 and LAMP2 showing the sites of glycosylation are given below.

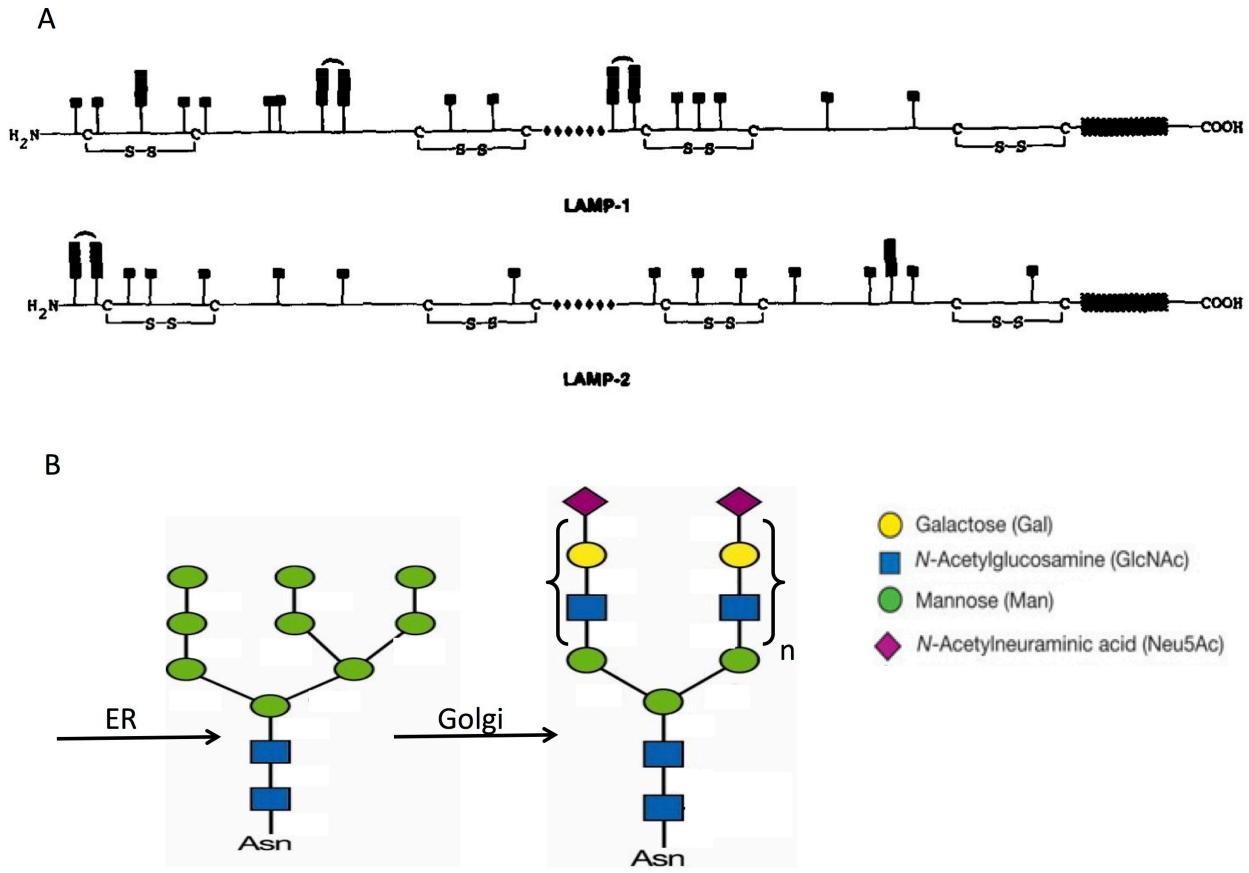

Image 5 Glycosylation Profile of the LAMPs **A.** N- to C-terminus maps of the LAMPs showing the N-linked sites of glycosylation represented by the squares and rectangles. O-linked glycosylation occurs in the middle linker region denoted by circles (80). **B.** N-linked glycan chains are added in the ER with $(GlcNac)_2$ attached to asparagine residues and harbor a complex mannose tree. In the Golgi, the mannose tree is trimmed to a tri-mannose structure and other sugars are added. In the LAMPs, the disaccharide (Gal-GlcNac) is repeated many times to form a poly-N-acetyllactosamine polymer. In panel A, the squares represent shorter polymers with n

= 1-4 while the rectangles are of longer chains with n = 15-20. An arc between two rectangles means one or the other N-linked chain has a long polymer. Usually, the N-linked glycans are capped by a class of charged sugars called N-acetyl-neuraminic acid.

The core peptides of LAMP1 and LAMP2 are calculated at 42 kDa, however, the observed weights are between 100-125 kDa depending on cell type (81). The additional molecular weight is due to the extensive glycosylation with significant contribution by the poly-N-acetyllactosamines chains added in the golgi apparatus.

Within the golgi apparatus, the cis- and trans- compartments have differential functions in N-linked glycan processing as shown in image 6 below.

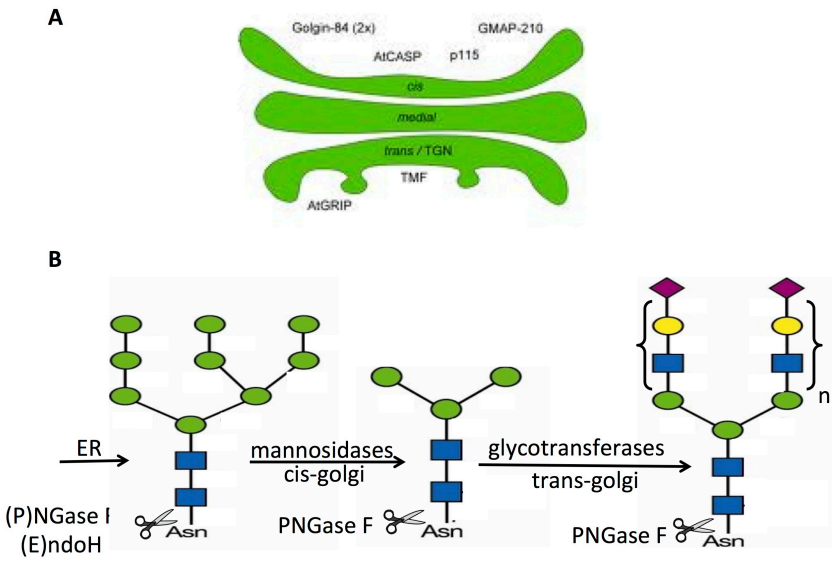

Image 6 Dissection of golgi-based glycosylation A. The golgi apparatus can be divided into cis, medial, and trans membranes that form a stacking structure. B. In the cis golgi the mannose tree is trimmed to a tri-mannose structure. Complete trimming to tri-mannose is required for the addition of other sugars in the trans-golgi. The endoglycosidase PNGaseF is able to cleave all N-linked glycan chain regardless of their level of processing by the golgi. However, Endoglycosidase H (EndoH) is only able to cleave an N-linked chain if it has **not** been processed

by the cis-golgi. That is, if the cis-golgi mannosidases do not form the tri-mannose structure, the EndoH will be able to cleave the N-linked glycan.

Methods

Endoglycosidase Study Total protein lysates following biphasic extraction were redissolved in a 0.5% SDS/1% triton solution in buffer specific for either Endoglycosidase H (Promega) or PNGase F (New England Biolabs) treatment. Instructions and buffers given with each enzyme were followed.

Immunofluorescence Immunofluorescence methods were used as described in previous chapters with the permeabilization reagent being 20 μM digitonin. The antibodies Golgin-97 (life sciences) and GM130 (Abcam) were used to stain the trans and cis golgi, respectively.

Brefeldin A and Sucrose Treatment For Brefeldin A (BFA) treatment, cells were exposed to concentrations of 500 ng/mL for 2 days before harvesting. The BFA was made at 1 mg/mL in DMSO and diluted for use. For the sucrose treatment experiment iPSC-CMs were cultured for 1 week to 1 month in 100 mM sucrose mixed with the RPMI/B27 media used for routine feeding.

2-D Western Blotting Electrophoresis in 2 dimensions began with the carrier ampholine method of isoelectric focusing (IEF) according to (82,83) within a glass tube containing 4% polyacrylamide and 2% of pH 3-10 isodalt servalytes (Serva, Heidelberg, Germany) in a 9M urea buffer. IEF was performed for 9600 volt-hrs with WGA glycoprotein extracts from 4 million cells boiled in a 5%SDS/5%βME solution and then mixed with 9M Urea/2M Thiourea in a 1:1 ratio before being applied to the acidic end of the tube. Following IEF, the tubes were equilibrated for 5 minutes in 10% glycerol, 50 mM DTT, 2.3% SDS and 0.0625 M tris at pH 6.8 and then boiled for 5 minutes in a water bath. The tube gels were sealed on a stacking gel overlaying a 7% acrylamide separating gel. SDS-PAGE occurred for 4 hrs at 15 mA. The gel

was then transferred to PVDF membrane for 18 hours and 1 minute at 22 V with a criterion tank blotter in Towbin's buffer. Western blotting was then identical to that described for the 1-D method. The 2-D lectin blots were performed with biotin conjugated lycopersicon esculentum (Vector labs, cat. B-1175) and a streptavidin conjugated fluorophore.

Nucleotide Sugar Measurements by HPLC Nucleotide sugars were extracted from confluent contracting cultures of iPSC-CMs with an ice cold 50% acetonitrile aqueous solution after rinsing once with PBS. The cells were then scraped off the surface in the extraction solution, added to 1.5 mL tubes at 1/mL per tube, sonicated, and then pelleted via centrifugation. The supernatant was transferred to new 1.5 mL tubes and dried under vacuum and mild heat with rotation in a speedvac device. The dried pellets were then resuspended in ddH2O, sonicated, and insoluble were pelleted. Supernatant were transferred into a new tube. The nucleotide sugar extracts were then separated on a carbopac PA-1 anion exchange column as the stationary phase and as a mobile phased used solution A: 3 mM NaOH and solution B: 3 mM NaOH, 1.5 M Sodium Acetate in varying ratios according to this separation protocol: 15 minutes 80% solution A, 20% solution B; 30 minutes to 20% solution A, 80% solution B in a linear gradient; 10 minutes at 80% solution B; 5 minutes back to 80% solution A in a linear gradient. Eluting nucleotide sugars were measured at 267 nm to detect the uracil or guanosine rings on the nucleotide sugars (84). Data was collected with the chromeleon software in the laboratory of Dr. Xuejun Pan at the alternative energy institute at the University of Wisconsin-Madison. Peak identification was performed with standard solutions of the nucleotide sugars (NS) purchased from Sigma that were spiked into the cellular NS samples. Increases in peak area implied that the spiked NS corresponded to the peak that experienced an increase in area.

Results

Lysosomal membrane proteins are hypoglycosylated in Pompe iPSC-CMs –We decided to investigate the cause for the differences in mobilities of the LAMPs in the Pompe iPSC-CMs by focusing on glycosylation since both of these proteins are heavily glycosylated by traditional N- and O-linked ER-to-golgi glycan biosynthesis pathways. In addition, several of the N-linked adducts are modified by long poly-N-acetyllactosamines added in the golgi apparatus (80,81,85,86). To test the hypothesis that a deficit in golgi-based glycosylation is the source of lower molecular weight LAMP species, iPSC-CMs were exposed to brefeldin A (BFA), a fungal metabolite that causes collapse of the golgi-stacks (87). Immunolabeling of Control and Pompe iPSC-CMs for the cis-golgi marker GM130 and trans-golgi marker golgin-97 (Fig. 12A) confirmed that BFA treatment dismantled the golgi stack cis-to-trans orientation moving outwards from the nucleus. As a result of golgi disruption, Control iPSC-CMs harbored the higher mobility forms of LAMP1 and LAMP2 normally present in the Pompe group (Fig. 12B). Similarily, the Pompe iPSC-CMs treated with BFA show an increase in the intensity of the higher mobility LAMPs at the cost of the lower mobility species. Therefore, we were able to reproduce in the Control lines the immunoblotting pattern of the LAMPs unique to the Pompe lines by interfering with the Control iPSC-CM golgi's ability to glycosylate proteins. Moreover, the Pompe disease-specific LAMP patterns were exaggerated in the Pompe iPSC-CMs through golgi disruption.

Since Pompe iPSC-CMs had no overt golgi structural pathology, we next tested if the hypoglycosylation of the LAMP proteins was a general response to lysosomal expansion or specific to lysosomal glycogen accumulation occurring in Pompe disease. We cultured the iPSC-CMs in 100 mM sucrose to induce a "sucrosome" storage disorder (88). In high sucrose

concentrations, cells lacking invertase activity gradually accumulate cytoplasmic sucrose, which enters the endosomal/autophagic system and is ultimately trapped in the lysosome. Control 2 iPSC-CMs demonstrate the intended effect of lysosomal expansion marked by LAMP1 due to sucrose uptake (Fig. 12C). However, immunoblot detection of LAMP1 and LAMP2 following sucrose culture (Fig. 12B) revealed no changes in species mobility in the Control 1 and Control 2 iPSC-CMs, suggesting that the higher mobility LAMPs from Pompe cells is not due to lysosomal expansion from accumulation of a nonmetabolizable carbohydrate. Sucrose treatment did increase the lower mobility LAMP1 and LAMP2 band intensities in the Pompe lines, indicating that the new LAMPs being synthesized were undergoing correct golgi-glycosylation.

The LAMPs have a significant number of sialic acid sugars added in the golgi (89). We hypothesized that incomplete golgi-based glycosylation in Pompe iPSC-CMs that affects apparent molecular weight would also change the pI due to incomplete addition of charged sugars such as the sialic acids. To evaluate for this, we performed isoelectric focusing in 2-D polyacrylamide gel electrophoresis. LAMP1 and LAMP2 immunodetection following 2-D separation of Control 1 iPSC-CM WGA-enriched glycoprotein reveals LAMP2 compressed at the pH 4 acidic edge and LAMP1 separated as 2 species near the pH 4 edge (Fig 13A). The LAMPs from Pompe 1 iPSC-CMs were detected at more basic pIs, with LAMP2 at approximately pH 5 near the calculated pI of 5.13 and LAMP1 as a smear ranging from pH 5 out to the basic edge at pH 9 compared to a calculated pI of 8.84. These results are consistent with a reduction of sialylation of LAMPs in Pompe iPSC-CMs.

We examined the impact of BFA-induced golgi disruption on LAMP immunodetection patterns separated in 2-dimensions (Fig. 13A). Control iPSC-CMs treated with BFA demonstrated a subtle, basic shift of the 2 prominent LAMP2 species that forms a tail fading out

to pH 5 as the apparent molecular weight gradually decreases. Although faint, a new observed streak of lower molecular weight and higher pI was produced following incubation with anti-LAMP1. Therefore, the loss of golgi structure in control iPSC-CMs results in a loss of LAMP protein acidity, reflecting lost sialylation that usually occurs in the trans-golgi. Of note, Pompe iPSC-CMs exposed to BFA showed a paradoxical acidic shift of LAMP1 and LAMP2.

The molecular weight and pI of LAMP1 from Pompe iPSC-CMs is similar to that observed with BFA treatment of control cells, although the faint streak towards the basic end observed in Pompe LAMP1 was either below detection or not present in the Control cells treated with BFA. LAMP2 physical properties in Pompe cells, on the other hand, are not precisely replicated via Control cell BFA treatment; Pompe LAMP2 has a more basic pI than the majority of LAMP2 intensity from BFA treated Control cells.

The differences observed between the Pompe and Control iPSC-CM 1D LAMP2 patterns following BFA exposure are also detected after 2D separation. Treatment of Pompe and Control cells with BFA produced two distinct spots for LAMP2, but while the LAMP2 spots in BFA treated control cells were vertically distributed between 100 and 75 kDa (similar pIs), the LAMP2 distribution from BFA treated Pompe cells was of a horizontal nature below 75 kDa and of differing pIs.

To localize further the deficit of glycosylation, protein lysates were tested for endoglycosidase sensitivity. Treatment of lysates from iPSC-CMs with Endoglycosidase F, which cleaves all N-linked glycans at their base between asparagine and the N-acetylglucosamine attachment, produces a core LAMP2 protein with a molecular weight of 35 kDa (Fig. 13B). Since the initial N-linked glycan chain mass is added in the ER and the higher mobilities of Pompe LAMP1 and LAMP2 are only 0-25 kDa below those from control iPSC-

CMs, the 65 kDa mass reduction upon EndoF treatment supports an intact ER-localized glycan chain addition. To determine if LAMP proteins in Pompe iPSC-CMs are entering the golgi stacks for cis-golgi terminal mannose sugar removal from the N-linked oligosaccharides added in the ER, protein lysates were also subject to endoglycosidase H (EndoH) treatment. EndoH only cleaves N-glycans if they have not been processed by the cis-golgi enzyme α-mannosidase I (αManI) (90). Control and Pompe lines showed a subtle increase in LAMP2 mobility upon EndoH treatment, implying that a sub-population of N-linked glycans are being trimmed (Fig. 9B). Equivalent EndoH sensitivity between control and Pompe protein suggests the deficit in golgi processing is not from lack of entry into the golgi or the inaction of golgi-glycosidases, but by reduced golgi-glycotransferase activity during modification of the trimmed mannose core.

In contrast to the different mobilities of LAMP1 and LAMP2 in Pompe and Control iPSC-CMs, no differences in LAMP protein mobilities were observed in undifferentiated iPS cells (Fig. 13C). The cell type dependence of LAMP hypoglycosylation has implications for understanding the tissue-specific manifestation of Pompe disease pathology.

The 2-D blots in Fig. 13A show two types of staining distribution. The horizontal streak represents the loss of acidic sugars, with molecular weight decreasing gradually as the streak extends towards the basic end. Vertical streaks where there is a dramatic change in molecular weight at the same pI represents differences in glycosylation with neutral carbohydrates. Since the LAMPs are major carriers of poly-N-acetyllactosamines (80,91), we hypothesized that the majority of molecular weight reduction of the LAMPs from Pompe cells was due to loss of poly-N-acetyllactosamines and that other proteins may also lack this group, which is often modified with a charged sugar at the terminal end.

To compare total lactosaminoglycan containing proteins, iPSC-CM glycoproteins were

purified with WGA – a lectin with specificity for N-acetylglucosamine and the sialic acids – and separated in 2 dimensions. Then, blots were probed with lycopersicon esculentum lectin (LEL), which has binding specificity for poly-N-acetyllactosamine (92). Glycoprotein from Control 1 iPSC-CMs (Fig. 14A) shows prominent staining above 250 kDa. In marked contrast, Pompe 1 glycoprotein (Fig. 14B) has an intense vertical smear between 37 and 75 kDa.

Exposure to BFA produced similar changes to the LEL patterns that occurred with the LAMPs. Both control (Fig. 14C) and Pompe (Fig. 14D) LEL bound protein have a downward shift in molecular weight in response to BFA. Also like the LAMPs, BFA produces a basic shift in LEL positive protein from the Control cells, but an acidic shift in protein detected by LEL from Pompe cells. Therefore, the absence of abundant high molecular weight lactosaminoglycan containing proteins in the Pompe glycoprotein pool, present in Control iPSC-CMs, points to a general deficit of glycan chain extension with galactose and N-acetylglucosamine in the golgi apparatus.

In order to explain how why proteins in Pompe iPSC-CMs are hypoglycosylated in the presence of normal golgi structure, we hypothesized that their may be a deficiency of nucleotide sugars that represent the building blocks of all glycosylations. We isolated intracellular nucleotide sugars from confluent cardiomyocyte cultures an subjected the samples to ion-exchange HPLC to separate, identify, and quantify each of the major nucleotide sugars (NS) in Pompe and Control iPSC-CMs (84). We first optimized the method with iPS cells, since one needs approximately 25-30 million cells for such an analysis. The chromatograms from Control 2 and Pompe 1 iPS-cells (Fig. 15A) demonstrate equivalent NS concentrations. The true identity of the peaks was determined by spiking the samples with a known NS and looking for which peak increased in area due to the higher concentration of that NS. HPLC chromatograms are

given for the Control 1 and Pompe 1 iPSC-CMs (Fig. 15B). A major difference noticed was the absence of an ATP/UTP peak in the Pompe line that was present in the Control line.

Discussion

We unexpectedly found changes in the electrophoretic mobility of LAMPs in Pompe iPSC-CMs during the autophagy studies (chapter 4). These changes were determined to be due to golgi-based hypoglycosylation of the LAMPs which typically include poly-N-acetyllactosamine and sialic acid. These studies unmask a previously unknown abnormality in protein processing in Pompe iPSC-CMs with features of hypoglycosylation similar to other congenital disorders of glycosylation (CDG) that also manifest hypertrophic cardiomyopathy (93-95). For example, hypoglycosylated LAMP2 has been observed in Cohen's syndrome – caused by mutations in a protein necessary for normal golgi structure (96). In two other CDG caused by loss of golgi organization due to mutations in the conserved oligomeric Golgi (COG) complex (97) or TMEM165 (98), LAMP2 is also reported as hypoglycosylated in HeLa cells or HEK293 cell culture models, respectively.

The LAMPs undergo extensive sialyation – 36.4 and 23.6 moles of sialic acid are added per mole LAMP1 or LAMP2, respectively (81). The higher pIs of LAMPs from Pompe iPSC-CMs is consistent with a major deficiency of sialic acid sugar transfer. Hyposialylation is a common, diagnostic feature of CDG (99-101).

The differences in the LEL binding pattern between Control and Pompe iPSC-CM glycoprotein is similar to LEL affinity data from type II CDGs where there is a loss of glycosidase or glycotransferase activity in the golgi. In the case of congenital dyserythropoietic anemia type II, a complete loss of LEL binding to erythrocyte membrane proteins separated by SDS-PAGE is common in patients (102). In CDG type IIa caused by lost N-

acetylglucosaminyltransferase II activity, LEL reactive erythrocyte membrane proteins have a downward shift in molecular weight compared to controls (103).

A key similarity amongst many of the CDGs is either a disruption of golgi structure, or the loss of a glycoprocessing protein's activity (104,105). In our work, we could not identify any obvious disruption in golgi stack structure nor does GAA have a known role in protein glycosylation. We speculate that a link between insufficient GAA activity and hypoglycosylation is secondary to changes in glycogen metabolism. A recent publication using a mouse model of Pompe Disease (33) demonstrated dramatically increased activity of glycogen synthase concomitant with reduced glycogen phosphorylase activity, particularity in the heart. Since glycogen synthesis and the nucleotide sugar synthesis pathways both use UTP and glucose-6-phosphate as substrates, perhaps these reactants are being disproportionately consumed in glycogen synthesis resulting in limited nucleotide sugar concentrations for golgi glycotransferase reactions.

Based on this reasoning, the ability for the acidotrope CQ to reverse the hypoglycosylation (chapter 4) could arise from the neutralization of the cis-to-trans golgi pH gradient, thereby slowing transport of proteins through the golgi (106), giving the LAMPs more time to be glycosylated in the environment of low substrate concentrations (86). That we observed no differences in LAMP mobility from the accumulation of lysosomal sucrose in Control iPSC-CMs is also supportive of glycogen biology being related to the observed hypoglycosylation. Glycogen storage disease (GSD) type 1b has also been identified as a CDG (107), giving precedence to a relationship between abnormal glycogen metabolism in a glycogen storage disorder (Pompe disease is also known as GSD type II) and deficits in golgi-glycosylation (108).

We attempted to address the limitation in nucleotide sugar hypothesis due to a disruption in glycogen metabolism by measuring nucleotide sugar (NS) concentrations with ion exchange HPLC. The measurements were excellent for iPS cells by using an icecold acetonitrile extraction protocol and showed that there was no significant differences between Pompe and Control iPS cell NS extracts. Comparisons of the iPSC-CMs was limited to one measurement each because of the enormous number of cardiomyocytes (25-30 million) needed for 1 measurement. We found that the UTP peak was absent in the Pompe iPSC-CMs, however, measurements might not be valid since the UTP peak is shared with ATP, which was very low in the Control and absent in the Pompe iPSC-CMs. We do not think that all the ATP was consumed during the time it takes to add the acetonitrile solution to the cells, so something may be confounding this measurement. ATP peaks in the iPS cells were prominent. Perhaps extraction from more iPSC-CMs will be necessary for conclusive measurements.

In conclusion, the iPSC-CM model of Pompe disease was used to identify a golgi-based glycosylation deficit potentially central to Pompe cardiac pathophysiology that gives reason to pursue therapeutic avenues aimed at restoring normal glycoprocessing. Future studies will be needed to define how the loss of lysosomal glycogen degradation in Pompe disease can cause changes in protein glycosylation and if hypoglycosylation of proteins (109-111) and lipids (112,113) involved in cardiomyocyte contractile function are implicated in the cardiomyopathy. Pompe iPS cell models will provide access to various human cell types relevant for further investigation of the disease and its treatment.

Figure Legends

Fig. 12. Effect of golgi structural disruption and induction of an artificial lysosomal storage disorder on LAMP1 and LAMP2 from Control and Pompe iPSC-CMs. A. The golgi apparatus stained with cis- and trans-golgi marker GM130 and Golgin-97, respectively, in Control and Pompe iPSC-CMs and after treatment with BFA. Scale bars = 10 μm. **B.** Immunoblots of LAMP1 and LAMP2 from iPSC-CMs with no treatments (No Tx), after 2 days of 500 ng/mL brefeldin A (BFA) treatment, and after 2-weeks of culture in 100 mM sucrose (S). GAPDH functions as the loading control **C.** Lysosomes stained with LAMP1 before and after 2-weeks of sucrose treatment in Control 2 iPSC-CMs. Scale bar = 10 μm. All nuclei are stained with DAPI in blue.

Fig. 13. Glycosylation analysis of LAMPs from Control and Pompe iPSC-CMs via 2-D glycoprotein separation and endoglycosidase treatment A. Glycoprotein extracts separated by pI and molecular weight along the horizontal and vertical axes, respectively. LAMP1 and LAMP2 were probed and detected separately and sequentially. Representative blots are of protein from Control 1 and Pompe 1 cells with and without BFA treatment. The region of the Control 1 blot within the square and marked by a "*" is expanded to the right of panel A. **B.** Endoglycosidase analysis of LAMP2 protein in Control 2 and Pompe 2 iPSC-CMs. Endoglycosidase F (EndoF) cleaves all N-linked glycan chains, revealing the core peptide chain with only O-linked glycosylations remaining. Endoglycosidase H (EndoH) cleaves N-linked glycan chains that have not yet been processed by α-mannosidase I in the cis-golgi. **C.** LAMP1 and LAMP2 immunoblots from undifferentiated iPS cell protein lysates.

Fig. 14. Lycopersicon Esculentum (tomato) lectin blots of 2-D separated glycoprotein from Control and Pompe iPSC-CMs A. Lectin probed PVDF membrane (lectin blot) containing

control 1 glycoprotein. The red arrow points to a reference streak flanked by clear areas. **B.** Lectin blot of Pompe 1 glycoprotein. The red arrow denotes a staining density of interest. **C.** Lectin blot of glycoprotein from Control 1 cells that have been treated with BFA. The red arrow points to the reference streak observed in panel A (the one flanked by clear areas). **D**. Glycoprotein from Pompe 1 cells treated with BFA and probed with tomato lectin. The red arrow tentatively identifies the same proteins marked in panel B. All PVDF membranes were imaged with the same exposure duration.

Figure 15 Ion Exchange HPLC elution chromatograms of nucleotide sugars from Control and Pompe iPS cells and IPC-CMs. A. Elution profile of nucleotide sugars (NS) from Control 2 and Pompe 1 iPS cells. **B.** NS profile from Control 1 and Pompe 1 iPSC-CMs. Peaks are labeled with NS identities.

Figure 12

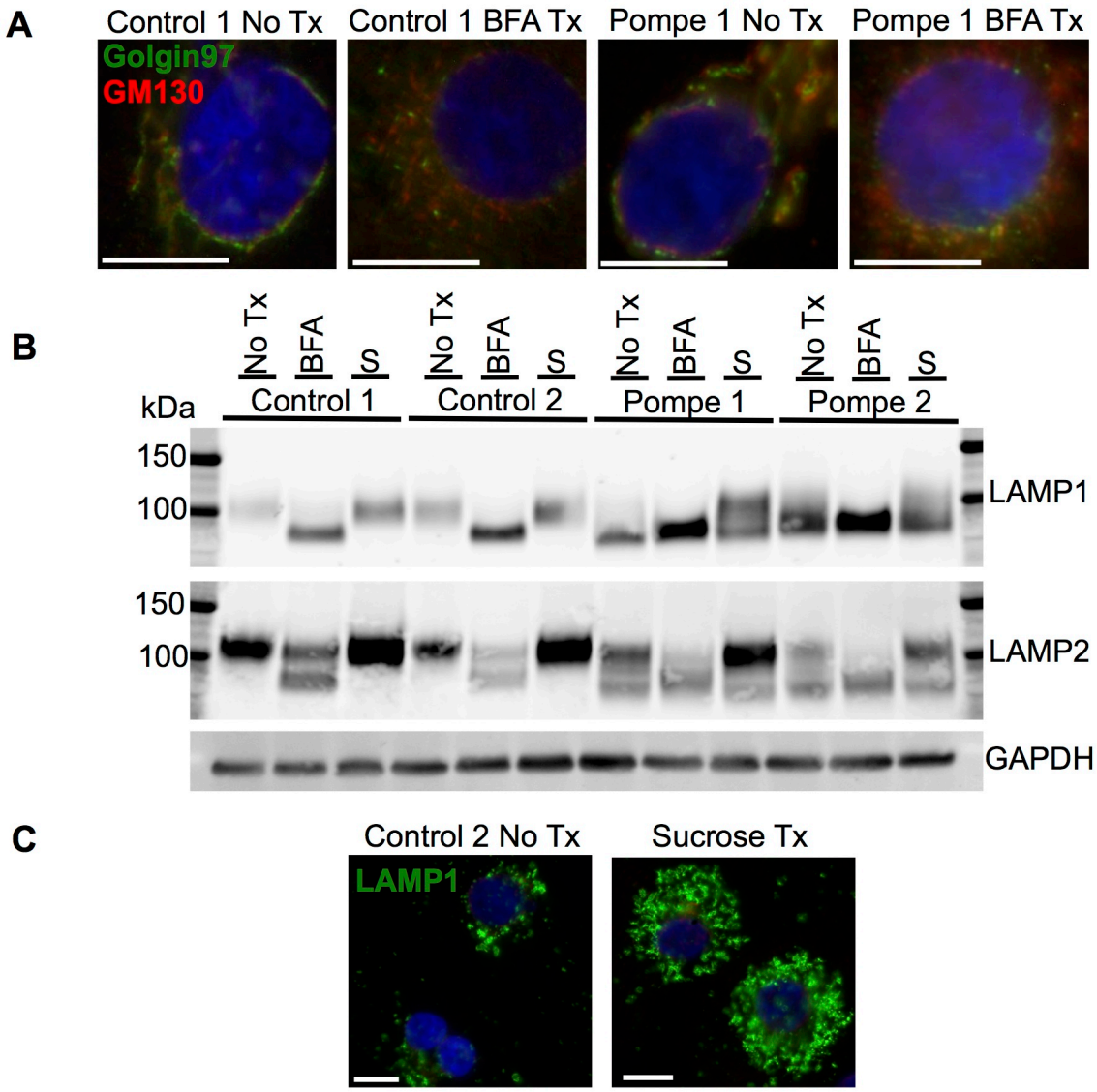
A
Control 1 No Tx
Control 1 BFA Tx
Pompe 1 No Tx
Pompe 1 BFA Tx
Golgin97
GM130
B
No Tx
BFA
S
Control 1
Control 2
Pompe 1
Pompe 2
kDa
150
100
LAMP1
150
100
LAMP2
GAPDH
C
Control 2 No Tx
Sucrose Tx
LAMP1

Figure 13

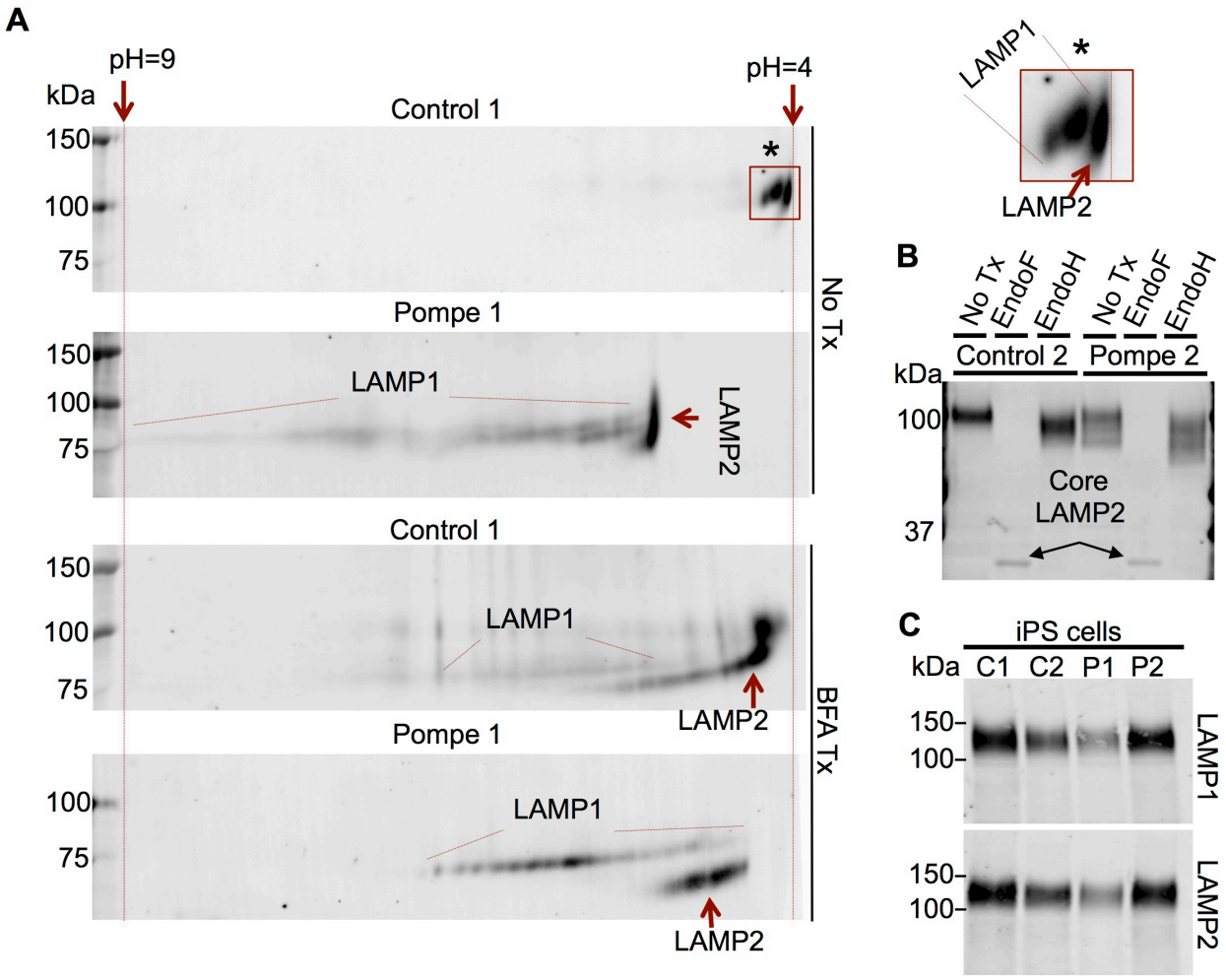
A
pH=9
pH=4
kDa
Control 1
150
100
75
*
Pompe 1
LAMP1
LAMP2
No Tx
Control 1
LAMP1
LAMP2
Pompe 1
LAMP1
LAMP2
BFA Tx
LAMP1
*
LAMP2
B
No Tx
EndoF
EndoH
No Tx
EndoF
EndoH
Control 2
Pompe 2
kDa
100
37
Core
LAMP2
C
iPS cells
kDa
C1
C2
P1
P2
150-
100-
LAMP1
150-
100-
LAMP2

Figure 14

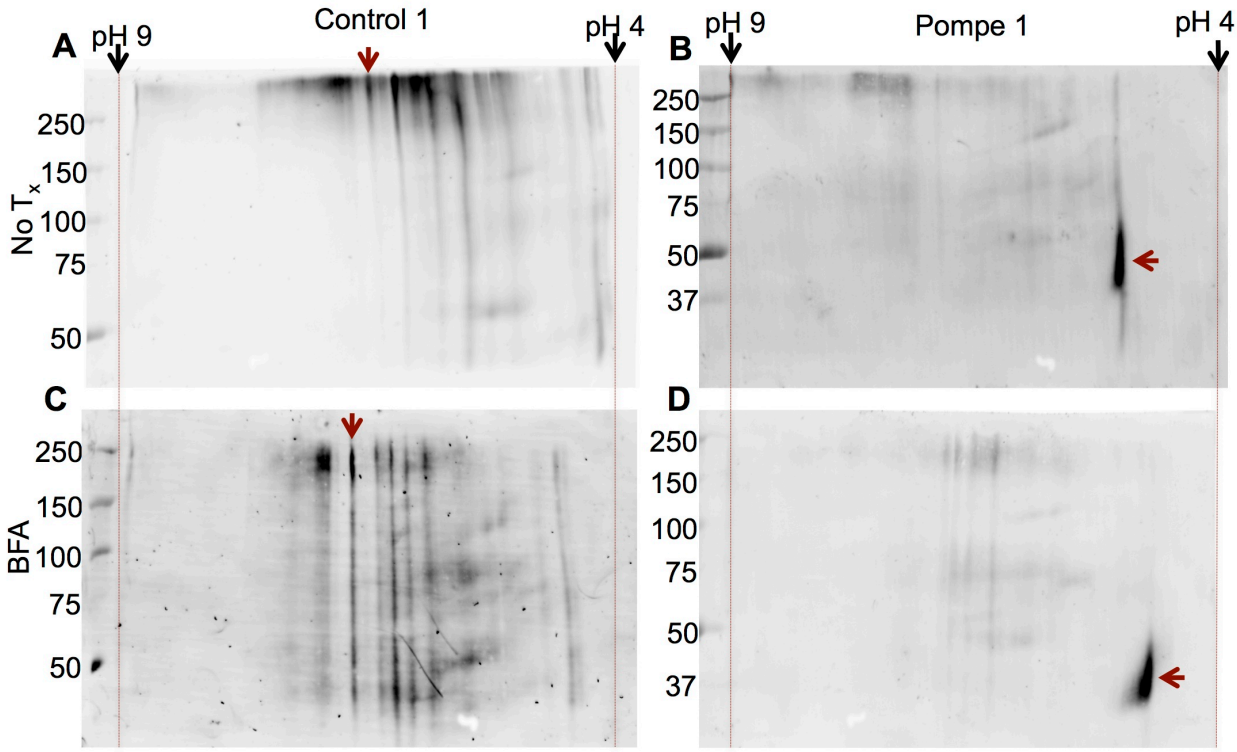
A
pH 9
Control 1
pH 4
250
150
100
75
50
No Tx
B
pH 9
Pompe 1
pH 4
250
150
100
75
50
37
C
250
150
100
75
50
BFA
D
250
150
100
75
50
37

Figure 15

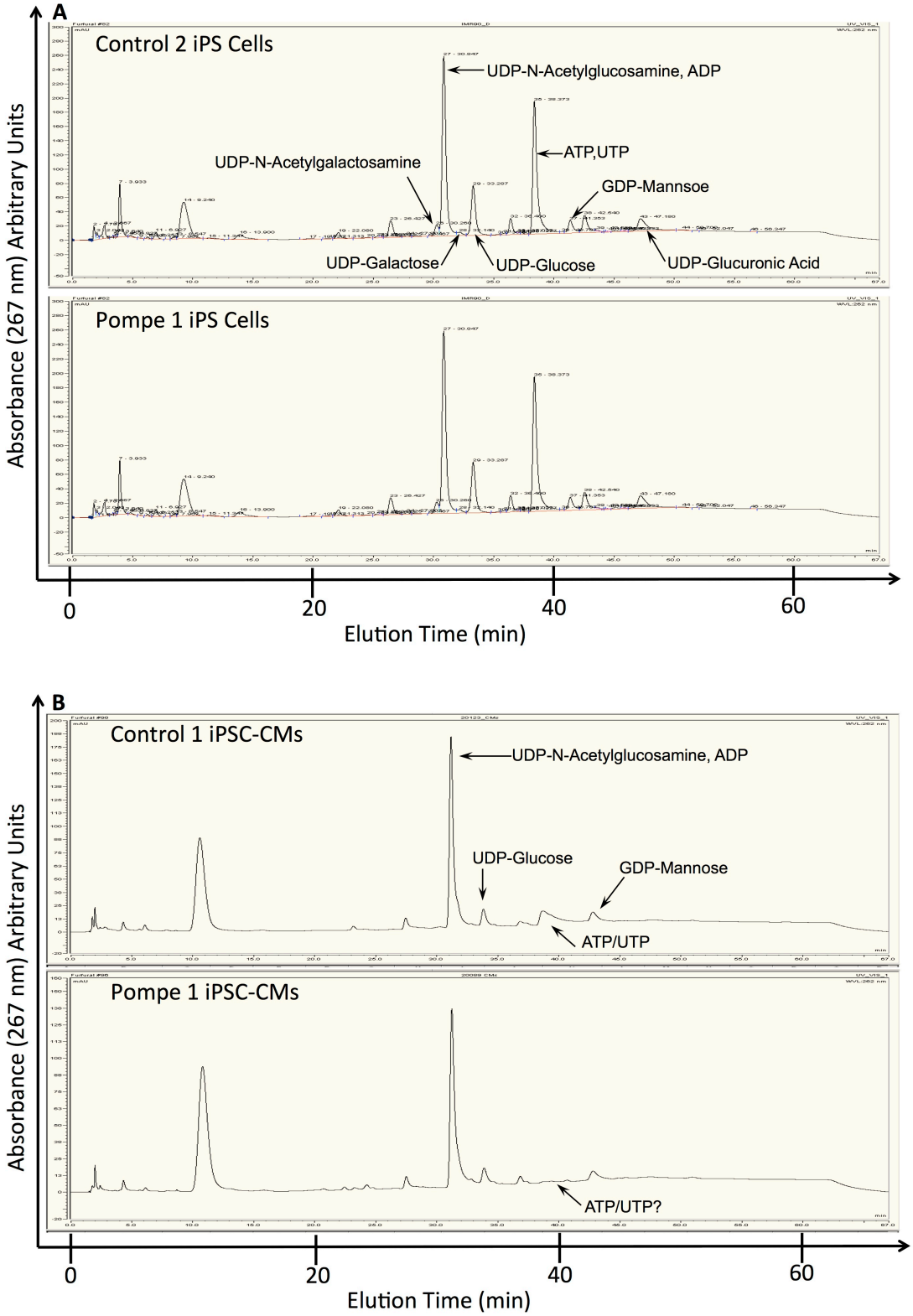
A
Control 2 iPS Cells
UDP-N-Acetylglucosamine, ADP
ATP,UTP
UDP-N-Acetylgalactosamine
GDP-Mannsoe
UDP-Galactose
UDP-Glucose
UDP-Glucuronic Acid
Pompe 1 iPS Cells
Absorbance (267 nm) Arbitrary Units
0
20
40
60
Elution Time (min)
B
Control 1 iPSC-CMs
UDP-N-Acetylglucosamine, ADP
UDP-Glucose
GDP-Mannose
ATP/UTP
Pompe 1 iPSC-CMs
ATP/UTP?
Absorbance (267 nm) Arbitrary Units
0
20
40
60
Elution Time (min)

Chapter 6:

The Glycosylation and Function of α-Dystroglycan

Although our characterization of LAMP protein hypoglycosylation supports the hypothesis that Glycogen Storage Disorder (GSD) type II (Pompe disease) may be a congenital disorder of glycosylation (CDG), we were lacking a distinct mechanism by which hypoglycosylation could lead cardiomyopathy. We asked the question, does a protein exist that 1) is necessary for normal cardiomyocyte function, 2) requires golgi-based glycosylation to carry out it's function, and 3) if incorrectly glycosylated in the golgi, results in cardiomyocyte dysfunction? Surprisingly, the answer was yes. This chapter characterizes the protein that met our 3 criteria, named α-Dystroglycan, in Pompe and Control iPSC-CMs.

Additional Background

After discovering that there was a glycosylation deficit in Pompe iPSC-CMs by studying LAMPs, we tried to extend the hypoglycosylation deficit to a protein involved in contractile function that requires correct glycosylation for its function. That is, we were looking for a protein that without correct golgi-based glycosylation would not function correctly and as a result of its malfunction, would change the way in which the cardiomyocyte contracts. After much searching, we identified the dystroglycan protein complex as our next target of investigation. The dystroglycan complex is a part of the larger dystrophin complex that links the sarcomeres at the Z-lines to the cell membrane and ultimately the extracellular matrix (ECM) (114). Although multiple proteins are involved, the link from the cell membrane to the ECM is facilitated by α-dystroglycan, which is able to bind to laminin (an ECM protein) via interaction of laminin with its golgi added O-linked glycosylations. Schematics of the dystrophin-dystroglycan complex are given below (115).

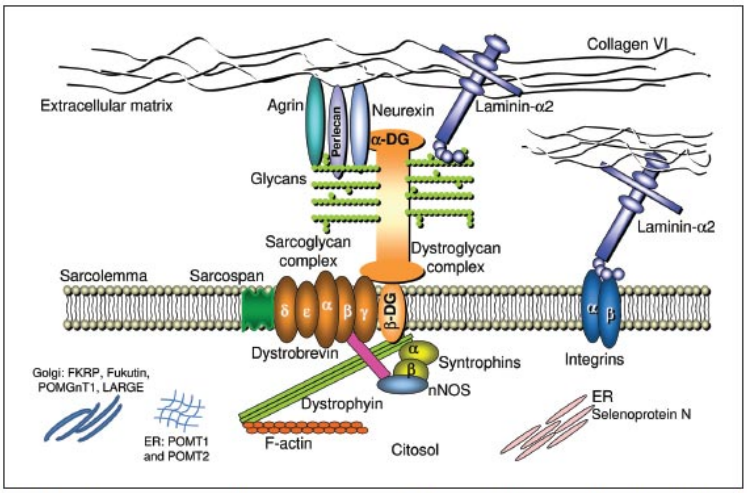

Image 8 Cartoon diagram of the dystrophin complex α-dystroglycan (DG) binds laminin in the ECM and interacts with its intramembrane subunit β-DG. Although multiple proteins are

involved, β-DG binds to the filamentous protein dystrophin, which is responsible for attaching to a single Z-line.

The single dystroglycan peptide is cleaved into two after synthesis into the ER to form the α- and β- dystroglycan (DG) chains. The α-DG experiences glycomanipulation in the ER by protein O-mannosyl transferase 1 and 2 (POMT1 and POMT2) that adds a mannose sugar to either a serine or threonine to begin the atypical α-DG glycosylation process that allows for laminin binding (116). In the golgi, α-DG is further manipulated by protein O-linked mannose N-acetylglucosaminyltransferase 1 (POMGNT1) and then by the most important glycotransferase called Like-acetylglucosaminyltransferase (LARGE) that extends the O-linked glycan with the disaccharide repeat (xylose-glucuronic acid)$_n$(117,118). This disaccharide repeat forms the binding site to laminin at the laminin globular (G) domains. The more disaccharide repeats that exist, the more laminin molecules are able to bind.

The loss of α-DG glycosylation results in an inability to bind laminin and a breakdown of the dystrophin complex (119). The function of the dystrophin complex is to link all the sarcomeric units to each other and to the extracellular space, which all have to contract in unison for effective movement. If there is no link between each sarcomere through the muscle to the ECM, then contractile force will not be equally distributed to the membrane and ECM, causing localized regions with higher and lower amounts of stress. These stresses will cause tears in the membrane, which ultimately lead to muscle necrosis through irreparable leaking of ions that maintain a cells electrochemical gradient. The global distribution of the dystrophin complexes form a beautiful pattern upon immunostaining of a dystropin complex associated protein that mirrors the organization of the sarcomeres. This patterning is called the “costamere” and an example is given below (120).

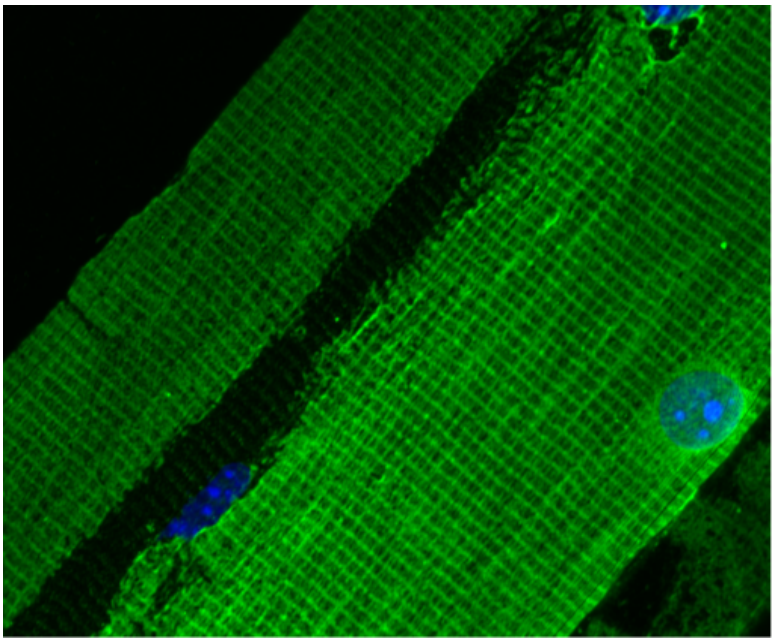

Image 9 Costameric structure of an isolated mouse ventricular myocyte. Vinculin staining, a protein of the dystrophin complex, reveals complex patterning that mirrors the sarcomeric arrangement throughout the cell.

The major diseases that are caused by lack or complete loss of the dystrophin protein are called Becker or Duchenne muscular dystrophy, respectively. In these diseases the costameric network shown above is destroyed and cause progressive skeletal muscle wasting that presents early in life and will lead to death if respiratory support is not given (the muscles of respiration are affected). Cardiac function also suffers from dilated remodeling that will lead to systolic dysfunction. From the clinical descriptions, the features of muscular dystrophy are similar to the presentation of Pompe disease, with skeletal and cardiac muscle being the primary sources of pathology. With our finding that a golgi based glycosylation deficit existed, we had the idea that perhaps in Pompe disease there was hypoglycosylation of α-DG, resulting in skeletal and cardiac muscle dystrophy. That is, perhaps Pompe disease was actually a form of muscular dystrophy!

Ultimately, we were unable to find hypoglycosylation of α-DG in the Pompe iPSC-CMs. In addition, both Pompe and Control iPSC-CMs were able to bind laminin to an equivalent extent in a α-DG specific manner. Therefore, we had to conclude that the glycosylation of α-DG was unaffected by Pompe etiology. Hypoglycosylated α-DG is a very specific kind of CDG that does not involve the N-linked glycan deficits observed in Pompe iPSC-CMs. All known α-DG CDGs are caused by mutations in specific glycotransferases involved in its non-classical synthesis pathways that do not affect the glycosylation of other proteins. Since we have identified a glycosylation deficit that affects the traditional N-linked pathway through the addition of N-acetylglucosamine, galactose, and sialic acids, it is logical that α-DG is correctly glycosylated in Pompe disease.

Methods

Dystroglycan Enrichment and Detection The dystroglycan complex was enriched from total protein lysates by using WGA-agarose beads purchased from Vector Labs. Total protein lysates were extracted from cells with 1% triton x-100 and incubated with the beads (100 μL beads/400 μL cell lysate from 1 million cells) overnight at 4 C. After washing with 0.1% triton x-100, the beads were boiled in 5% SDS (150 μL). The SDS solution then subjected to biphasic extraction (methanol/chloroform/water) and the precipitated glycoprotein dried for 5 minutes before being resolubilized in 5% SDS for 1D-western blotting. α-DG was detected with antibodies to the glycoepitopes required for laminin binding (clones IIH6c4 and VIA4-1 from the DSHB). β-DG was detected with clone 43DAG1/8D5 from abcam.

Laminin overlay assays Laminin binding to α-DG separated and immobilized on the PVDF membrane was performed according to (119). Briefly, EHS laminin (sigma, L9393) was incubated with the blot overnight, washed, and the incubated with an anti-laminin antibody (Sigma). For the live cell laminin overlay EHS laminin was added to the cell culture media at 10 μM for 2 days, the cells were fixed, and detected with the anti-laminin antibody.

Results

The golgi-based glycosylation and laminin binding capability of α-dystroglycan is preserved in Pompe iPSC-CMs– From the finding that the deficit of Pompe LAMP glycosylation was in the golgi, we hypothesized that α-dystroglycan (αDG) is also hypoglycosylated in Pompe iPSC-CMs, since αDG undergoes O-linked glycosylation via the like-acetylglucosaminyltransferase (LARGE) located in the golgi (121). The disaccharide polymer (xylose-glucuronic acid)$_n$ (117) added by LARGE function as the binding domain for laminin that when lacking cause a class of muscular dystrophies called the dystroglycanopathies (117,119,122). Since Pompe disease shares a similar clinical presentation with dystroglycanopathies (123), we tested the hypothesis that a loss of laminin binding by αDG contributes to Pompe cardiomyopathy.

Antibody clones IIH6c4 and VIA4-1 that only recognize the LARGE processed form of αDG (124,125) were used in quantitative immunoblot assays of WGA-enriched glycoprotein extracts from Pompe and control iPSC-CMs. The glycosylated αDG (VIA4-1, IIH6c4) to βDG band density ratios were the same between Pompe and Control iPSC-CMs (Fig. 16A and 16B), implying that a consistent Pompe deficit of αDG glycosylation did not existed. To confirm that glycosylated αDG in Pompe iPSC-CMs was functionally able to bind laminin, we performed a laminin overlay assay. Both control and Pompe iPSC-CMs exhibited comparable αDG specific laminin binding (Fig. 16B and 16C). As a final test, a dramatic increase in surface laminin fluorescence following 2 days of culture in laminin containing media occurred in both Control and Pompe iPSC-CMs in Fig. 16D and 16E, respectively. The co-localization of IIH6c4 and laminin fluorescence is in support of αDG mediated laminin binding (126,127).

We also looked at costamere development in Pompe and Control iPSC-CMs. We used antibody against the α2 domain of laminin, the specific part of the laminin molecule that binds to

the glycosylations of α-DG and an antibody against vinculin, an intracellular protein that associates with the dystrophin complex. The laminin α2 protein formed a rib-like pattern over the myofilaments (Fig. 17A). One can appreciate the alternating pattern between the myosin heads stained in red and laminin α2 stained in green that aligns on the extracellular surface above the z-lines of the sarcomere (Fig. 17B). For the laminin α2 staining, cells were not permeabilized to ensure that the staining was only extracellular. The patterning of laminin on the myofilaments was a rare occurance in a population of cardiomyocytes. Most of the time the laminin stain resembled a large lake in the middle of a cell (Fig. 17A). The vinculin staining pattern also has examples of costameric patterning over myofilaments (Fig. 17C). Laminin α2 and vinculin patterns were also noted in Pompe iPSC-CMs. Thus, iPSC-CMs have the potential to form advanced costameric patterns similar to skeletal muscle myotubes (128).

Discussion

Given the known pathology of hypoglycosylated αDG resulting in a loss of laminin binding in a subset of muscular dystrophies, which can have associated cardiomyopathies (129,130), we examined the glycosylation of αDG specifically. We did not detect differences in αDG glycosylation or laminin binding between Pompe and Control iPSC-CMs, suggesting that this specific glycosylation pathway is intact in Pompe disease and unlikely to be central to the pathophysiology.

The presence of costameres in iPSC-CMs has not been reported in the literature and so demonstrates that these differentiated cardiomyocytes are capable of higher order CM structures. Using the presence of costameres as a marker for maturation may be useful in future methods that aim to produce an adult-like cardioymocyte from iPSC-CMs cells.

Figure Legends

Fig. 16. Dystroglycan glycosylation and laminin binding in Control and Pompe iPSC-CMs **A.** Immunoblots of glycoprotein from both control (C1, C2) and Pompe (P1, P2) iPSC-CMs probed with anti-αDG antibodies IIH6c4 and VIA4-1 that exclusively detect the laminin binding glyco-epitope. Each lane within 1 cell line represents protein from iPSC-CMs differentiated from different iPS cell passages. **B.** Laminin overlay assay to measure laminin binding ability specific to α-DG. Binding of laminin occurs at the molecular weight of αDG recognized by IIH6c4 and VIA4-1. **C.** Quantification of α/β dystroglycan ratios in panel A and laminin binding to βDG ratios in panel D. No significant differences were noticed between control and Pompe groups. **D&E.** Laminin and αDG (IIH6c4) immunofluorescence of iPSC-CMs fixed after 2 days of incubation with exogenous laminin (bottom row) compared to normal culture conditions (top row) in Control 2 (**D**) and Pompe 2 (**E**) iPSC-CMs. Scale bar = 20 μm. All nuclei are stained with DAPI in blue.

Figure 17 Costameres in iPSC-CMs as visualized by Laminin and Vinculin immunostaining A. An example of Laminin α2 costameric patterning in Control 2 iPSC-CMs at the whole cell level. **B.** Positional relationship between Laminin α2 and MHC immunostaining at the myofilament level. **C.** Vinculin immunostaining in Control 2 iPSC-CMs. All scale bars = 10 μm and DAPI stains the nuclei blue.

Figure 16

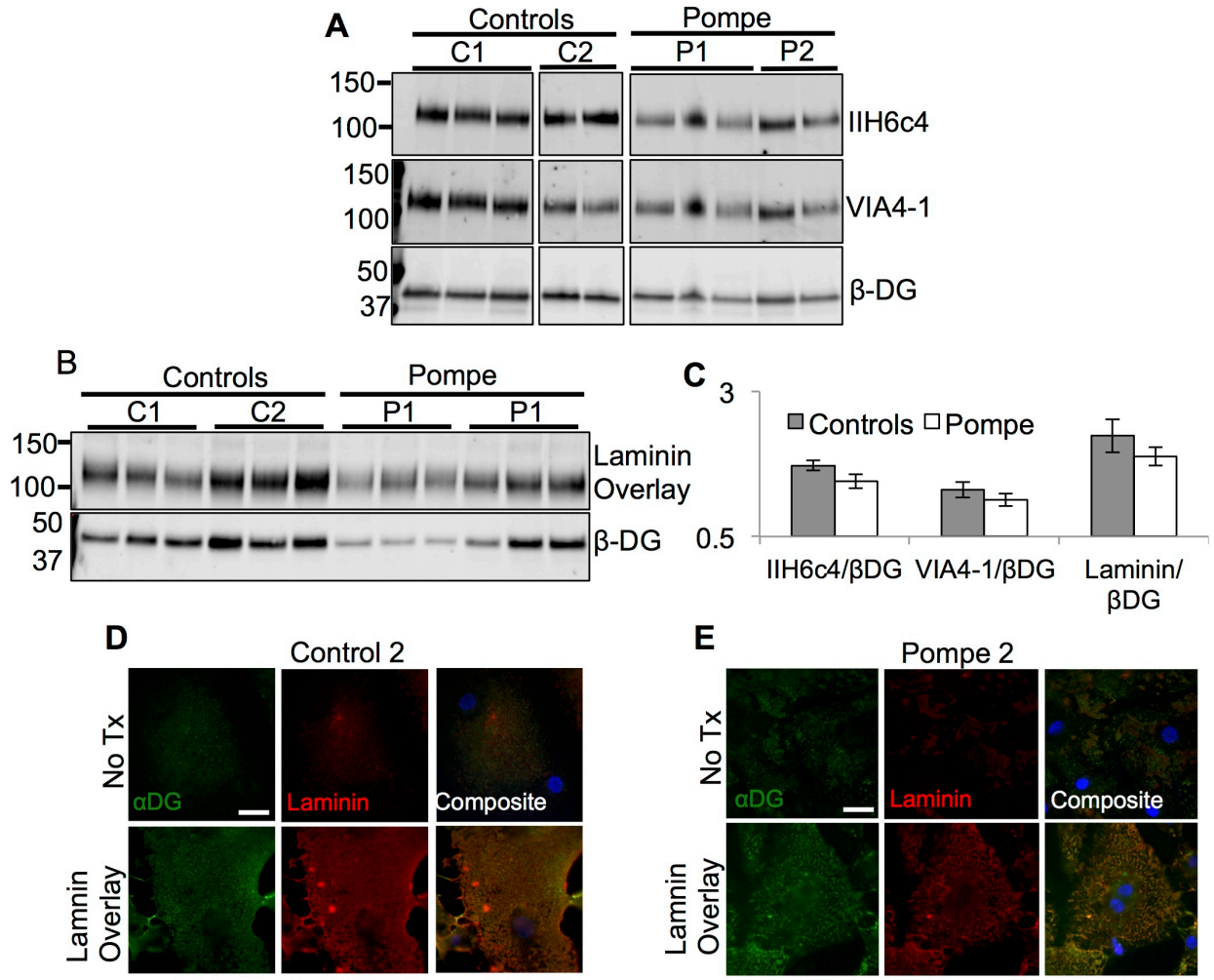
A
Controls
Pompe
C1
C2
P1
P2
150
100
150
100
50
37
IIH6c4
VIA4-1
β-DG
B
Controls
Pompe
C1
C2
P1
P1
150
100
50
37
Laminin Overlay
β-DG
C
3
0.5
Controls
Pompe
IIH6c4/βDG
VIA4-1/βDG
Laminin/ βDG
D
Control 2
No Tx
Lamnin Overlay
αDG
Laminin
Composite
E
Pompe 2
No Tx
Lamnin Overlay
αDG
Laminin
Composite

Figure 17

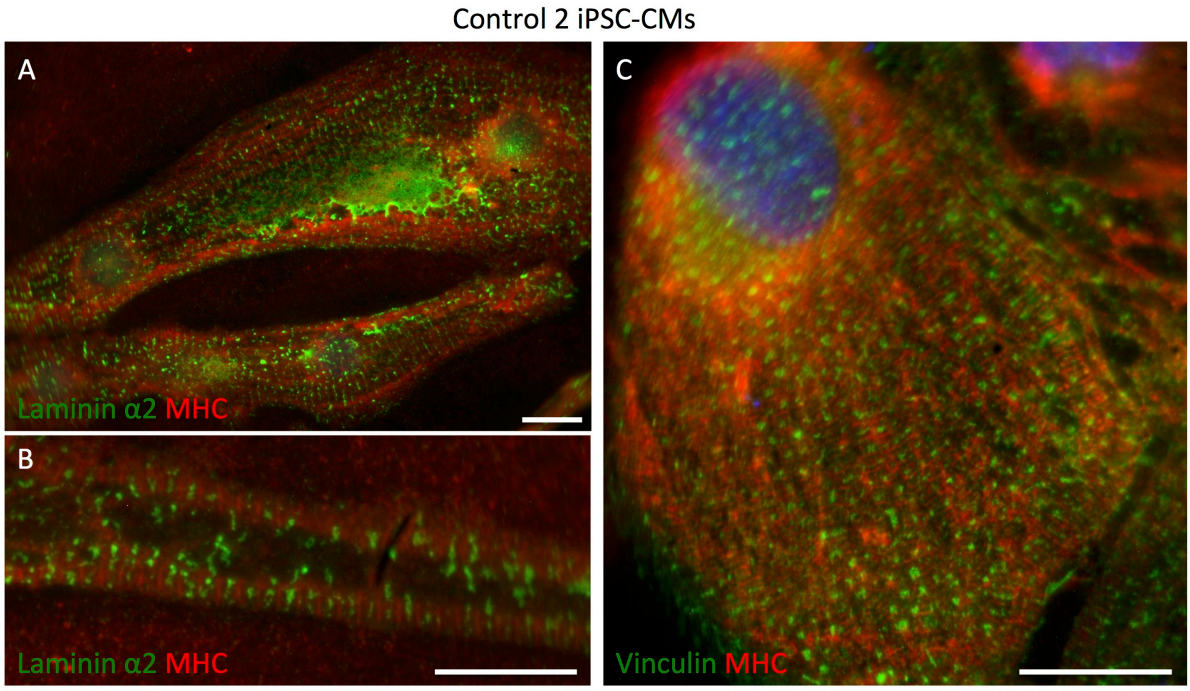
Control 2 iPSC-CMs
A
Laminin α2 MHC
B
Laminin α2 MHC
C
Vinculin MHC

Chapter 7: Future Directions

I had the opportunity to listen to a talk by Oliver Smithies, father of the mouse model, at an American Heart Association meeting. He took us through his scientific career, with his laboratory notebooks as a guide. Concepts that are common knowledge today were just being discovered during his time in graduate school; in one example he showed us part of his preliminary exam where he was asked to predict the metabolites involved in mitochondrial oxidative respiration. Today this process is called the tri-carboxylic acid cycle (Kreb's cycle) and I will say his answer was almost correct. As he reached the last page of his most recent notebook (yes, the man still does bench work), he asked us "so, what's on the next page?" I could feel anticipation in the audience. "Well, that's for you to find out!"

The most exciting part of research, in my view, is what to do next. This chapter lets you know what would be on my next page.

Why is there a golgi-based glycosylation deficit in Pompe disease?

If Pompe disease is a CDG, then an answer is demanded as to the mechanism by which golgi-based N-linked glycosylation is impacted by the inability for glycogen to be degraded into glucose within the lysosomes. The question is intriguing because the two processes seem unrelated. We begin our reasoning with the observation that there is a similar deficit of N-linked golgi based glycosylation in glycogen storage disease (GSD) type I (107) and type XIV(131) due to the inability of the trans-golgi to add galactose and sialic acids. Recall that Pompe disease is also called GSD type II.

In all 3 diseases (GSD type I, II, and XIV) there is an accumulation of glycogen within tissues that rely on the missing enzyme. In classic GSD type I (type 1a), the enzyme catalyzing the dephosphorylation of glucose-6-phosphate (G6P) into free glucose (glucose-6-phoshatase) is non-functional. In GSD type 1b, the enzyme that transports G6P into the ER for dephosphorylation by glucose-6-phosphatase (G6P transporter) is non-functional. Therefore, G6P accumulates within the cytoplasm. In GSD type XIV, cells are unable to convert between the two phosorylated glucose molecules G6P and glucose-1-phosphate (G1P) due to the lack of phosphoglucomutase. In GSD type II (Pompe disease), a report (33) shows that G6P concentrations and glycogen synthesis activity were elevated 15- and 20- fold, respectively, in both skeletal and cardiac muscle. We hypothesize that disrupted G6P metabolism in all three disorders is causing a deficiency of UDP-galactose in the golgi that then limits the extension of N-linked glycan chains in the trans-golgi according to the image below.

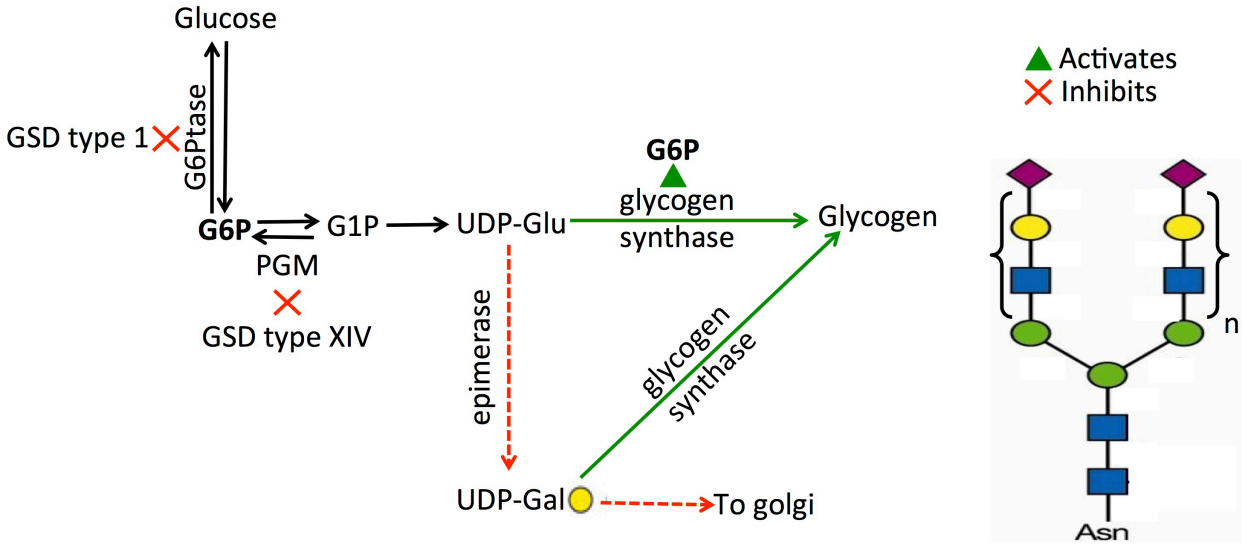

Image 10 Hypothesis for hypoglycosylation in the GSDs due to a deficiency in UDP-Gal

Elevated G6P concentrations allosterically activate glycogen synthase, which consumes all of the cytoplasmic UDP-glucose and UDP-galactose for glycogen synthesis. As a result, insufficient UDP-galactose reaches the golgi lumen. G6P = Glucose-6-phosphate, G1P = Glucose-1-Phosphate, epimerase = UDP-4-glucose epimerase, UDP-gal = UDP-galactose, G6Ptase = Glucose-6-phosphatase, PGM = Phosphoglucomutase.

G6P is a powerful allosteric activator of glycogen synthase, with the ability to override all inhibitory phosphorylation signals if the G6P concentration is high enough. The enhanced glycogen synthase activity in Pompe disease due to G6P allosteric activation may be depleting the UDP-Glu concentrations to the extent that the conversion of UDP-glu to UDP-gal through the epimerase reaction is inadequate. In addition, the UDP-gal that does exist may also be incorporated into glycogen, due to the high glycogen synthase activity (glycogen synthase can incorporate galactose into glycogen with UDP-gal substrate), before it has time to diffuse to and enter the golgi. With limited UDP-gal in the golgi, glycan chain extension of the tri-mannose

structure in the trans-golgi becomes limited. The same mechanism is thought to occur in GSD type I and type XIV.

The elevation in G6P that triggers the cascade to depleted UDP-gal in GSD type I and type XIV can be directly related to the enzyme that is missing in those disorders; in both, the inactive enzyme is responsible for converting G6P into another form. The higher G6P in Pompe disease is less obvious because acid α-glucosidase degrades glycogen into free glucose within the lysosome – there is no direct relation to G6P. However, recent evidence shows that the surface of the lysosome is the site for cellular nutritional sensing via the mammalian target of rapamycin complex 1 (mTORC1) (132).

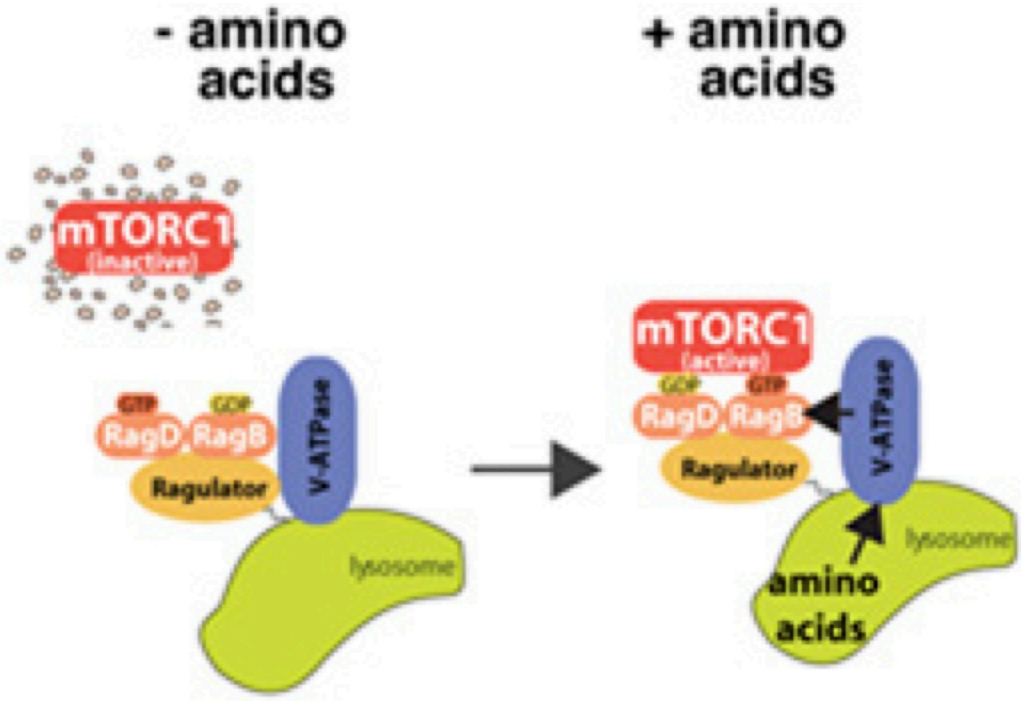

Image 11 Hypothesis for the elevation in G6P in Pompe skeletal and cardiac muscle The mTORC1 complex in the inactive state is free in the cytoplasm and signals a low nutritional state. Upon sufficient lysosomal release of amino acids, mTORC1 docks on the lysosomal membrane via its interaction with the V-ATPase and signals for an energy rich state.

The mechanism by which the cell senses its free amino acid levels is not through the levels that exist in the cytoplasm, but by the amount that is being release by lysosomes via hydrolase activity. The vacuolar ATPase (vATPase), that is responsible for maintaining the acidic environment of the lysosomal, has been demonstrated to be the amino acid sensor. Upon sensing high levels of amino acids in the lysosome, the vATPase becomes available for mTORC1 binding and activation, signaling an energy rich state. We hypothesize that glucose sensing by the cell also occurs via a lysosome-centric method. The vATPase has been shown in vitro to dissociate in the presence of low glucose (133). Therefore, vATPase may also be sensing the concentration of free glucose in the lysosome. If glucose is low, the vATPase dissociates and will not allow mTORC1 to dock on the surface to be activated. The major deficit of Pompe lysosomes are their inability to hydrolyze glycogen into free glucose. Since this is the only mechanism by which glucose can be produced by the lysosome, the vATPase may be in a perpetually unstable state, not allowing for the activation of mTORC1. Thus, mTORC1 in Pompe disease may be in a constant inactive state, signaling a low nutritional state and calling for the import of more glucose from the outside. Data exists that the glucose transporters (GLUT) that bring in extracellular glucose are elevated on the surface of Pompe myocytes(134). In addition, measurements of lysosomal acidity in expanded glycogen-filled lysosomes shows a more basic lumen, indicating that dissociated vATPases may not be maintaining the low pH levels(25).

In summary, the inability to hydrolyze glycogen in the lysosome causes the glucose concentration in the lysosome to be negligible. With low glucose concentrations, the vATPase dissociates from the lysosomal surface and prevent the docking and activation of mTORC1. Inactive mTORC1 signals for a low energy state, and triggers the overexpression of GLUT on

the cell surface, causing higher levels of glucose entry into the cell. The high intracellular glucose allosterically activates hexokinase, which causes G6P to accumulate. The accumulated G6P allosterically activates glycogen synthase, depleting the UDP-galactose pools. Without UDP-galactose in the golgi, glycan chain extension becomes insufficient.

The HCM of Pompe disease can also be explained by a deficit in golgi-based glycosylation and constitutes our final hypothesis. In addition to proteins, lipid glycosylation also occurs in the golgi.

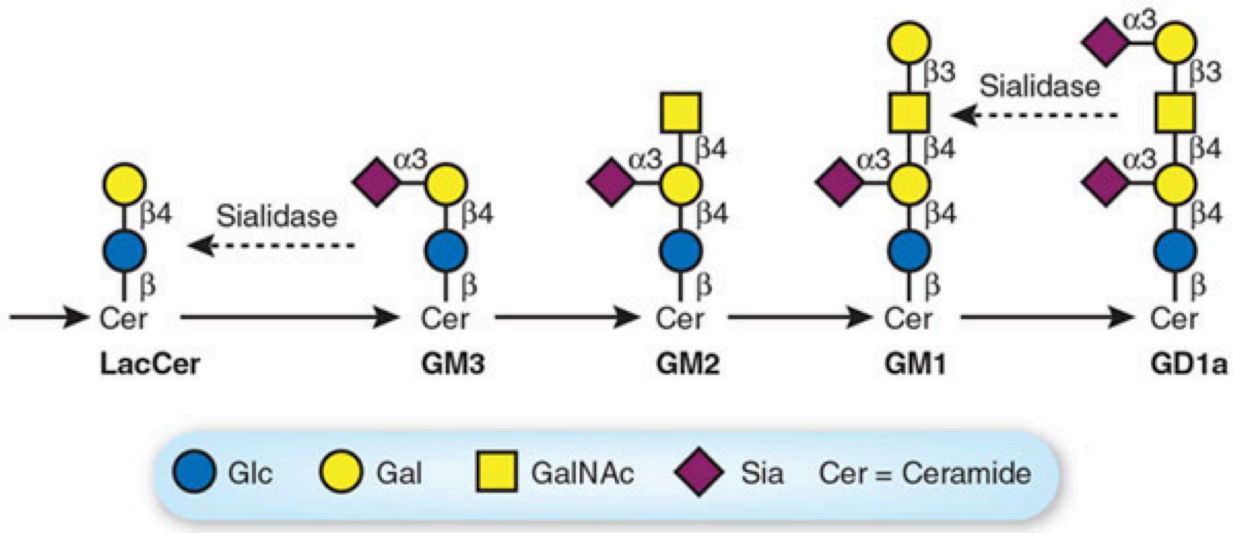

Image 12 Glycosylation of cermide to form the spingolipids Galactose linked sialic acid addition to form the sphingolipids of the cardiomyocyte sarcolemma are necessary to prevent the non-channel leak of calcium into the cytoplasm (112).

Without correct sphingolipid sialylation, intracellular cardiomyocyte calcium concentrations rise. Chronically higher cytoplasmic calcium is known to trigger cardiac hypertrophy via the calcium-calcineurin-NFAT signaling pathway (46). Therefore, chromatographic techniques to separate the glycolipid composition and non-channel calcium currents of Control and Pompe iPSC-CMs may be a fruitful pursuit.

References

1. O'Donnell, K. pompestory.blogspot.com
2. JC, P. (1932) Over idiopathische hypertrophie van het hart. *Ned Tijdschr Geneeskd* **76**, 304-311
3. van der Ploeg, A. T., and Reuser, A. J. (2008) Pompe's disease. *Lancet* **372**, 1342-1353
4. Thurberg, B. L., Lynch Maloney, C., Vaccaro, C., Afonso, K., Tsai, A. C., Bossen, E., Kishnani, P. S., and O'Callaghan, M. (2006) Characterization of pre- and post-treatment pathology after enzyme replacement therapy for Pompe disease. *Lab Invest* **86**, 1208-1220
5. Hesselink, R. P., Schaart, G., Wagenmakers, A. J., Drost, M. R., and van der Vusse, G. J. (2006) Age-related morphological changes in skeletal muscle cells of acid alpha-glucosidase knockout mice. *Muscle & nerve* **33**, 505-513
6. Katz, A. M. (2011) *Physiology of the heart*, 5th ed., Wolters Kluwer Health/Lippincott Williams & Wilkins Health, Philadelphia, PA
7. Ramay, H. R., and Vendelin, M. (2009) Diffusion restrictions surrounding mitochondria: a mathematical model of heart muscle fibers. *Biophysical journal* **97**, 443-452
8. Arber, S., Hunter, J. J., Ross, J., Jr., Hongo, M., Sansig, G., Borg, J., Perriard, J. C., Chien, K. R., and Caroni, P. (1997) MLP-deficient mice exhibit a disruption of cardiac cytoarchitectural organization, dilated cardiomyopathy, and heart failure. *Cell* **88**, 393-403
9. Omens, J. H., Usyk, T. P., Li, Z., and McCulloch, A. D. (2002) Muscle LIM protein deficiency leads to alterations in passive ventricular mechanics. *American journal of physiology. Heart and circulatory physiology* **282**, H680-687
10. Drost, M. R., Hesselink, R. P., Oomens, C. W., and van der Vusse, G. J. (2005) Effects of non-contractile inclusions on mechanical performance of skeletal muscle. *Journal of biomechanics* **38**, 1035-1043
11. Hesselink, R. P., Van Kranenburg, G., Wagenmakers, A. J., Van der Vusse, G. J., and Drost, M. R. (2005) Age-related decline in muscle strength and power output in acid 1-4 alpha-glucosidase knockout mice. *Muscle & nerve* **31**, 374-381
12. Xu, S., Galperin, M., Melvin, G., Horowits, R., Raben, N., Plotz, P., and Yu, L. (2010) Impaired organization and function of myofilaments in single muscle fibers from a mouse model of Pompe disease. *J Appl Physiol (1985)* **108**, 1383-1388
13. Lynch, C. M., Johnson, J., Vaccaro, C., and Thurberg, B. L. (2005) High-resolution light microscopy (HRLM) and digital analysis of Pompe disease pathology. *J Histochem Cytochem* **53**, 63-73
14. Codogno, P. (2014) Shining light on autophagy. *Nature reviews. Molecular cell biology* **15**, 153
15. Kubli, D. A., and Gustafsson, A. B. (2012) Mitochondria and mitophagy: the yin and yang of cell death control. *Circulation research* **111**, 1208-1221
16. Xie, Z., and Klionsky, D. J. (2007) Autophagosome formation: core machinery and adaptations. *Nature cell biology* **9**, 1102-1109
17. Melendez, R., Melendez-Hevia, E., and Cascante, M. (1997) How did glycogen structure evolve to satisfy the requirement for rapid mobilization of glucose? A

problem of physical constraints in structure building. *Journal of molecular evolution* **45**, 446-455
18. Zirin, J., Nieuwenhuis, J., and Perrimon, N. (2013) Role of autophagy in glycogen breakdown and its relevance to chloroquine myopathy. *PLoS biology* **11**, e1001708
19. Raben, N., Hill, V., Shea, L., Takikita, S., Baum, R., Mizushima, N., Ralston, E., and Plotz, P. (2008) Suppression of autophagy in skeletal muscle uncovers the accumulation of ubiquitinated proteins and their potential role in muscle damage in Pompe disease. *Hum Mol Genet* **17**, 3897-3908
20. Raben, N., Baum, R., Schreiner, C., Takikita, S., Mizushima, N., Ralston, E., and Plotz, P. (2009) When more is less: excess and deficiency of autophagy coexist in skeletal muscle in Pompe disease. *Autophagy* **5**, 111-113
21. Geddes, R., and Stratton, G. C. (1977) The influence of lysosomes on glycogen metabolism. *The Biochemical journal* **163**, 193-200
22. Hawes, M. L., Kennedy, W., O'Callaghan, M. W., and Thurberg, B. L. (2007) Differential muscular glycogen clearance after enzyme replacement therapy in a mouse model of Pompe disease. *Molecular genetics and metabolism* **91**, 343-351
23. Drost, M. R., Schaart, G., van Dijk, P., van Capelle, C. I., van der Vusse, G. J., Delhaas, T., van der Ploeg, A. T., and Reuser, A. J. (2008) Both type 1 and type 2a muscle fibers can respond to enzyme therapy in Pompe disease. *Muscle & nerve* **37**, 251-255
24. Raben, N., Danon, M., Gilbert, A. L., Dwivedi, S., Collins, B., Thurberg, B. L., Mattaliano, R. J., Nagaraju, K., and Plotz, P. H. (2003) Enzyme replacement therapy in the mouse model of Pompe disease. *Molecular genetics and metabolism* **80**, 159-169
25. Takikita, S., Myerowitz, R., Zaal, K., Raben, N., and Plotz, P. H. (2009) Murine muscle cell models for Pompe disease and their use in studying therapeutic approaches. *Mol Genet Metab* **96**, 208-217
26. Raben, N., Wong, A., Ralston, E., and Myerowitz, R. (2012) Autophagy and mitochondria in Pompe disease: nothing is so new as what has long been forgotten. *Am J Med Genet C Semin Med Genet* **160C**, 13-21
27. Raben, N., Ralston, E., Chien, Y. H., Baum, R., Schreiner, C., Hwu, W. L., Zaal, K. J., and Plotz, P. H. (2010) Differences in the predominance of lysosomal and autophagic pathologies between infants and adults with Pompe disease: implications for therapy. *Mol Genet Metab* **101**, 324-331
28. Nascimbeni, A. C., Fanin, M., Masiero, E., Angelini, C., and Sandri, M. (2012) The role of autophagy in the pathogenesis of glycogen storage disease type II (GSDII). *Cell Death Differ* **19**, 1698-1708
29. Tanida, I., Ueno, T., and Kominami, E. (2008) LC3 and Autophagy. *Methods in molecular biology* **445**, 77-88
30. Li, L., Chen, Y., and Gibson, S. B. (2013) Starvation-induced autophagy is regulated by mitochondrial reactive oxygen species leading to AMPK activation. *Cellular signalling* **25**, 50-65
31. Mizushima, N., Yamamoto, A., Matsui, M., Yoshimori, T., and Ohsumi, Y. (2004) In vivo analysis of autophagy in response to nutrient starvation using transgenic mice expressing a fluorescent autophagosome marker. *Molecular biology of the cell* **15**, 1101-1111

32. Douillard-Guilloux, G., Raben, N., Takikita, S., Ferry, A., Vignaud, A., et al. (2010) Restoration of muscle functionality by genetic suppression of glycogen synthesis in a murine model of Pompe disease. *Human molecular genetics* **19**, 684-696
33. Taylor, K. M., Meyers, E., Phipps, M., Kishnani, P. S., Cheng, S. H., Scheule, R. K., and Moreland, R. J. (2013) Dysregulation of multiple facets of glycogen metabolism in a murine model of Pompe disease. *PLoS One* **8**, e56181
34. Grahame Hardie, D. (2014) AMP-activated protein kinase: a key regulator of energy balance with many roles in human disease. *Journal of internal medicine*
35. Arad, M., Benson, D. W., Perez-Atayde, A. R., McKenna, W. J., Sparks, E. A., Kanter, R. J., McGarry, K., Seidman, J. G., and Seidman, C. E. (2002) Constitutively active AMP kinase mutations cause glycogen storage disease mimicking hypertrophic cardiomyopathy. *The Journal of clinical investigation* **109**, 357-362
36. Kishnani, P. S., Corzo, D., Leslie, N. D., Gruskin, D., Van der Ploeg, A., et al. (2009) Early treatment with alglucosidase alpha prolongs long-term survival of infants with Pompe disease. *Pediatric research* **66**, 329-335
37. Chen, L. R., Chen, C. A., Chiu, S. N., Chien, Y. H., Lee, N. C., Lin, M. T., Hwu, W. L., Wang, J. K., and Wu, M. H. (2009) Reversal of cardiac dysfunction after enzyme replacement in patients with infantile-onset Pompe disease. *J Pediatr* **155**, 271-275 e272
38. Hagemans, M. L., Winkel, L. P., Van Doorn, P. A., Hop, W. J., Loonen, M. C., Reuser, A. J., and Van der Ploeg, A. T. (2005) Clinical manifestation and natural course of late-onset Pompe's disease in 54 Dutch patients. *Brain : a journal of neurology* **128**, 671-677
39. Kishnani, P. S., Hwu, W. L., Mandel, H., Nicolino, M., Yong, F., Corzo, D., and Infantile-Onset Pompe Disease Natural History Study, G. (2006) A retrospective, multinational, multicenter study on the natural history of infantile-onset Pompe disease. *J Pediatr* **148**, 671-676
40. Rees, A., Elbl, F., Minhas, K., and Solinger, R. (1976) Echocardiographic evidence of outflow tract obstruction in Pompe's disease (glycogen storage disease of the heart). *The American journal of cardiology* **37**, 1103-1106
41. Yu, J., Vodyanik, M. A., Smuga-Otto, K., Antosiewicz-Bourget, J., Frane, J. L., et al. (2007) Induced pluripotent stem cell lines derived from human somatic cells. *Science* **318**, 1917-1920
42. Takahashi, K., Tanabe, K., Ohnuki, M., Narita, M., Ichisaka, T., Tomoda, K., and Yamanaka, S. (2007) Induction of pluripotent stem cells from adult human fibroblasts by defined factors. *Cell* **131**, 861-872
43. Grskovic, M., Javaherian, A., Strulovici, B., and Daley, G. Q. (2011) Induced pluripotent stem cells--opportunities for disease modelling and drug discovery. *Nature reviews. Drug discovery* **10**, 915-929
44. Carvajal-Vergara, X., Sevilla, A., D'Souza, S. L., Ang, Y. S., Schaniel, C., et al. (2010) Patient-specific induced pluripotent stem-cell-derived models of LEOPARD syndrome. *Nature* **465**, 808-812
45. Wesselschmidt, R. L. (2011) The teratoma assay: an in vivo assessment of pluripotency. *Methods in molecular biology* **767**, 231-241
46. Wilkins, B. J., and Molkentin, J. D. (2004) Calcium-calcineurin signaling in the regulation of cardiac hypertrophy. *Biochem Biophys Res Commun* **322**, 1178-1191

47. Sun, N., Yazawa, M., Liu, J., Han, L., Sanchez-Freire, V., et al. (2012) Patient-specific induced pluripotent stem cells as a model for familial dilated cardiomyopathy. *Science translational medicine* **4**, 130ra147
48. Wang, G., McCain, M. L., Yang, L., He, A., Pasqualini, F. S., et al. (2014) Modeling the mitochondrial cardiomyopathy of Barth syndrome with induced pluripotent stem cell and heart-on-chip technologies. *Nature medicine* **20**, 616-623
49. Raval, K. K., and Kamp, T. J. (2014) Cardiomyopathy, mitochondria and Barth syndrome: iPSCs reveal a connection. *Nature medicine* **20**, 585-586
50. Barth, P. G., Scholte, H. R., Berden, J. A., Van der Klei-Van Moorsel, J. M., Luyt-Houwen, I. E., Van 't Veer-Korthof, E. T., Van der Harten, J. J., and Sobotka-Plojhar, M. A. (1983) An X-linked mitochondrial disease affecting cardiac muscle, skeletal muscle and neutrophil leucocytes. *J Neurol Sci* **62**, 327-355
51. Bione, S., D'Adamo, P., Maestrini, E., Gedeon, A. K., Bolhuis, P. A., and Toniolo, D. (1996) A novel X-linked gene, G4.5. is responsible for Barth syndrome. *Nat Genet* **12**, 385-389
52. Feinberg, A. W., Feigel, A., Shevkoplyas, S. S., Sheehy, S., Whitesides, G. M., and Parker, K. K. (2007) Muscular thin films for building actuators and powering devices. *Science* **317**, 1366-1370
53. Huang, H. P., Chen, P. H., Hwu, W. L., Chuang, C. Y., Chien, Y. H., et al. (2011) Human Pompe disease-induced pluripotent stem cells for pathogenesis modeling, drug testing and disease marker identification. *Hum Mol Genet* **20**, 4851-4864
54. Selak, M. A., de Chadarevian, J. P., Melvin, J. J., Grover, W. D., Salganicoff, L., and Kaye, E. M. (2000) Mitochondrial activity in Pompe's disease. *Pediatric neurology* **23**, 54-57
55. Chen, C. A., Chien, Y. H., Hwu, W. L., Lee, N. C., Wang, J. K., et al. (2011) Left ventricular geometry, global function, and dyssynchrony in infants and children with pompe cardiomyopathy undergoing enzyme replacement therapy. *Journal of cardiac failure* **17**, 930-936
56. Moore, J. R., Leinwand, L., and Warshaw, D. M. (2012) Understanding cardiomyopathy phenotypes based on the functional impact of mutations in the myosin motor. *Circ Res* **111**, 375-385
57. De Lange, W. J., Grimes, A. C., Hegge, L. F., Spring, A. M., Brost, T. M., and Ralphe, J. C. (2013) E258K HCM-causing mutation in cardiac MyBP-C reduces contractile force and accelerates twitch kinetics by disrupting the cMyBP-C and myosin S2 interaction. *J Gen Physiol* **142**, 241-255
58. de Lange, W. J., Hegge, L. F., Grimes, A. C., Tong, C. W., Brost, T. M., Moss, R. L., and Ralphe, J. C. (2011) Neonatal mouse-derived engineered cardiac tissue: a novel model system for studying genetic heart disease. *Circ Res* **109**, 8-19
59. Yu, J., Hu, K., Smuga-Otto, K., Tian, S., Stewart, R., Slukvin, II, and Thomson, J. A. (2009) Human induced pluripotent stem cells free of vector and transgene sequences. *Science* **324**, 797-801
60. Ludwig, T. E., Levenstein, M. E., Jones, J. M., Berggren, W. T., Mitchen, E. R., et al. (2006) Derivation of human embryonic stem cells in defined conditions. *Nat Biotechnol* **24**, 185-187

61. Lian, X., Hsiao, C., Wilson, G., Zhu, K., Hazeltine, L. B., et al. (2012) Robust cardiomyocyte differentiation from human pluripotent stem cells via temporal modulation of canonical Wnt signaling. *Proc Natl Acad Sci U S A* **109**, E1848-1857
62. Lian, X., Zhang, J., Azarin, S. M., Zhu, K., Hazeltine, L. B., Bao, X., Hsiao, C., Kamp, T. J., and Palecek, S. P. (2013) Directed cardiomyocyte differentiation from human pluripotent stem cells by modulating Wnt/beta-catenin signaling under fully defined conditions. *Nature protocols* **8**, 162-175
63. Wessel, D., and Flugge, U. I. (1984) A method for the quantitative recovery of protein in dilute solution in the presence of detergents and lipids. *Anal Biochem* **138**, 141-143
64. Moreland, R. J., Jin, X., Zhang, X. K., Decker, R. W., Albee, K. L., et al. (2005) Lysosomal acid alpha-glucosidase consists of four different peptides processed from a single chain precursor. *The Journal of biological chemistry* **280**, 6780-6791
65. Ausems, M. G., Kroos, M. A., Van der Kraan, M., Smeitink, J. A., Kleijer, W. J., Ploos van Amstel, H. K., and Reuser, A. J. (1996) Homozygous deletion of exon 18 leads to degradation of the lysosomal alpha-glucosidase precursor and to the infantile form of glycogen storage disease type II. *Clin Genet* **49**, 325-328
66. Knaapen, M. W., Vrolijk, B. C., and Wenink, A. C. (1997) Ultrastructural changes of the myocardium in the embryonic rat heart. *Anat Rec* **248**, 233-241
67. Higuchi, T., Kawagoe, S., Otsu, M., Shimada, Y., Kobayashi, H., et al. (2014) The generation of induced pluripotent stem cells (iPSCs) from patients with infantile and late-onset types of Pompe disease and the effects of treatment with acid-alpha-glucosidase in Pompe's iPSCs. *Molecular genetics and metabolism* **112**, 44-48
68. Schaaf, S., Shibamiya, A., Mewe, M., Eder, A., Stohr, A., et al. (2011) Human engineered heart tissue as a versatile tool in basic research and preclinical toxicology. *PLoS One* **6**, e26397
69. Hansen, A., Eder, A., Bonstrup, M., Flato, M., Mewe, M., et al. (2010) Development of a drug screening platform based on engineered heart tissue. *Circ Res* **107**, 35-44
70. Nunes, S. S., Miklas, J. W., Liu, J., Aschar-Sobbi, R., Xiao, Y., et al. (2013) Biowire: a platform for maturation of human pluripotent stem cell-derived cardiomyocytes. *Nat Methods* **10**, 781-787
71. Kemi, O. J., Haram, P. M., Wisloff, U., and Ellingsen, O. (2004) Aerobic fitness is associated with cardiomyocyte contractile capacity and endothelial function in exercise training and detraining. *Circulation* **109**, 2897-2904
72. Sun, H., Gaspo, R., Leblanc, N., and Nattel, S. (1998) Cellular mechanisms of atrial contractile dysfunction caused by sustained atrial tachycardia. *Circulation* **98**, 719-727
73. Klionsky, D. J., Abdalla, F. C., Abeliovich, H., Abraham, R. T., Acevedo-Arozena, A., et al. (2012) Guidelines for the use and interpretation of assays for monitoring autophagy. *Autophagy* **8**, 445-544
74. Slater, A. F. (1993) Chloroquine: mechanism of drug action and resistance in Plasmodium falciparum. *Pharmacology & therapeutics* **57**, 203-235
75. Lieberman, A. P., Puertollano, R., Raben, N., Slaugenhaupt, S., Walkley, S. U., and Ballabio, A. (2012) Autophagy in lysosomal storage disorders. *Autophagy* **8**, 719-730

76. Meikle, P. J., Brooks, D. A., Ravenscroft, E. M., Yan, M., Williams, R. E., et al. (1997) Diagnosis of lysosomal storage disorders: evaluation of lysosome-associated membrane protein LAMP-1 as a diagnostic marker. *Clin Chem* **43**, 1325-1335
77. Raben, N., Fukuda, T., Gilbert, A. L., de Jong, D., Thurberg, B. L., et al. (2005) Replacing acid alpha-glucosidase in Pompe disease: recombinant and transgenic enzymes are equipotent, but neither completely clears glycogen from type II muscle fibers. *Mol Ther* **11**, 48-56
78. Takikita, S., Myerowitz, R., Schreiner, C., Baum, R., Raben, N., and Plotz, P. H. (2009) The values and limits of an in vitro model of Pompe disease: the best laid schemes o' mice an' men. *Autophagy* **5**, 729-731
79. Spampanato, C., Feeney, E., Li, L., Cardone, M., Lim, J. A., et al. (2013) Transcription factor EB (TFEB) is a new therapeutic target for Pompe disease. *EMBO Mol Med* **5**, 691-706
80. Carlsson, S. R., and Fukuda, M. (1990) The polylactosaminoglycans of human lysosomal membrane glycoproteins lamp-1 and lamp-2. Localization on the peptide backbones. *The Journal of biological chemistry* **265**, 20488-20495
81. Carlsson, S. R., Roth, J., Piller, F., and Fukuda, M. (1988) Isolation and characterization of human lysosomal membrane glycoproteins, h-lamp-1 and h-lamp-2. Major sialoglycoproteins carrying polylactosaminoglycan. *The Journal of biological chemistry* **263**, 18911-18919
82. O'Farrell, P. H. (1975) High resolution two-dimensional electrophoresis of proteins. *The Journal of biological chemistry* **250**, 4007-4021
83. Burgess-Cassler, A., Johansen, J. J., Santek, D. A., Ide, J. R., and Kendrick, N. C. (1989) Computerized quantitative analysis of coomassie-blue-stained serum proteins separated by two-dimensional electrophoresis. *Clin Chem* **35**, 2297-2304
84. del Val, I. J., Kyriakopoulos, S., Polizzi, K. M., and Kontoravdi, C. (2013) An optimized method for extraction and quantification of nucleotides and nucleotide sugars from mammalian cells. *Analytical biochemistry* **443**, 172-180
85. Carlsson, S. R., Lycksell, P. O., and Fukuda, M. (1993) Assignment of O-glycan attachment sites to the hinge-like regions of human lysosomal membrane glycoproteins lamp-1 and lamp-2. *Arch Biochem Biophys* **304**, 65-73
86. Nabi, I. R., and Dennis, J. W. (1998) The extent of polylactosamine glycosylation of MDCK LAMP-2 is determined by its Golgi residence time. *Glycobiology* **8**, 947-953
87. Fujiwara, T., Oda, K., Yokota, S., Takatsuki, A., and Ikehara, Y. (1988) Brefeldin A causes disassembly of the Golgi complex and accumulation of secretory proteins in the endoplasmic reticulum. *The Journal of biological chemistry* **263**, 18545-18552
88. Isaac, E. L., Karageorgos, L. E., Brooks, D. A., Hopwood, J. J., and Meikle, P. J. (2000) Regulation of the lysosome-associated membrane protein in a sucrose model of lysosomal storage. *Exp Cell Res* **254**, 204-209
89. Chen, J. W., Pan, W., D'Souza, M. P., and August, J. T. (1985) Lysosome-associated membrane proteins: characterization of LAMP-1 of macrophage P388 and mouse embryo 3T3 cultured cells. *Arch Biochem Biophys* **239**, 574-586
90. Alberts, B. (1989) *Molecular biology of the cell*, 2nd ed., Garland Pub., New York
91. Zhou, D. (2003) Why are glycoproteins modified by poly-N-acetyllactosamine glyco-conjugates? *Curr Protein Pept Sci* **4**, 1-9

92. Wang, S. H., Wu, S. W., and Khoo, K. H. (2011) MS-based glycomic strategies for probing the structural details of polylactosaminoglycan chain on N-glycans and glycoproteomic identification of its protein carriers. *Proteomics* **11**, 2812-2829
93. Footitt, E. J., Karimova, A., Burch, M., Yayeh, T., Dupre, T., et al. (2009) Cardiomyopathy in the congenital disorders of glycosylation (CDG): a case of late presentation and literature review. *J Inherit Metab Dis* **32 Suppl 1**, S313-319
94. Gehrmann, J., Sohlbach, K., Linnebank, M., Bohles, H. J., Buderus, S., Kehl, H. G., Vogt, J., Harms, E., and Marquardt, T. (2003) Cardiomyopathy in congenital disorders of glycosylation. *Cardiol Young* **13**, 345-351
95. Kranz, C., Basinger, A. A., Gucsavas-Calikoglu, M., Sun, L., Powell, C. M., Henderson, F. W., Aylsworth, A. S., and Freeze, H. H. (2007) Expanding spectrum of congenital disorder of glycosylation Ig (CDG-Ig): sibs with a unique skeletal dysplasia, hypogammaglobulinemia, cardiomyopathy, genital malformations, and early lethality. *Am J Med Genet A* **143A**, 1371-1378
96. Duplomb, L., Duvet, S., Picot, D., Jego, G., El Chehadeh-Djebbar, S., et al. (2014) Cohen syndrome is associated with major glycosylation defects. *Hum Mol Genet*
97. Shestakova, A., Zolov, S., and Lupashin, V. (2006) COG complex-mediated recycling of Golgi glycosyltransferases is essential for normal protein glycosylation. *Traffic* **7**, 191-204
98. Foulquier, F., Amyere, M., Jaeken, J., Zeevaert, R., Schollen, E., et al. (2012) TMEM165 deficiency causes a congenital disorder of glycosylation. *Am J Hum Genet* **91**, 15-26
99. Sparks, S. E., and Krasnewich, D. M. (1993) Congenital Disorders of N-linked Glycosylation Pathway Overview. in *GeneReviews(R)* (Pagon, R. A., Adam, M. P., Ardinger, H. H., Bird, T. D., Dolan, C. R., Fong, C. T., Smith, R. J. H., and Stephens, K. eds.), Seattle (WA). pp
100. Wopereis, S., Grunewald, S., Morava, E., Penzien, J. M., Briones, P., Garcia-Silva, M. T., Demacker, P. N., Huijben, K. M., and Wevers, R. A. (2003) Apolipoprotein C-III isofocusing in the diagnosis of genetic defects in O-glycan biosynthesis. *Clinical chemistry* **49**, 1839-1845
101. Carchon, H. A., Chevigne, R., Falmagne, J. B., and Jaeken, J. (2004) Diagnosis of congenital disorders of glycosylation by capillary zone electrophoresis of serum transferrin. *Clin Chem* **50**, 101-111
102. Denecke, J., and Marquardt, T. (2009) Congenital dyserythropoietic anemia type II (CDAII/HEMPAS): where are we now? *Biochim Biophys Acta* **1792**, 915-920
103. Charuk, J. H., Tan, J., Bernardini, M., Haddad, S., Reithmeier, R. A., Jaeken, J., and Schachter, H. (1995) Carbohydrate-deficient glycoprotein syndrome type II. An autosomal recessive N-acetylglucosaminyltransferase II deficiency different from typical hereditary erythroblastic multinuclearity, with a positive acidified-serum lysis test (HEMPAS). *European journal of biochemistry / FEBS* **230**, 797-805
104. Freeze, H. H., and Schachter, H. (2009) Genetic Disorders of Glycosylation. in *Essentials of Glycobiology* (Varki, A., Cummings, R. D., Esko, J. D., Freeze, H. H., Stanley, P., Bertozzi, C. R., Hart, G. W., and Etzler, M. E. eds.), 2nd Ed., Cold Spring Harbor (NY). pp
105. Freeze, H. H., and Aebi, M. (2005) Altered glycan structures: the molecular basis of congenital disorders of glycosylation. *Curr Opin Struct Biol* **15**, 490-498

106. Pous, C., Guibourdenche, J., Drechou, A., and Durand, G. (1994) Differential secretion of alpha 1-acid glycoprotein occurs in the Golgi complex of isolated rat hepatocytes. Evidence of partial retention in the Golgi. *Eur J Biochem* **219**, 1073-1079
107. Hayee, B., Antonopoulos, A., Murphy, E. J., Rahman, F. Z., Sewell, G., et al. (2011) G6PC3 mutations are associated with a major defect of glycosylation: a novel mechanism for neutrophil dysfunction. *Glycobiology* **21**, 914-924
108. Freeze, H. H., Chong, J. X., Bamshad, M. J., and Ng, B. G. (2014) Solving glycosylation disorders: fundamental approaches reveal complicated pathways. *Am J Hum Genet* **94**, 161-175
109. Ednie, A. R., Horton, K. K., Wu, J., and Bennett, E. S. (2013) Expression of the sialyltransferase, ST3Gal4, impacts cardiac voltage-gated sodium channel activity, refractory period and ventricular conduction. *Journal of molecular and cellular cardiology* **59**, 117-127
110. Norring, S. A., Ednie, A. R., Schwetz, T. A., Du, D., Yang, H., and Bennett, E. S. (2013) Channel sialic acids limit hERG channel activity during the ventricular action potential. *FASEB journal : official publication of the Federation of American Societies for Experimental Biology* **27**, 622-631
111. Fermini, B., and Nathan, R. D. (1991) Removal of sialic acid alters both T- and L-type calcium currents in cardiac myocytes. *The American journal of physiology* **260**, H735-743
112. Marengo, F. D., Wang, S. Y., Wang, B., and Langer, G. A. (1998) Dependence of cardiac cell Ca2+ permeability on sialic acid-containing sarcolemmal gangliosides. *J Mol Cell Cardiol* **30**, 127-137
113. Post, J. A. (1992) Removal of sarcolemmal sialic acid residues results in a loss of sarcolemmal functioning and integrity. *Am J Physiol* **263**, H147-152
114. Ehmsen, J., Poon, E., and Davies, K. (2002) The dystrophin-associated protein complex. *Journal of cell science* **115**, 2801-2803
115. Lisi, M. T., and Cohn, R. D. (2007) Congenital muscular dystrophies: new aspects of an expanding group of disorders. *Biochimica et biophysica acta* **1772**, 159-172
116. van Reeuwijk, J., Janssen, M., van den Elzen, C., Beltran-Valero de Bernabe, D., Sabatelli, P., et al. (2005) POMT2 mutations cause alpha-dystroglycan hypoglycosylation and Walker-Warburg syndrome. *Journal of medical genetics* **42**, 907-912
117. Inamori, K., Yoshida-Moriguchi, T., Hara, Y., Anderson, M. E., Yu, L., and Campbell, K. P. (2012) Dystroglycan function requires xylosyl- and glucuronyltransferase activities of LARGE. *Science* **335**, 93-96
118. Barresi, R., Michele, D. E., Kanagawa, M., Harper, H. A., Dovico, S. A., et al. (2004) LARGE can functionally bypass alpha-dystroglycan glycosylation defects in distinct congenital muscular dystrophies. *Nature medicine* **10**, 696-703
119. Michele, D. E., Barresi, R., Kanagawa, M., Saito, F., Cohn, R. D., et al. (2002) Post-translational disruption of dystroglycan-ligand interactions in congenital muscular dystrophies. *Nature* **418**, 417-422
120. Ervasti, J. M. (2003) Costameres: the Achilles' heel of Herculean muscle. *The Journal of biological chemistry* **278**, 13591-13594
121. Brockington, M., Torelli, S., Prandini, P., Boito, C., Dolatshad, N. F., Longman, C., Brown, S. C., and Muntoni, F. (2005) Localization and functional analysis of the

LARGE family of glycosyltransferases: significance for muscular dystrophy. *Hum Mol Genet* **14**, 657-665
122. Kanagawa, M., Saito, F., Kunz, S., Yoshida-Moriguchi, T., Barresi, R., et al. (2004) Molecular recognition by LARGE is essential for expression of functional dystroglycan. *Cell* **117**, 953-964
123. Sparks, S., Quijano-Roy, S., Harper, A., Rutkowski, A., Gordon, E., Hoffman, E. P., and Pegoraro, E. (1993) Congenital Muscular Dystrophy Overview. in *GeneReviews(R)* (Pagon, R. A., Adam, M. P., Bird, T. D., Dolan, C. R., Fong, C. T., Smith, R. J. H., and Stephens, K. eds.), Seattle (WA). pp
124. Ervasti, J. M., and Campbell, K. P. (1993) A role for the dystrophin-glycoprotein complex as a transmembrane linker between laminin and actin. *The Journal of cell biology* **122**, 809-823
125. Michele, D. E., and Campbell, K. P. (2003) Dystrophin-glycoprotein complex: post-translational processing and dystroglycan function. *The Journal of biological chemistry* **278**, 15457-15460
126. Cohen, M. W., Jacobson, C., Yurchenco, P. D., Morris, G. E., and Carbonetto, S. (1997) Laminin-induced clustering of dystroglycan on embryonic muscle cells: comparison with agrin-induced clustering. *J Cell Biol* **136**, 1047-1058
127. Montanaro, F., Lindenbaum, M., and Carbonetto, S. (1999) alpha-Dystroglycan is a laminin receptor involved in extracellular matrix assembly on myotubes and muscle cell viability. *J Cell Biol* **145**, 1325-1340
128. Quach, N. L., and Rando, T. A. (2006) Focal adhesion kinase is essential for costamerogenesis in cultured skeletal muscle cells. *Developmental biology* **293**, 38-52
129. Wells, L. (2013) The o-mannosylation pathway: glycosyltransferases and proteins implicated in congenital muscular dystrophy. *The Journal of biological chemistry* **288**, 6930-6935
130. Kabaeva, Z., Meekhof, K. E., and Michele, D. E. (2011) Sarcolemma instability during mechanical activity in Largemyd cardiac myocytes with loss of dystroglycan extracellular matrix receptor function. *Human molecular genetics* **20**, 3346-3355
131. Tegtmeyer, L. C., Rust, S., van Scherpenzeel, M., Ng, B. G., Losfeld, M. E., et al. (2014) Multiple phenotypes in phosphoglucomutase 1 deficiency. *The New England journal of medicine* **370**, 533-542
132. Zoncu, R., Bar-Peled, L., Efeyan, A., Wang, S., Sancak, Y., and Sabatini, D. M. (2011) mTORC1 senses lysosomal amino acids through an inside-out mechanism that requires the vacuolar H(+)-ATPase. *Science* **334**, 678-683
133. Diakov, T. T., and Kane, P. M. (2010) Regulation of vacuolar proton-translocating ATPase activity and assembly by extracellular pH. *The Journal of biological chemistry* **285**, 23771-23778
134. Orth, M., and Mundegar, R. R. (2003) Effect of acid maltase deficiency on the endosomal/lysosomal system and glucose transporter 4. *Neuromuscular disorders : NMD* **13**, 49-54

The Epilogue

Attempting the PhD has been my most challenging experience to date. I have learned that being in school (high school, undergrad, medical school) where information is handed to you to understand and digest is a far easier task, no matter the volume of information, than creating that knowledge yourself. No process is as frustrating as not knowing what to do next in the face of continuous failure. There is much I could complain about, but I will refrain because I decided to try for the PhD and enduring all types of perceived inequalities and hardships is part of the challenge. In the end, I think whether or not I am granted the title of PhD should not depend on the quantity of first author publications, which I anticipate as being at 1, but on what PhD actually means. Am I a philosopher – am I one who loves knowledge?

I think the research lab can be divided into groups of people. There are the technicians, who are able to conduct an experiment at the highest quality. But clearly that alone does not qualify one as a philosopher. Then there are the scientists, who are able to generate a hypothesis, design an experiment to test that hypothesis, conduct the experiment (like the technician), analyze the data, reformulate the hypothesis based on the new data, and perform another experiment. That cycle is repeated until some new conclusion can be reached. This entire thesis has shown, I think, that I am capable of doing just that process. However, does scientist equal philosopher? I don't think so because there are capable scientists who do science as a means to an end, not the end itself. For example, from my experience with and as a medical student, I think if someone offered all of us the guarantee of any residency position at any location if we were able to publish one paper, I think some would be up to that task and have the ability to complete that task. However, those medical students would not be doing research out of the love for knowledge. It would be done out of necessity. To be a philosopher, I believe, one has to do

research for the purpose of being able to do more research. This definition of a degree is not easy to quantify or confirm, so I understand one only has to prove one can be a scientist in order to be given the degree of doctor of philosophy. However, I hope through my thesis you can see that I did not do all these experiments and put in so much thought just to walk away from it all at the end. My hope is that I have the opportunity to do research once again after I complete my medical training, which may take some time. I wish to always be a traveler – an explorer – on that journey with no end we call science. Thank you so much.

Kunil Raval